INVESTIGATION OF ANION-PI INTERACTIONS IN INORGANIC, ORGANIC AND BIOLOGICAL SYSTEMS

A Thesis

by

EDWARD STERLING FUNCK

Submitted to the Office of Graduate Studies of
Texas A&M University
in partial fulfillment of the requirements for the degree of

MASTER OF SCIENCE

May 2011

Major Subject: Chemistry

INVESTIGATION OF ANION-PI INTERACTIONS IN INORGANIC, ORGANIC AND BIOLOGICAL SYSTEMS

A Thesis

by

EDWARD STERLING FUNCK

Submitted to the Office of Graduate Studies of
Texas A&M University
in partial fulfillment of the requirements for the degree of

MASTER OF SCIENCE

Approved by:

Chair of Committee,	Kim R. Dunbar
Committee Members,	François P. Gabbaï
	Timothy R. Hughbanks
	Thomas R. Ioerger
	James C. Sacchettini
Head of Department,	David H. Russell

May 2011

Major Subject: Chemistry

ABSTRACT

Investigation of Anion-pi Interactions in Inorganic, Organic and Biological Systems.

(May 2011)

Edward Sterling Funck, B.S., Grove City College

Chair of Advisory Committee: Dr. Kim R. Dunbar

Despite an ever growing number of reports concerning the anion-π interaction, controversy surrounding the nature of these weak supramolecular interactions continues. In an effort to further explore the nature and properties of anion-π interactions, experimental and computational methods were employed to study their occurrence in inorganic, organic and biological systems.

As part of ongoing research in the Dunbar group on the topic of anion-π based supramolecular interactions, the ligand 3,6-bis(2′-pyrimidyl)-1,2,4,5-tetrazine (bmtz) was synthesized and reacted with $[Cu(NCMe)_4][BF_4]$ to form the octanuclear complex $[Cu_8(bmtz)_6][BF_6]_6 \cdot 6MeCN$. Crystallographic evidence indicates an *in situ* reduction of two of the complexed bmtz ligands to radical anions. A second blue compound has also been observed in this reaction, and recent work has resulted in a direct synthesis of this compound. Preliminary results indicate that this second compound contains Cu(II) centers, as expected. Further work is necessary to identify the second blue compound.

In an effort to explore the fundamental question of whether or not anion-π interactions can occur between complex anions and olefins a series of Density

Functional Theory and *ab initio* computations have been preformed for the tetracyanoethylene, 7,7,8,8-tetracyanoquinodimethane, 7,7,8,8-tetracyano-1,2,4,5-tetrafluoroquinodimethane and octacyanoquinodimethane molecules with the anions tetrafluoroborate and hexaflurophosphate. These optimizations indicate favorable interactions for all cases and are further supported by critical point analysis, performed using the Atoms in Molecules theory, and Natural Bond Orbitals analysis.

DFT and NBO computations were also employed to explore the simultaneous anion-π and π-type charge transfer interactions observed between 1,4,5,8,9,12-hexaazatriphenylene-hexacarbonitrile and the chloride, bromide and iodide anions, as observed previously by the Dunbar group. Computations involving chloride and bromide anions are in full agreement with the previously reported spectroscopic and crystallographic evidence.

Finally, the question of whether or not anion-π interactions occur in proteins was investigated by searching the Protein Data Bank for interactions between chloride or iodide anion and the aromatic moieties of the phenylalanine, tyrosine and tryptophan residues. Computer scripts were specifically written for this search and revealed promising interactions between chloride anions and all three amino acids. Procedural and statistical considerations preclude these examples from being definitive.

DEDICATION

This thesis is dedicated to my wife, Kristen Funck, whose support was instrumental to the writing of this document.

If you have a theory that states the moon is made out of blue cheese but is able to accurately predict the orbit of moon, then you have a useful theory.

~ Paraphrased from Dr. F. Albert Cotton regarding VSEPR theory, Fall 2005.

ACKNOWLEDGEMENTS

I would like to thank Dr. Kim R. Dunbar for her mentorship, guidance and patience during my graduate studies. I greatly appreciate the opportunities that she provided to me at Texas A&M University and I am grateful and honored to have worked in her group. I would also like to thank my research committee: Dr. François P. Gabbaï, Dr. Timothy R. Hughbanks, Dr. Thomas R. Ioerger and Dr. James C. Sacchettini, as well as Dr. Steven E. Wheeler. The advice, feedback and criticism that they provided played a large part in my growth as a student and the development of my research.

Over the five years I was at Texas A&M, the Dunbar group underwent many changes as older students graduated and postdocs moved on and new faces arrived to take their places. One aspect that did not change is that the group consistently provided a network of support and friendship. This support was important to me during my time at Texas A&M and I would like to thank all of the members of the Dunbar group for that work environment. I would also like to thank all of my family (Funck and Chambers) for their unwavering support and love during my graduate career.

Finally, I would like to especially thank my wife, Kristen. You have been a blessing in my life and I can honestly say I would not have been able to come this far without you.

This thesis would not have been completed without the support and guidance of my family, friends, teachers and co-workers. I am indescribably grateful for that support. Thank you all.

TABLE OF CONTENTS

CHAPTER Page

CHAPTER Page

LIST OF FIGURES

FIGURE Page

FIGURE Page

LIST OF SCHEMES

LIST OF TABLES

TABLE Page

NOMENCLATURE

$\alpha_{\parallel}$	Polarizability in the direction perpendicular to plane of an aromatic ring.
AIM	Atoms in Molecules Theory
B3LYP	The Becke3 parameter hybrid exchange functional and Lee-Yang-Parr correlation function
bmtz	3,6-bis(2′-pyrimidyl)-1,2,4,5-tetrazine
bppn	3,6-bis(2′-pyridyl)-1,2-pyridazine
bptz	3,6-bis(2′-pyridyl)-1,2,4,5-tetrazine
BSSE	Basis Set Superposition Error
CH-bonding	Hydrogen bonding (carbon based) intearctions
CH-π	Hydrogen-π (carbon based) interactions
CP	Critical Point (resulting from AIM analysis)
CSD	Cambridge Structural Database
CT	Charge-Transfer
DFT	Density Functional Theory
ECP	Electrostatic Core Potential
E_{CT}	Charge-Transfer Energy
EPR	Electron Paramagnetic Resonance
ESI	Electrospray Ionization
ESP	Electrostatic Potential
E_t	Energy of Interaction

$HAT(CN)_6$	1,4,5,8,9,12-hexaazatriphenylene-hexacarbonitrile
H-bonding	Hydrogen bonding interactions
H-π	Hydrogen-π interactions
L.P.-π	Lone-pair π interactions
MP2	Second order Møller-Plesset perturbation theory
NBO	Natrual Bond Orbitals Theory
NMR	Nuclear Magnetic Resonance
MS	Mass Spectrometry
Q_{zz}	Quadrupole moment for an aromatic ring
PDB	Protein Data Bank
TCNE	tetracyanoethylene
TCNQ	7,7,8,8-tetracyanoquinodimethane
$TCNQ(CN)_4$	octacyanoquinodimethane
$TCNQF_4$	7,7,8,8-tetracyano-1,2,4,5-tetrafluoroquinodimethane
THF	tetrahydrofuran

CHAPTER I

INTRODUCTION AND GENERAL REVIEW OF ANION-PI INTERACTIONS

Introduction to Supramolecular Chemistry

To arrive at a precise definition of supramolecular chemistry is a challenging task. At its simplest, supramolecular chemistry can be defined as "chemistry beyond the molecule".[1] While this concise definition is widely quoted, it is quite vague. Generally, this simple definition is taken to mean that supramolecular interactions are noncovalent. Supramolecular chemistry can also refer to the chemistry of molecules or complexes that are comprised of separate components, either molecules or moieties, which collectively contribute unique properties to the final assembled product.[2] This definition is used specifically by supramolecular photochemists to describe compounds possessing multiple active centers separated by spacers.[2] Unlike the first definition, this second definition does not discount covalent bonding as a possible supramolecular interaction. Instead of defining the compound as supramolecular or molecular simply by structure, the second definition focuses on the segregation of distinct chemical properties within a given compound allowing for overlap between supramolecular and molecular chemistry. For the purposes of this thesis, supramolecular chemistry will be defined as the chemistry of noncovalent interactions between discrete molecules and atoms. Given the fact that so much science revolves around weak interactions and the self-assembly of molecules that can mimic nature, supramolecular chemistry continues to be an active and

---

This thesis follows the style of the *Journal of the American Chemical Society.*

growing field of interest for many researchers.

There are many types of reported supramolecular interactions in the literature involving both neutral and charged species. Electrostatic, hydrogen bonding (H-bonding), π-π and cation coordination including cation-π, interactions are widely accepted supramolecular interactions. Less common are the anion coordination[3-4] and the anion-π interaction,[5-7] which will be the focus of this thesis. More exotic interactions, namely lone pair-π[8-16] (L.P.-π) and hydrogen-π (H-π) interactions,[13,17-28] have also been reported in recent years.

Introduction to Anion-π Interactions

Katapinates (Scheme 1.1), the first host molecules to encapsulate an anionic guest, were developed by Park and Simmons at DuPont in 1968.[29] Also at DuPont, Pederson reported the development of crown ethers in 1967;[30] a seminal event in the field of cation coordination. While the complexation of metal cations by crown ethers received much attention, anion coordination remained a dormant field of study until Jean-Marie Lehn revitalized it during the 1970s.[4]

Reports by Schneider, *et al*. in the early 1990s, marked the first appearance of the term "anion-π",[31-32] but it would take another ten years and almost simultaneous reports by Alkorta, *et al*.,[33] Mascal, *et al*.[34] and Quiñonero, *et al*.[35] in 2002, before any significant attention was given to the anion-π interaction. Since these early reports, the interest in anion-π interactions has grown dramatically (Figure 1.1).

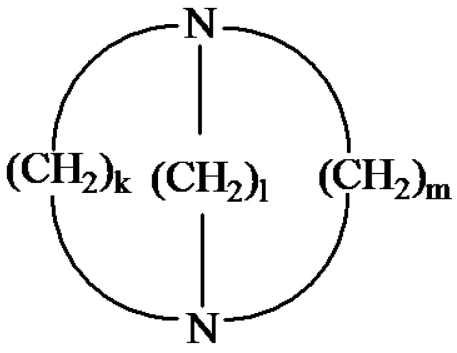

k	l	m
7	7	7
8	8	8
9	9	9
10	10	10

Scheme 1.1. Schematic representation of the katapinate molecules. k, l and m values are for those molecules that coordinate chloride anion.[29,36]

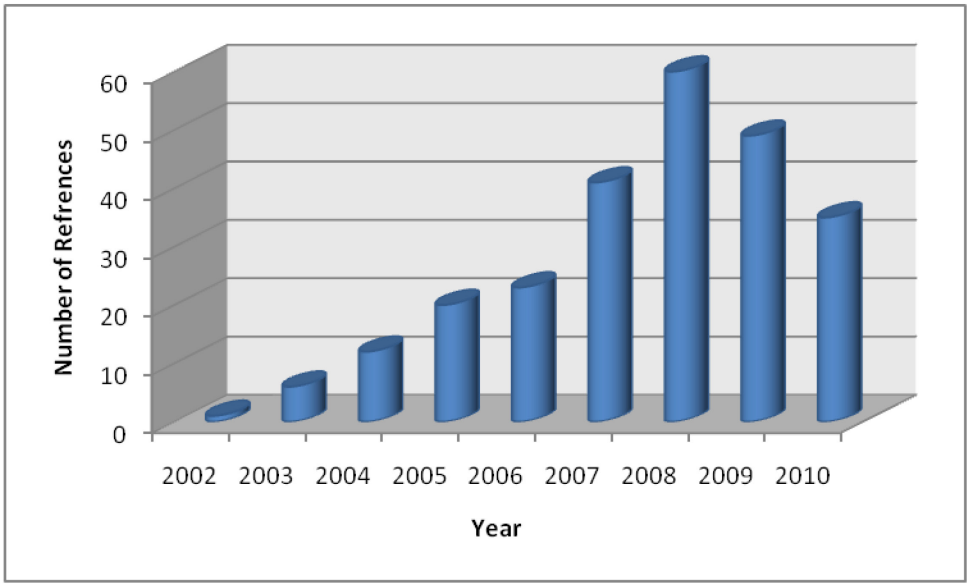

Figure 1.1. Histogram showing the number of publications on the topic of anion-π interactions. The information was obtained by searching the term "anion-pi" in Web of Science on September 27, 2010. While the values are not entirely accurate, as far as number of publications, the general trend is apparent.

Despite ongoing research the true nature of anion-π interactions still remains controversial. The first concise definition was provided by Garau, *et al*. in 2004 and described anion-π interactions as being the noncovalent interaction between an anion and an electron deficient aromatic ring.[37] Under this model, the interaction is governed by electrostatics, specifically the quadrupole moment, Q_{zz} and molecular polarizability in the direction perpendicular to the plane of the ring, $\alpha_{\parallel}$, of the aromatic ring.[37] In other words, π-acidic (electron deficient) aromatic rings, rings possessing a positive quadrupole moment, could interact electrostatically with an anion. If the Q_{zz} value is small, then a sufficiently large molecular polarizability can allow for an anion-π interaction to be induced, by the anion, in non-electron deficient aromatic rings. Recent work published by the Houk group however, makes the point, that for the case of fluorinated benzene, the apparent electron-deficient character of the ring and the purported anion-π interactions are actually not due to an electron-deficient π-system as had been previously proposed.[38] Houk and Wheeler maintain that the attraction between the benzene ring and the anion is actually due to the C-F dipoles along the C-F σ bonds. In this analysis, it is concluded that the electron withdrawing effect is on the carbon atoms as result of σ bonding and the π-system itself retains its electron rich character which is actually repulsive with respect to an anion.

Other authors have also tried to deconstruct the exact interaction(s) between an anion and an aromatic ring. One of the earliest reports regarding anion···arene interactions was published in 1968 by Buncel, *et al*.[39] While this report predates the concept of anion-π interactions, the authors do report spectroscopic evidence for what

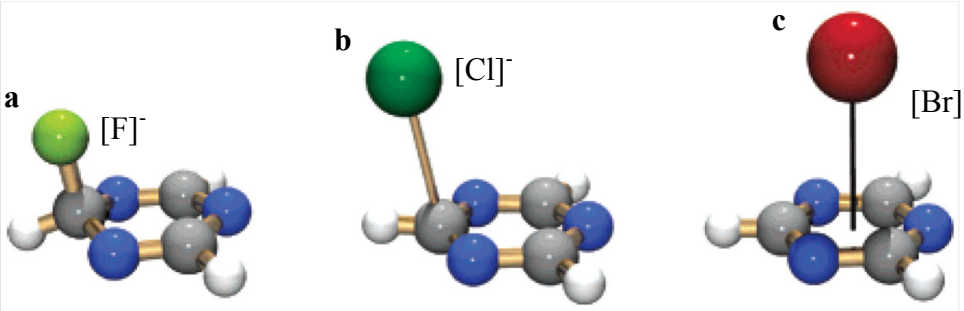

Figure 1.2. Computational results of Berryman, *et al*. depicting the σ-type charge-transfer (**a**), π-type charge-transfer (**b**) and anion-π (**c**) interactions. (Adapted with permission from Berryman, *et al*.[40]).

they refer to as a π-complex, a term used to describe a charge-transfer interaction between an anion (or some other electron rich molecule) and a π-electron deficient nucleus of an aromatic ring. The idea of this "π-complex" was also discussed in a more recent report. It was reported by Berryman, *et al*. that there are three different interactions that could occur between an anion and the face of an aromatic ring (Figure 1.2).[40] The authors define the anion-π as being an electrostatic interaction, with negligible (ideally no) charge-transfer, in which the anion is positioned directly over or near the centroid of the aromatic ring (Figure 1.2c). The authors also identify two different charge transfer interactions, σ- and π-type charge-transfer (CT) (the latter sounding much like the π-complex described by Buncel, *et al*.) Both types of CT interactions feature a structure in which the anion has moved away from the centroid of the aromatic ring and is positioned over the periphery of the molecule (Figure 1.2a,b). The only real difference between the two is the degree of CT. The π-type CT interaction features a smaller degree of CT and larger distances between the ring atoms and the anion than the σ-type (also known as a Meisenheimer complex). Deformation of the aromatic ring is expected in the σ-type CT (Figure 1.2a). It should be noted that in the computational studies and Cambridge Structural Database (CSD) search performed by Berryman, *et al*., the charge-transfer motifs were the most common.[40]

It is generally accepted that anion-π interactions can be characterized by anion to ring distances less than the sum of the van der Waals radii of the participating atoms and at such a position that the anion – ring centroid vector is perpendicular to the plane of the aromatic ring (the structure described by Berryman, *et al*. in Figure 1.2c).[7,40] While

certainly this is the ideal structure of an anion-π interaction, not all researchers agree that this rigid definition (*i.e.* the anion *must* be positioned over the centroid of the aromatic ring and the interaction *must* be electrostatic[40]) is sufficient but rather prefer a broader definition. In the Dunbar group, we use as an operative definition that any interaction between the anion and the π-system of an aromatic ring is an anion-π interaction, regardless of position (over the π-face of the ring) and with or without CT interactions.

One useful approach is to follow in the description of anion coordination structures inspired by the well established terminology of cation coordination structures. Structural types typically observed around cations are described for host-anionic guest complexes using similar terminology with the understanding that the driving force to adopt the structures is very different.[41] Likewise, the term "anion-π" could be used to describe a particular structure, namely a situation in which an anion is located above the π-face of an aromatic ring, with the caveat that the nature of the interaction (*i.e.* charge–quadrupole, charge–dipole, CT or some combination thereof) will be highly dependent on the identities of anion and ring as well as other environmental factors.

Support for the above argument can be found in a report by Hay, *et al*.[42] The conclusion of Hay, *et al*. can be summarized as: less nucleophilic anions and arenes with moderate electron affinity favor the anion-π interaction. As the nucleophilicy of the anion or electron affinity of the arene increases, so does the preference for a CT complex (particularly the σ-type).[42] Since subtle changes in the properties of either the anion or the aromatic ring can affect the exact structure and strength of the anion···arene interaction, it is reasonable to conclude that these various interaction types observed by

Berryman, *et al*.[40] are all related. In fact, the σ-type CT, π-type CT and anion-π interactions all involve both electrostatic and CT components, although the CT component of the anion-π interaction is negligible to zero. Given this case, it seems reasonable to use one term to describe all three types of interactions. For the purposes of clarity, the nomenclature proposed by Berryman, *et al*. (σ-type CT, π-type CT and anion-π) will be used in this thesis as described by the authors.[40]

While the earliest studies on anion-π interactions were computational[33-35,43] and computations still play a large role in the ongoing research,[38,44-49] there is a growing body of experimental support for anion-π interactions.[46,50-55]

Applications of Anion-π Interactions

While anion-π interactions have been predicted to be comparable in energy to cation-π interactions,[56] there is also evidence that anion-π interactions are in fact weaker than cation-π interactions.[57] The only experimentally derived energies for anion-π interactions, that we are aware of, are enthalpies of interaction from a gas phase study in 1987, which finds of enthalpies of 10.4 - 16.8 kcal/mol for $(C_6F_6)_n\cdots[X]^-$ (n=1,2, X=Cl,Br,I).[58] In comparison, cation-π interactions have been shown to have energies between 1 and 19 kcal/mol (the 19 kcal/mol value refers to $C_6H_6\cdots K^+$ in the gas phase).[2] These energies support the conclusion that these two interactions are comparable in energy and underscore the potential utility of the anion-π interaction.

The most obvious application is in the area of anion detection and sequestration via new receptors incorporating the anion-π interaction.[59-63] It has also been

demonstrated that anions can template supramolecular architectures through anion-π interactions[45,55,64-65] and recent work has revealed the possibility of anion-π interactions being used to mediate a reaction.[47] Using anion-π interactions as a source of anion transport has also generated a great deal of interest.[66-67] In summary, anion-π interactions are of interest for environmental,[6-7,61] crystal engineering,[45,64-65] catalytic [7,68] and biological/medicinal applications.[6-7,69]

It should be noted that several of the examples discussed below deal involve substituted benzene molecules as the π-system in question. While the recent report by Wheeler, *et al*.[38] maintains that these interactions (between an anion and a substituted phenyl ring) arise from charge-dipole interactions and not charge-quadrupole interactions, it is clear that the interaction between the anion and the π-face of the phenyl ring is important in all of the example compounds.

Anion Receptor Design

Mascal, *et al*. proposed a series of four cylindrical anion receptors based on the molecule [1,3,5]cyclophane (one of which is based on two triazine moieties).[62] Computational studies of these molecules have predicted that these receptors should show selectivity toward the fluoride anion encapsulation as opposed to chloride anion encapsulation. Later experimental work confirmed this prediction when Mascal, *et al*. synthesized a cylindrophane based on two cyanuric acid moieties (Scheme 1.2a).[63] It should be noted that this receptor incorporates anion-π, H-bonding and ion pairing interactions.

A report by Berryman, *et al*. demonstrates cooperation between anion-π interactions and H-bonding.[60] It was shown that by replacing the phenyl ring of a sulfonamide based halide acceptor with a pentafluorophenyl ring (Scheme 1.2b) the halide (chloride, bromide, iodide) association constants, as determined by ^{1}H-NMR, could be increased substantially. Hartree-Fock calculations support the conclusion that the increased halide binding affinity is due to the presence of the of the pentafluorophenyl ring.[60] Similar compounds were the subject of recent work by Albrecht, *et al*.[59] In this case the pentafluorophenyl substituted ammonium and pyridinium salts (Scheme1.2c) exhibit cooperative anion-π and carbon based hydrogen-bonding (CH-bonding) interactions. It is interesting to note that the position of the anion with respect to the aromatic ring depends on the identity of the anion (chloride, bromide, iodide, hexafluorophosphate) and the exact crystallization conditions.[59] By borrowing from traditional coordination chemistry, the authors described the position of the anion using an η^{x} (x = 1,2,3,6) notation.

Another example of cooperation between supramolecular interactions is provided in a recent report by Quinonero, *et al*. In this work, the authors use a triazine based ligand, 6*R*,2,4-bis(pyrazol-1-yl)triazine, to synthesize copper(II) and zinc(II) clusters designed to incorporate carbon based hydrogen-π (CH-π) and anion-π interactions (with tetrafluoroborate anion).[49] The resulting structures, as well as computational studies, support the conclusion that the anion-π interaction is stronger than the CH-π and that the presence of one interaction added further stability to the other.

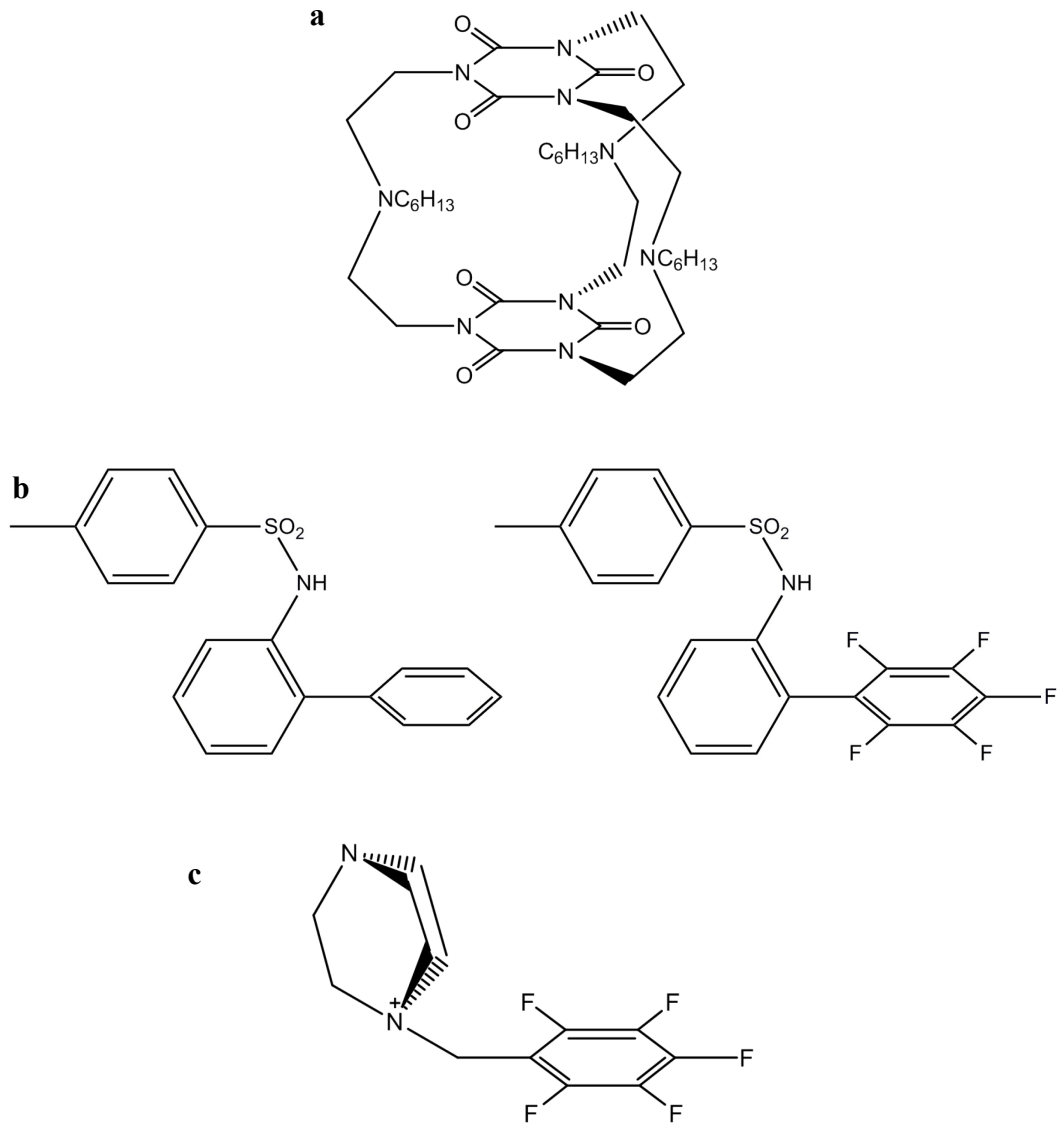

Scheme 1.2. Schematic representations of the anion receptors synthesized by Mascal, *et al*.[63] (**a**) Berryman, *et al*.[60] (**b**) and one of the receptors syntehsized by Albrecht, *et al*. (**c**).[59]

Anion Templation and Crystal Engineering

Early reports by the Dunbar group in the publications of Campos-Fernández, *et al*.[64] and Schottel, *et al*.[65] focused the dependence of molecular geometry on anion identity. As this topic is directly relevant to the results described in **Chapter II**, a more detailed discussion of these reports is provided therein. This dependence was also investigated by Wan, *et al*. in their recent work regarding silver complexes of a new dipyrazinyl sulfoxide ligand.[55] The two pyrazinyl groups of this ligand were shown to form a "pincer" around the anion (nitrate, hexafluorophosphate, perchlorate, trifluoroacetate) via anion-π interactions (Figure 1.3). The different sizes of the anions resulted in varying angles between the two arms of the ligand and ultimately a variety of structures. Similar results were also observed for zinc(II) and cadmium(II).[55]

A later report of two supramolecular assemblies consisting of magnesium malonate, perchlorate anion and either protonated 2-aminopyridine or protonated 2-amino-4-picoline by Das, *et al*. revealed a network incorporating π-π, lone pair-π and anion-π interactions in the solid state.[45] Computational studies were also employed to probe these noncovalent interactions, the results of which indicate that these interactions are present in this structure. While the discovery of this structure was not an attempt at design, the authors underscore the importance of understanding structures incorporating various types of weak supramolecular- interactions as the field of crystal engineering advances.[45]

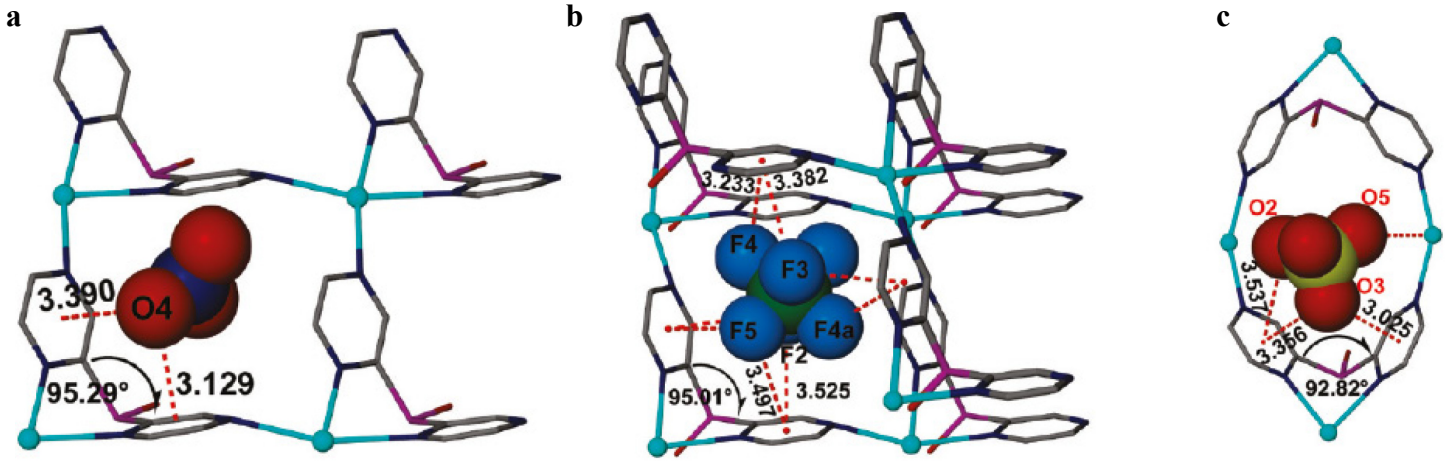

Figure 1.3. Depiction of the anion encapsulation observed in the structures of $\{[Ag(pyz_2SO)][NO_3]\cdot MeCN\}_\infty$ (**a**), $\{[Ag(pyz_2SO)][PF_6]\}_\infty$ (**b**) and $\{[Ag_3(pyz_2SO)_2][ClO_4]_3\}_\infty$ (**c**). pyz_2SO refers to dipyrazinylsulfoxide. Silver atoms (teal), carbon atoms (gray), nitrogen atoms (purple), sulfur atoms (magenta), oxygen atoms (red), phosphorus atom (green), chlorine atom (yellow). (Adapted with permission from Wan, *et al*.[55]).

Reaction Mediation

An investigation of the synthesis of 1,2,4-trinitrobenze from 1-fluoro-2,4-dinitrobenzene was recently reported by Jones, *et al*.[47] The reaction is typically performed in ethanol and proceeds through a nucleophilic substitution (S_NAr) of the fluoro group by an ethanol molecule resulting in the formation of an ether intermediate. It was discovered that the rate of reaction for this synthesis increases in the ionic liquid [Bmin][$N(SO_2CF_3)_2$] (Bmin = 1-butyl-3-methylimidazolium) as compared to ethanol. A combination of experimental and computational work led the authors to conclude that the anionic component of the ionic liquid is playing a significant role in the lowering of reaction barrier. The computational data demonstrate that the anionic component of the liquid prefers to interact with the π-face of the benzene ring, while the cationic component interacts with the periphery of the ring or the substituents on the ring (Figure 1.4) pointing to anion-π interactions, or anion···arene interactions in general, playing a role in the mediation of this reaction.[47]

Anion Transport

A synthetic trans-membrane chloride anion channel utilizing anion-π interactions was reported by Gorteau, *et al*.[67] This anion-π "slide" has generated significant interest[66] and will be discussed in more detail in **Chapter V**. Research involving chloride channels is of particular import due to the role that chloride channels play in cystic fibrosis.[67]

Biological Relevance of Weak Supramolecular Interactions

Supramolecular interactions have been shown to play a significant role in biological systems.[1] While there has been little evidence for anion-π interactions occurring biologically, there is still significant interest in their potential role.[6-7] (This particular topic will be discussed in **Chapter V**).

A major reason for the interest and optimism regarding the biological role of anion-π interactions is the occurrence of other weak supramolecular interactions in biomolecules. To clarify this definition, weak supramolecular interactions do not refer to electrostatic,[70] H-bonding,[71] π-π[71] or cation-π interactions.[72] (These types of interactions have all been shown to play a significant role in biology and give substantial credence to the idea that other supramolecular interactions can also play a role in biology.) The term weak is meant to indicate the anion-π, lone pair (L.P.)-π[10] and H-π[23] interactions. Analysis of crystal structures of RNA and DNA, coupled with computational studies, lead Egli, *et al*. to originally propose L.P-π interactions as a biologically relevant supramolecular interaction.[10] While examples of this interaction, in biological molecules, are still limited, recent experimental[14] and computational[9,11,14] results provide further evidence for these interactions. Of particular interest is the report of Convertino, *et al*. which discusses the mechanisms by which 9,10-anthroquinone and anthracene can inhibit amyloid aggregation, a process linked to many neurological disorders, including Alzheimer's.[9] The authors discuss the presence of what they refer to as $\pi^{+}\delta^{-}$ interactions in the 9,10-anthroquinone-β-amyloid complex (the authors used a heptapeptide sequence of β-amyloid for this work).

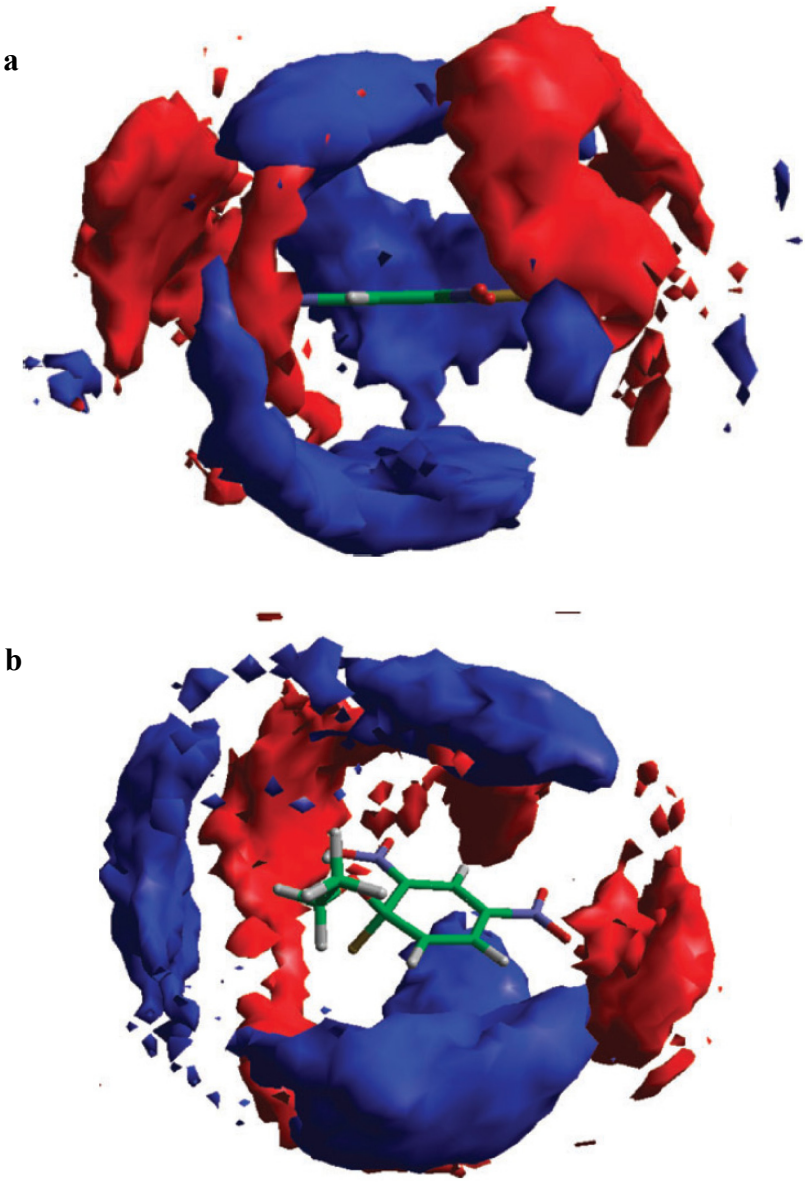

Figure 1.4. Computational models of 1-fluoro-2,4-dinitrobenzene (**a**) and an ethanol substituted intermediate (**b**) in [Bmin][$N(SO_2CF_3)_2$]. Blue regions refer to anion interactions and the red regions refer to cation interactions. (Adapted with permission from Jones, *et al*.[47] – Reproduced by permission of the PCCP Owner Societies, http://dx.doi.org/10.1039/b920131a)

Egli, *et al*. comment on the research surrounding H-π interactions in biomolecules as a contrast to the counterintuitive L.P.-π interactions.[10] (The same contrasted was noted in the early reports of anion-π interactions.[43]) The more intuitive H-π interaction is still a topic of research as evidenced by a recent report by Plevin, *et al*.[23] The authors were able to demonstrate the existence for CH-π interactions in protein structures through NMR spectroscopic measurements supported by a combination of Density Functional Theory (DFT) computations and database searching. It is worth mentioning, that Plevin, *et al*. were focusing on the less studied CH- π interactions arising from methyl···arene interactions.[23]

Exploration of Anion-π Interactions in this Thesis

While the field of anion-π chemistry is steadily growing, there are still many questions that remain unanswered. In an effort to explore both the fundamental and applied facets of the anion-π interaction, a new series of experimental and computational studies have been performed.

As part of ongoing attempts to design clusters template by anion-π interactions,[64-65] a new cluster capable of engaging in anion-π interactions has been synthesized.

Fundamental questions regarding the potential for anion-π interactions involving non-aromatic molecules have been addressed by a new series of computations.

Further investigations into the simultaneous CT and anion-π interactions exhibited by the molecule 1,4,5,8,9,12-hexaazatriphenylene-hexacarbonitrile[51,73] have been pursued utilizing computational methods.

Finally, in an attempt to provide clear evidence for anion-π interactions in proteins, a series of computer scripts have been written and used to conduct systematic searches of the Protein Data Bank.

CHAPTER II

SYNTHESIS AND CHARACTERIZATION OF A NEW OCTANUCLEAR COPPER(I) COMPLEX EXHIBITING ANION-PI INTERACTIONS

Introduction

The design and synthesis of new supramolecular architectures has been an ongoing theme in the Dunbar group since the discovery of anion-π templated squares[74] and pentagons[75] by Campos-Fernández, *et al*. It was reported that the substituted tetrazine molecule, 3,6-bis(2′-pyridyl)-1,2,4,5-tetrazine (bptz) (Figure 2.1a) was capable of forming squares with fully solvated nickel(II) cations in the presence of the complex anion tetrafluoroborate, $[Ni_4(bptz)_4(NCMe)_8][BF_4]_8$ (Figure 2.2a).[74] Further work by Campos-Fernández demonstrated that the identity of the architecture can be controlled by the counter anion and that the pentagon $[Ni_5(bptz)_5(NCMe)_{10}][SbF_6]_{10}$ (Figure 2.2b) can be prepared if hexafluoroantimonate anion is used.[75] It was later demonstrated that the square architecture could be synthesized using $[Zn(NCMe)_6][BF_4]$ or the corresponding perchlorate salts of both nickel(II) and zinc(II).[64] An interesting property exhibited by the square and pentagon architectures formed with the nickel(II) salts is the ability to interconvert between the two structures by addition of excess amounts of the appropriate anion. By taking advantage of this fact, the nickel-pentagon was used to synthesize the square architecture incorporating a variety of anions.[64]

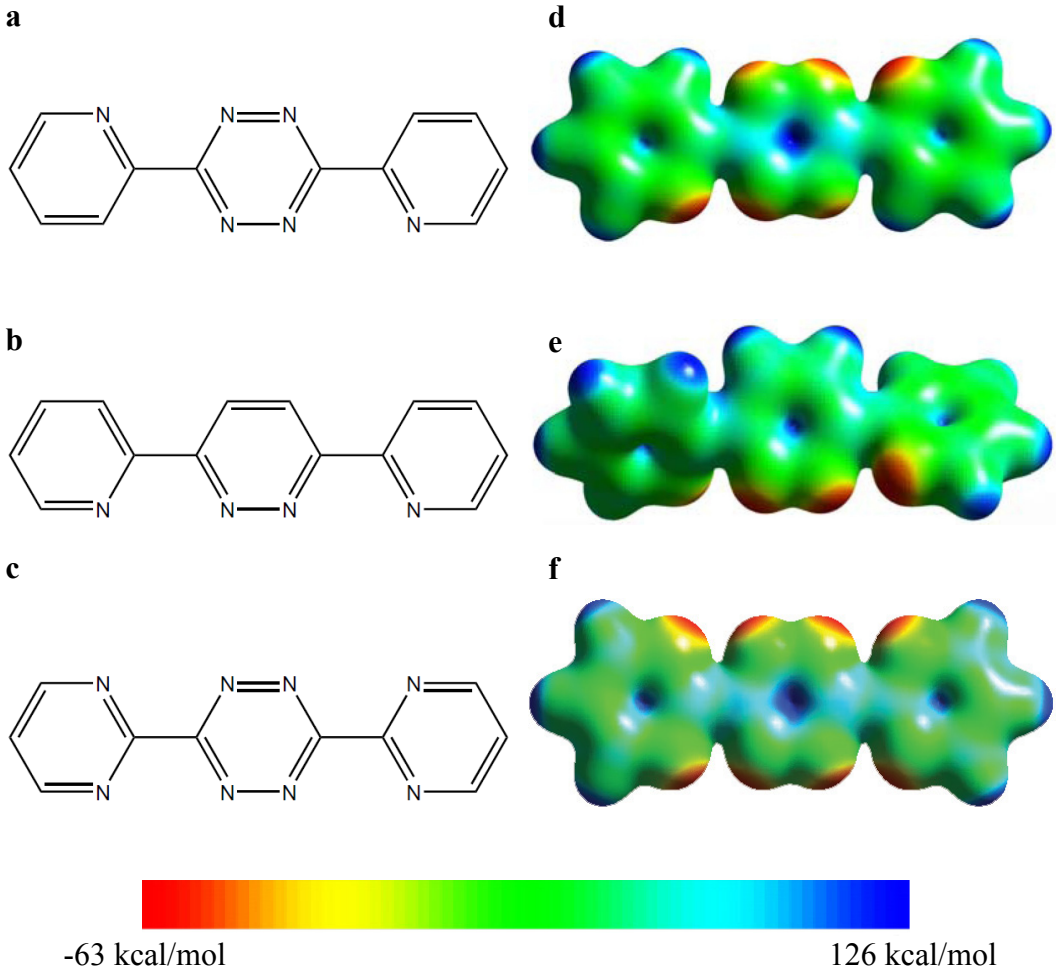

Figure 2.1. Schematic representations of the molecules 3,6-bis(2′-pyridyl)-1,2,4,5-tetrazine (bptz) (**a**), 3,6-bis(2′-pyridyl)-1,2-pyridazine (bppn) (**b**) and 3,6-bis(2′-pyrimidyl)-1,2,4,5-tetrazine (bmtz) (**c**) along with their respective electrostatic potential (ESP) maps. The ESP maps for bptz (**d**) and bppn (**e**) are Adapted with permission Schottel, *et al*.[65] The ESP map for bmtz (**f**) was generated by Cerius^2 4.10 using the geometry optimized structure obtained through B3LYP/6-311++G(d,p). All maps were made with an isodensity value of 0.02.

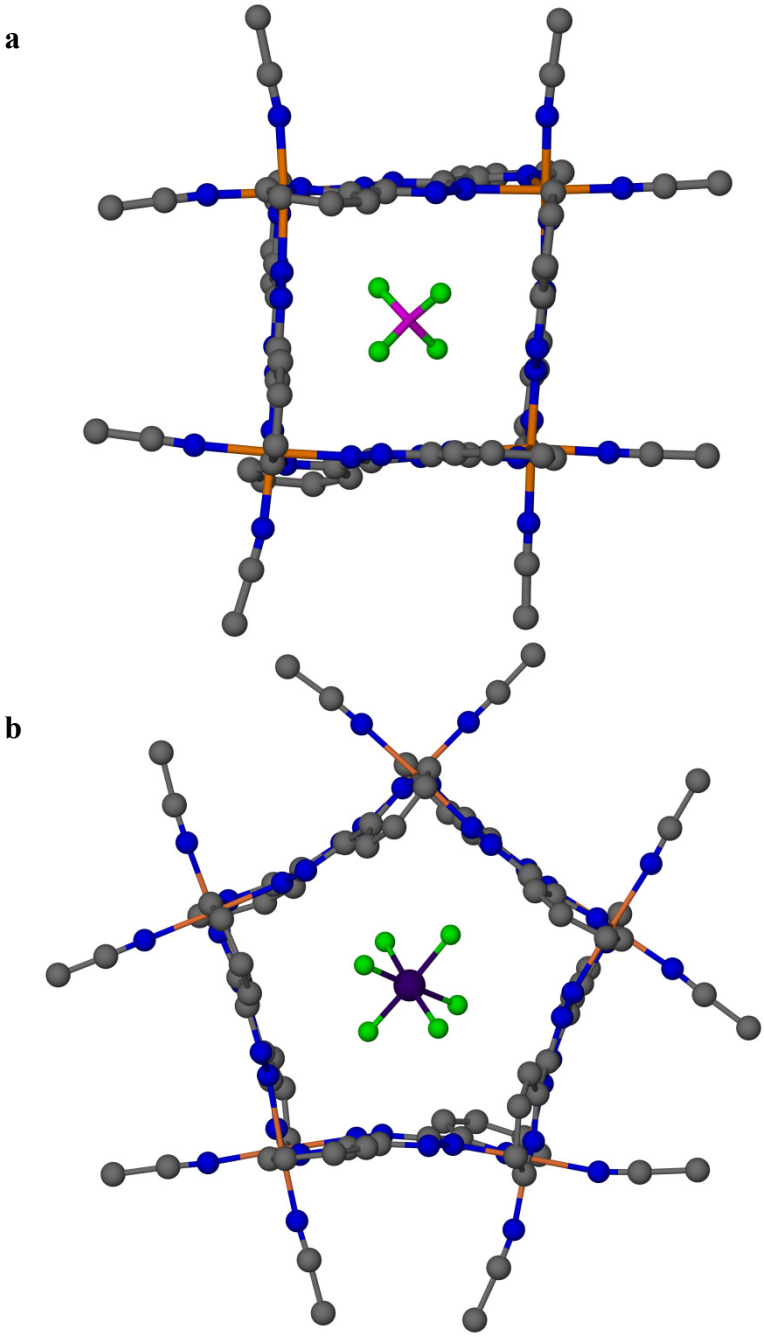

Figure 2.2. Crystal structures of $[Ni_4(bmtz)_4(NCMe)_8][BF_4]_8$ (**a**) and $[Ni_5(bmtz)_5(NCMe)_{10}][SbF_6]_{10}$ (**b**). Non-encapsulated anions are omitted for the sake of clarity. Carbon atoms(gray), nitrogen atoms (blue), nickel atoms (orange), fluorine atoms (green), boron atom (pink), phosphorus atom (purple).

The results of these studies prompted Schottel, *et al*. to investigate the reaction between bptz and silver(I) cations.[65,76] It was discovered that, unlike previous reactions between silver(I) cations and related ligands which generally form extended structures,[76] the silver(I)-bptz reaction yielded a dinuclear paddlewheel, $[Ag_2(bptz)_3][SbF_6]_2$, which packs in a hexagonal fashion with anion-π interactions between six of the clusters and a single anion (Figure 2.3a,b).[76] By changing the ligand from bptz, to 3,6-bis(2′-pyridyl)-1,2-pyridazine (bppn) (Figure 2.1b) a dinuclear grid structure, $[Ag_4(bppn)_4][SbF_6]_4$ was isolated (Figure 2.3c).[65] It is particularly interesting to note that the silver(I)-bptz structure is dominated by anion-π interactions whereas the silver(I)-bppn structure is dominated by π-π interactions, the anion-π interactions being less prominent.[65]

It should be noted that while bptz is capable of binding two metal ions in both the *syn* and *anti* configurations, both bptz and bppn are coordinated to the silver(I) ions in the *syn* configuration in these structures. The only difference between the bptz and bppn molecules is the central core of the ligand (Figure 2.1a,b). The central tetrazine core of bptz has been shown to be more electropositive than the central pyridazine core of bppn (Figure 2.1d,e).[77] Given that a decrease in the electropositive nature of the ligand resulted in a drastic change in the produced, it is reasonable to expect that an increase in the electropositive nature of the ligand would have an effect on the structure as well. To this end the ligand, 3,6-bis(2′-pyrimidyl)-1,2,4,5-tetrazine (bmtz) (Figure 2.1c,f) was synthesized in order to use for the assembly of cationic architectures.

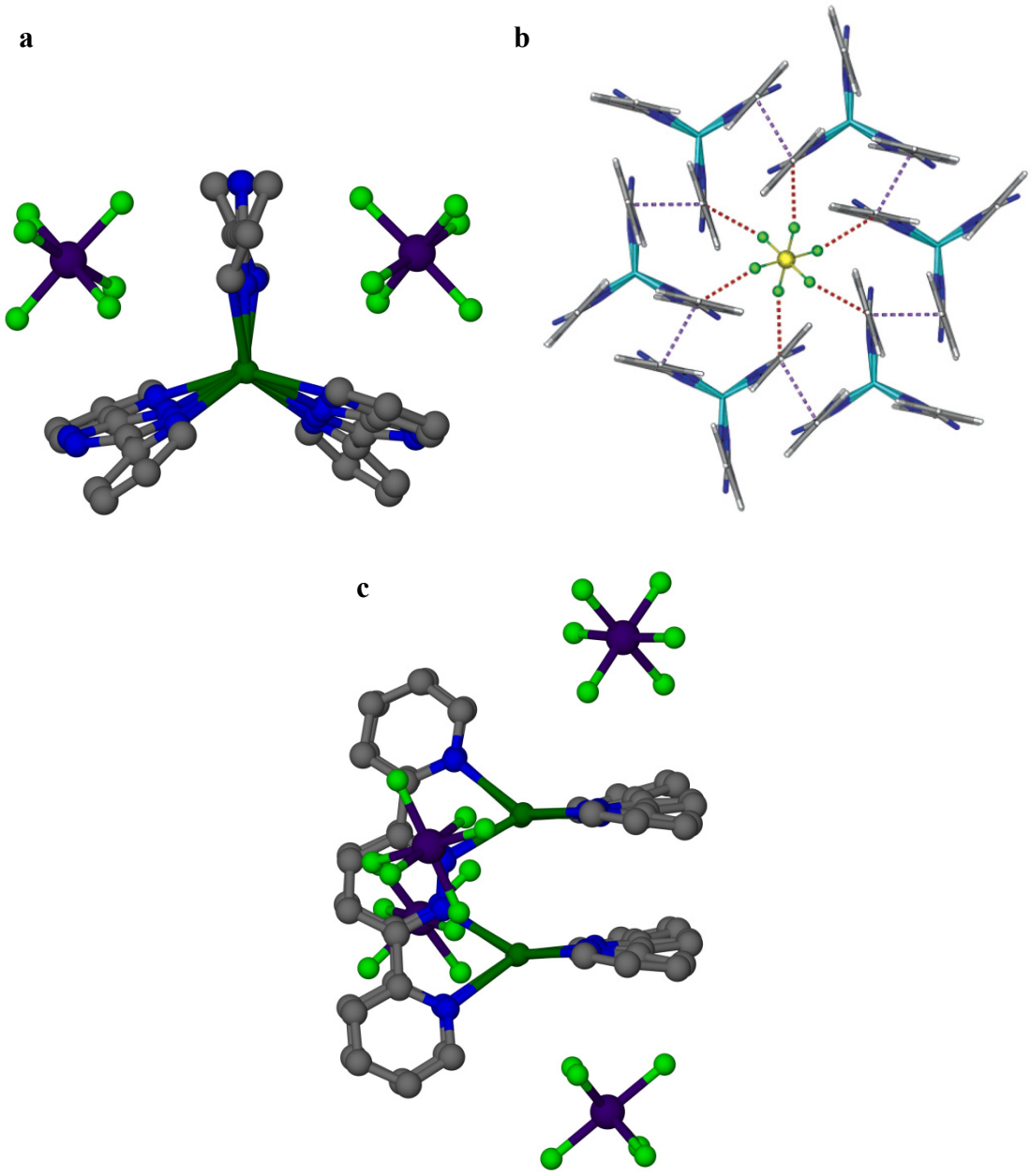

Figure 2.3. Crystal structures of $[Ag_2(bptz)_3][SbF_6]_2$ (**a**) and $[Ag_4(bppn)_4][SbF_6]_4$ (**c**). A portion of the packing diagram for $[Ag_2(bptz)_3][SbF_6]_2$ is also shown (**b**). In **b** it can be seen that the hexagonal arrangement of $[Ag_2(bptz)_3]^{2+}$ clusters is templated by the anion-π interactions. (Adapted with permission Schottel, *et al.*[65]) Carbon atoms (gray), nitrogen atoms (blue), silver atoms (dark green or teal), fluorine atoms (light green), antimony atoms (purple or yellow).

Experimental

Materials

The starting materials 2-cyanopyrimidine (Aldrich), hydrazine hydrate (Aldrich), hydrochloric acid (EMD), sodium nitrate (EM Science), copper(I) oxide (Fisher), tetrafluoroboric acid (48% in water) (Aldrich), hexafluoroantimonic acid hexahydrate (Aldrich), glacial acetic acid (EMD), ammonium hydroxide (EM Science), nitric acid (EM Science) and tetrahydrofuran (EMD) were all purchased and used without further purification. The precursor salt $[Cu(NCMe)_4][PF_6]$ (Aldrich) was stored under a nitrogen atmosphere and used without further purification. Copper foil (Aldrich) and copper powder (Fisher) were used without further purification. Diethyl ether (Aldrich), tetrahydrofuran (Alfa Aesar), benzene (Aldrich) and toluene (Alfa Aesar) were dried and deoxygenated using an MBraun Solvent Purification System. Acetonitrile (EMD), dichloromethane (EMD) and nitromethane (Aldrich) were distilled, under a nitrogen atomosphere, over calcium hydride, diphosphorus pentoxide, and calcium hydride, respectively, prior to use; Acetonitrile and dichloromethane were stored over 4 Å molecular sieves prior to distillation.

Syntheses

$[Cu(NCMe)_4][X]$ (X = BF_4, SbF_6). $[Cu(NCMe)_4][X]$ (X = BF_4, SbF_6) were prepared by slight modification of a literature method.[78] The hexafluorophosphoric acid called for in the original preparation was replaced by tetrafluoroboric acid (48% in water) or hexafluoroantimonic acid hexahydrate to form the appropriate salt. The $[Cu(NCMe)_4][SbF_6]$ salt was prepared by a previous member of the Dunbar group, Dr.

Michael Shatruk (Department of Chemistry and Biochemistry, The Florida State University).

2,5-dihydro-3,6-bis(2′-pyrimidyl)-1,2,4,5-tetrazine (H_2bmtz). H_2bmtz was synthesized using a modified literature preparation.[79-80] A sample of 2-cyanopyrimidine (6.0 g, 0.057 mol) was dissolved in tetrahydrofuran (THF) (80 mL) to which concentrated HCl (8.0 mL) was added resulting in a pale yellow solution; the solution was then brought to reflux. The dropwise addition of hydrazine hydrate (4.0 mL) resulted in the formation of a dark red solution after a few minutes. (If the solution does not darken to red, the addition of another 4.0 mL of hydrazine hydrate may be required). Reflux continued overnight (Kaim, *et al*.[80] only report a 4 hour reflux) after which distilled water (80 mL) was added to give an orange precipitate which was collected by suction filtration. Rotoevaporation of the reaction solution to remove THF resulted in additional precipitation of an orange solid which was removed by filtration. Additional crude product can be isolated by extraction from the remaining solution with dichloromethane (3 x 100 mL). An orange powder is then isolated by removal of the dichloromethane *via* rotoevaporation.

The orange powders were recombined and purified by recrystallization from 500 mL of boiling water. Orange needle crystals. Yield: 5.6 g (82%). ^{1}H-NMR spectrum in $CDCl_3$ (δ, ppm): 8.85 (d), 8.52 (s), 7.40 (t). ESI-MS: *m/z* 241.1 $[H_2bmtz+H]^+$.

3,6-bis(2′-pyrmidyl)-1,2,4,5-tetrazine (bmtz). The bmtz molecule was synthesized using a modified literature preparation.[79-80] It should be noted that Kaim, *et al*. report that bmtz is readily reduced to H_2bmtz, particularly in protic solvents.[80]

A suspension of H_2bmtz (2.4 g, 1.0 mmol) in a 3:2 glacial acetic acid:THF solution (225 mL) was prepared and cooled using an ice bath to 6 °C. A concentrated solution of $NaNO_2$ (4.1 g, 59 mmol) was prepared in distilled water (6.0 mL) and slowly added dropwise to the H_2bmtz suspension taking care to maintain the temperature of the reaction below 10 °C. The suspension darkened to purple and evolved brown NO gas. The reaction was stirred for 23 minutes and the pH was then adjusted to basic conditions (pH=8) with the slow addition of concentrated NH_4OH (270 mL) taking care to ensure that the reaction temperature did rise above 20 °C. (In general, the reaction should be kept as cold as possible). The resulting purple powder was isolated by filtration from the remaining orange solution.

The product can be purified by washing with benzene (200 mL) and, if needed, recrystallized from boiling dicholormethane (800 mL). Purple needle crystals. ^{1}H-NMR spectrum in $CDCl_3$ (δ, ppm): 9.17 (d), 7.63 (t). ESI-MS: *m/z* 239.1 $[bmtz+H]^+$.

$[Cu_8(bmtz)_6][BF_4]_6 \cdot$ 6 MeCN (1). This reaction was performed under nitrogen and under anhydrous conditions. White $[Cu(NCMe)_4][BF_4]$ (0.18 g, 0.58 mmol) and purple bmtz (0.069 g, 0.29 mmol) were dissolved in 50 mL of distilled acetonitrile resulting in a dark brown solution which was stirred overnight. (It should be noted that this particular reaction was left to stand for three days under nitrogen). Undissolved bmtz was isolated from the reaction *via* suction filtration. Layering with diethyl ether, under nitrogen, in a thin tube resulted in the formation of brown block crystals after three months.

Further attempts to react $Cu^{0/1+}$ and bmtz. Other attempts to synthesize Cu-bmtz complexes are summarized in Tables 2.1 and 2.2. All of these reactions followed the

same basic procedure as **1** with the variations being limited to the Cu:bmtz ratio, reaction volume and crystallization conditions (Table 2.1). It should be noted that these samples were not allowed to stand before crystallization as is the case in **1**. These attempts generally resulted in the formation of a blue precipitate or a mixture of dark blue and brown precipitates. Reactions involving $[Cu(NCMe)_4][X]$ ($X = [PF_6]^-$, $[SbF_6]^-$), were performed in an attempt to grow crystals of analogues of **1** while the reactions involving Cu^0 were intended to be attempts at controlling redox chemistry in the formation of this complex (Table 2.2) (see **Discussion**). (Glöckle, *et al*. were able to reduce bmtz, using Cu^0 in the presence of triphenylphosphine.[81])

Blue precipitate (2). It was discovered that the blue precipitate observed in many of the reactions of $[Cu(NCMe)_4][BF_4]$ and bmtz could be synthesized exclusively by the following method(s). A clear solution of $[Cu(NCMe)_4][BF_4]$ (0.098 g, 0.31 mmol) in distilled CH_2Cl_2 (10 mL) and a fuchsia solution of bmtz (0.044 g, 0.18 mmol) in distilled CH_2Cl_2 were prepared under nitrogen. Addition of the bmtz solution to the $[Cu(NCMe)_4][BF_4]$ solution resulted in the instantaneous formation of a dark blue precipitate which can be isolated by vacuum filtration.

Alternatively, a slow diffusion reaction can be set up in a three chambered cell (Scheme 2.1) by placing solutions of $[Cu(NCMe)_4][BF_4]$ (0.050 g, 0.16 mmol) in distilled CH_2Cl_2 (~15 mL) and bmtz (0.025 g, 0.11 mmol) in distilled CH_2Cl_2 (~15 mL) into opposite chambers of the cell with distilled CH_2Cl_2 (~15 mL) in the central chamber

Table 2.1. Summary of reaction and crystallization attempts to synthesize **1**. This table does not include information reported for the synthesis of **2**.

$[Cu(NCMe)_4][BF_4]$ (g)	**bmtz (g)**	**Molar Ratio**	**MeCN (mL)**	**Crystallization Condition***	**Result†**
0.18	0.069	2 : 1	50	layered with diethyl ether	1[a] or **2**
0.18	0.069	2 : 1	50	layered with benzene	**2**
0.18	0.069	2 : 1	50	layered with nitromethane	-----
0.18	0.069	2 : 1	50	added diethyl ether (40 mL)[c]	‡
0.55	0.20	2 : 1	20, 80[b]	added diethyl ether (40 mL)[d]	‡
0.18	0.069	2 : 1	50	vapor diffusion with diethyl ether	**2**
0.18	0.10	4 : 3	50	layered with diethyl ether	**1**
0.10	0.061	4 : 3	50	layered over toluene	**2** or **1**[e]
0.10	0.061	4 : 3	50	layered over toluene[d]	-----
0.18	0.10	4 : 3	50	layered with THF	**2**
0.18	0.10	4 : 3	50	added THF (95 mL)[c]	‡
0.69	0.35	3 : 2	50 mL	added diethyl ether[f]	‡

*all crystallization attempts were performed on a small scale in thin crystallization tubes unless otherwise stated.
†all blue precipitates observed are assumed to be **2.**
‡these attempts yielded a black precipitate: based on observations of recrystallization attempts it is possibly a mixture of **1** and **2**.
[a]the information in red is a result of the synthesis reported for **1**.
[b]the volumes of MeCN used to dissolve $[Cu(NCMe)_4][BF_4]$ and bmtz, respectively. The $[Cu(NCMe)_4][BF_4]$ solution was added to the bmtz solution.
[c]bulk crystallization attempt that was placed in the freezer.
[d]the reaction was layered in a Schlenk tube (bulk scale).
[e]a brown powder was observed, presumed to be **1**.
[f]precipitating solvent was added slowly until a solid was observed.

Table 2.2. Summary of reaction and crystallization attempts to synthesize clusters related to **1**. This table does not include information reported for the synthesis of **2**.

$[Cu(NCMe)_4][PF_6]$ (g)	bmtz (g)	Molar Ratio	MeCN (mL)	Crystallization Condition	Result
0.83	0.37	3 : 2	50 mL	added diethyl ether[f]	‡

$[Cu(NCMe)_4][SbF_6]$ (g)	bmtz (g)	Molar Ratio	MeCN (mL)	Crystallization Condition	Result
1.2	0.50	4 : 3	30 mL	added THF[f]	-----
1.2	0.50	4 : 3	40 mL	added diethyl ether (40 mL)[f]	‡

Cu^0 (g)[g]	bmtz (g)	Molar Ratio	CH_2Cl_2 (mL)	Crystallization Condition	Result
0.021 (foil)	0.081	1 : 1	15 mL		no reaction
0.50 (powder)	0.079	24 : 1	35 mL		no reaction

‡these attempts yielded a black precipitate, based on observations of recrystallization attempts it is possibly a mixture of **1** and **2**.

[f]precipitating solvent was added slowly until a solid was observed.

[g]the copper metal was activated with nitric acid.

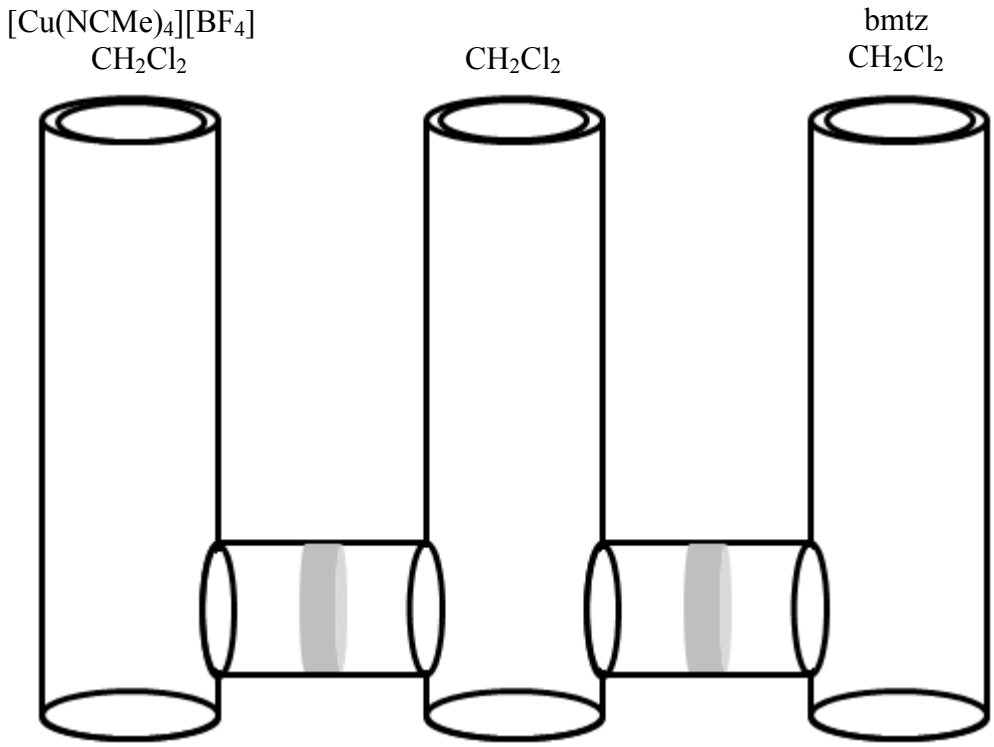

Scheme 2.1. Schematic diagram of a three chambered cell used in a crystallization attempt of **2**.

separating the other two solutions. After several days a mixture of precipitate and microcrystals were observed.

Physical Measurements

Nuclear Magnetic Resonance (NMR) Spectroscopy. The ^{1}H NMR spectra were recorded at 20 °C on a 300 MHz Mercury spectrometer. The ^{1}H NMR spectra were referenced relative to the residual proton impurities in the deuterated solvent ($CDCl_3$).

Mass Spectrometry (MS). Electrospray mass spectral data were acquired on a Sciex API QStar Pulsar mass spectrometer using an electrospray ionization (ESI) source. ~1 mg/mL solutions of the samples were used, and the data were acquired in the positive-ion mode. The ion spray voltage was set at ~4800 V, and the nozzle skimmer potential was adjusted to 10 V to minimize fragmentation. Theoretical isotope ratio calculations were performed using the program IsoPro 3.0.

Electron Paramagnetic Resonance (EPR) Spectroscopy. X-band EPR spectra were recorded on a Bruker EMX spectrometer equipped with a Hewlett-Packard 5352B microwave frequency counter, an ER4102 ST cavity, and the Oxford Instruments ESR 900 Crysostat. Data were collected in the solid state at 4 K and plotted with the SpinCount 3.1.2[82] software.

Magnetic Susceptibility Measurements. Magnetic susceptibility measurements were performed on a Quantum Design SQUID MPMS-XL magnetometer. Measurements were carried out in the DC mode in an applied flied of 0.1 T in the 2-300 K range.

Single Crystal X-ray Diffraction Studies

The crystal selected for study was suspended in polybutene oil (Aldrich), mounted on a cryoloop and placed in a N_2 cold stream. Single-crystal X-ray data were collected on a Bruker SMART 1000 diffractometer equipped with a CCD detector. The data sets were recorded as two ω-scans of 600 frames each, at 0.3° step width, and two ω-scans of 400 frames each, at 0.5° step width. The Bruker SAINT[83] software package was used to integrate the data. The absorption correction (SADABS[84]) was based on fitting a function to the empirical transmission surface as sampled by multiple equivalent measurements. Solution and refinement of the crystal structure was carried out using the SHELX[85] suite of programs and the graphical interface X-SEED.[86] Preliminary indexing of the data sets established a triclinic unit cell for the compound and systematic extinctions indicated that they belonged to the space group *P-1* (No. 2). The structures were solved by direct methods, which resolved the positions of all the atoms in the cluster and some of the anion and solvent atoms. The remaining non-hydrogen atoms were located by alternating cycles of least-squares refinements and difference Fourier maps. All hydrogen atoms were placed in calculated positions. The final refinements were carried out with anisotropic thermal parameters for all non-hydrogen atoms. A summary of pertinent information relating to unit cell parameters, data collection and refinement statistics is provided in Table 2.3.

Computational Methods

Geometry optimization of bmtz was performed using density functional theory (DFT)[87] as contained in the Gaussian03[88] program suite. The Becke3 parameter hybrid

exchange functional[89] and Lee-Yang-Parr correlation function[90] (B3LYP) was also used. A Pople style triple-ζ basis set with an optimized p and d-polarization functions[91-92] (6-311++G(d,p)) was used. The electrostatic potential map was generated using Cerius^2 4.10[93] with an isodensity value was set at 0.02.

Results

Synthesis

Most reaction attempts resulted in a blue powder that is most likely **2**. This assignment is by no means certain, as there is no evidence other than color to support any conclusion. The single largest difficulty for this reaction was the small quantities of solid material isolated from most reactions, and the inability to determine if the powder isolated is actually a pure compound (it will be shown that there are at least two separate compounds **1** and what is referred to as product **2** that are being formed during the synthesis). This conclusion is supported by the appearance of both blue and brown powder in the crystallization tubes during some of the crystallization attempts reported in Table 2.1. Despite these difficulties, crystals of **1** were grown on three separate occasions (though only a few crystals were harvested each time and only single crystal X-ray data was gathered each time). The recent discovery of a direct synthesis for **2** will also enable identification of **2** which is proposed to be a kinetic product on the way to **1**, the thermodynamic product. (It should be noted that attempts to reflux the reaction mixture during the synthesis of **1** still yielded mixtures of **1** and **2**).

Single Crystal X-ray Diffraction Studies

Single crystal X-ray studies revealed that the crystals of **1** crystallize in the space group *P-1*. Crystallographic parameters are listed in Table 2.3. The structure consists of eight copper atoms bound to six bmtz ligands forming a rectangular prism (Figure 2.4). Each copper atom is bound to two bmtz ligands in a pseudo-tetrahedral environment with N-Cu-N angles between 80.47° and 82.25° (109.5° ideal). The four μ^2-bound bmtz ligands are distorted to accommodate binding to the copper centers (Figure 2.5). Two of the six anions are located over the tetrazine rings of the μ^4-bound bmtz ligands, while the other four are located over the pyrimidine rings of the μ^2-bound bmtz ligands (Figure 2.6). The six solvent molecules are located in the crystal interstices and do not appear to interact with the cluster. All of the anions and solvent molecules are related by the inversion center located in the center of the cluster.

Intramolecular π-π interactions dominate the cluster and intermolecular π-π (Figure 2.7, Table 2.4a), anion-π (Figure 2.6, Table 2.4b) and carbon based hydrogen bonding (Figure 2.8, Table 2.4b) interactions regulate the crystal packing. There are two distinct cases of π-π stacking occurring: one case exhibits substantial overlap (two of the three rings of the bmtz ligand interacting with the equivalent ligand in the next cluster over (Figure 2.7b)) and the second case exhibits minimal π-π interactions (only two atoms of a pyrimidine ring interacting with the equivalent atoms in the next cluster (Figure 2.7c)). Distances observed for all of the π-π interactions observed in the previously reported range for metal complexed pyridine-pyridine interactions (3.4-3.8 Å).[94]

Table 2.3. Crystallographic data and structural refinement parameters for compound **1**.

	$[Cu_8(bmtz)_6][BF_4]_6 \cdot 6MeCN$
chemical formula	$C_{72}H_{54}N_{54}B_6F_{24}Cu_8$
asymmetric unit formula	$C_{36}H_{27}N_{27}B_3F_{12}Cu_4$
formula weight	2704.78
space group	*P-1* (No. 2)
A	13.628 (2) Å
B	15.175 (2) Å
C	15.460 (2) Å
A	113.922 (2)°
B	115.585 (2)°
Γ	93.858 (2)°
Volume	2519.6 (6) $Å^3$
Z	2
Temperature	110 K
density (calc)	1.7823 g/cm^3
abs coeff (μ)	1.788 mm^{-1}
crystal color and habit	brown block
crystal size (mm^3)	0.28 × 0.27 × 0.23
Radiation	Mo Kα, 0.71073 Å
θ range	1.54-28.27°
reflections collected	24047 [R_{int} = 0.0314]
data/parameters/restraints	11537/742/0
R_1	0.0498
wR_2	0.1353
GOF (F^2)	1.026
max./min. residual densities ($e \cdot Å^{-3}$)	1.306, -0.620

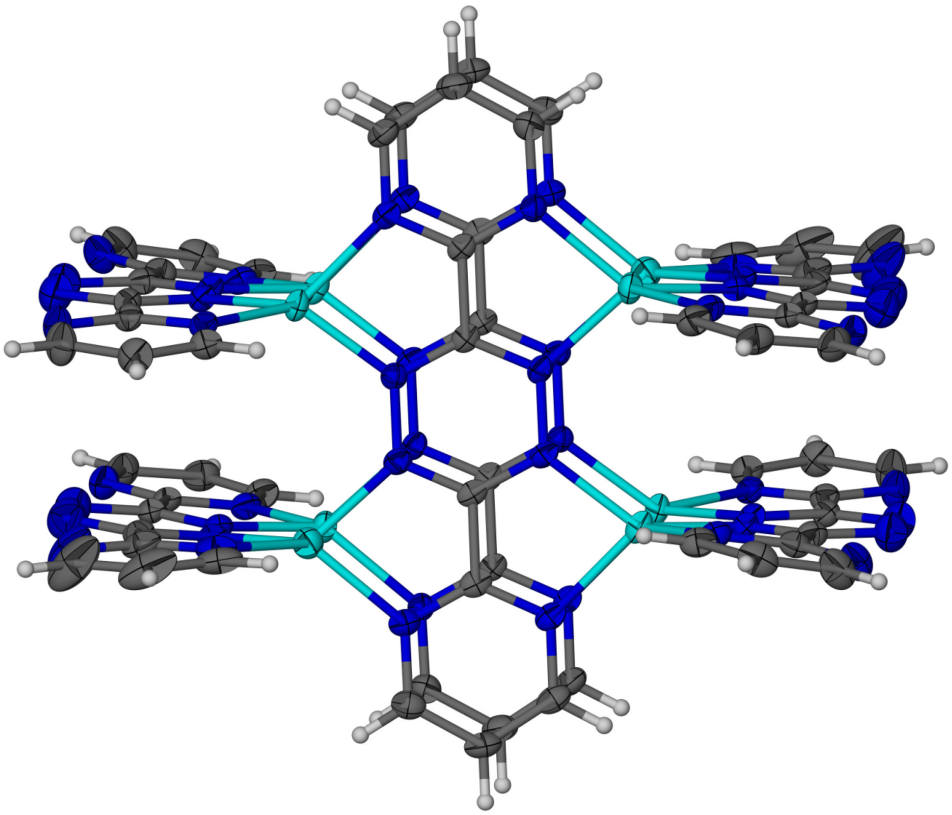

Figure. 2.4. Thermal ellipsoid plot of $[Cu_8(bmtz)_6][BF_4]_6 \cdot 6$ MeCN (**1**) drawn at the 50% probability level. Hydrogen atoms are in calculated positions. Anions and solvent molecules omitted for clarity. Copper atoms (teal), carbon atoms (black), nitrogen atoms (blue), hydrogen atoms (gray).

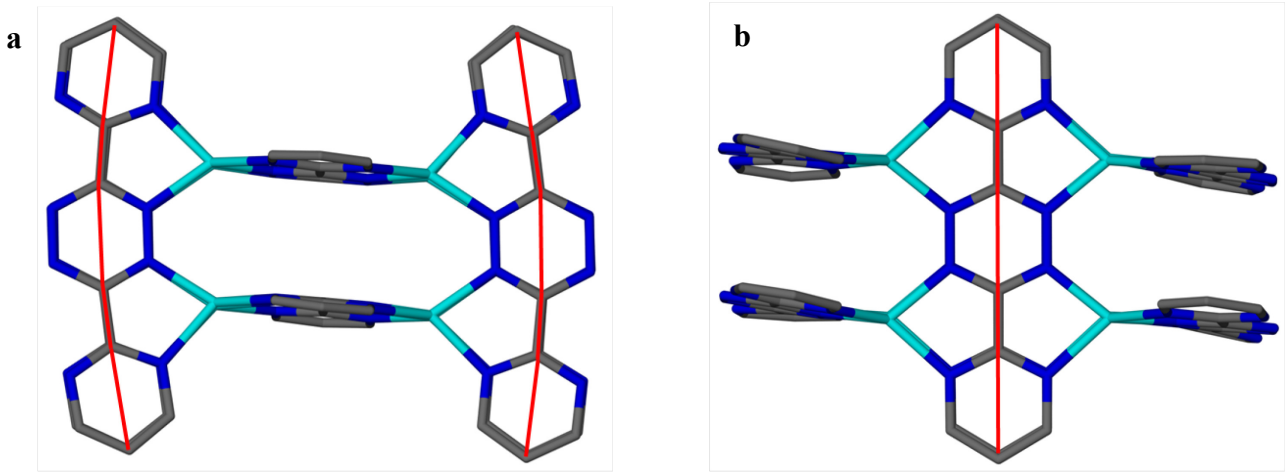

Figure 2.5. Depiction of the structure of **1** with the μ^2 bound bmtz ligands in the plane of the paper (**a**). Crystal structure of **1** with the μ^4 bound bmtz ligands in the plane of the paper (**b**). The red lines are added to depict the curvature of the ligand (they are straight lines between the respective carbon atoms). Copper atoms (teal), carbon atoms (black), nitrogen atoms (blue).

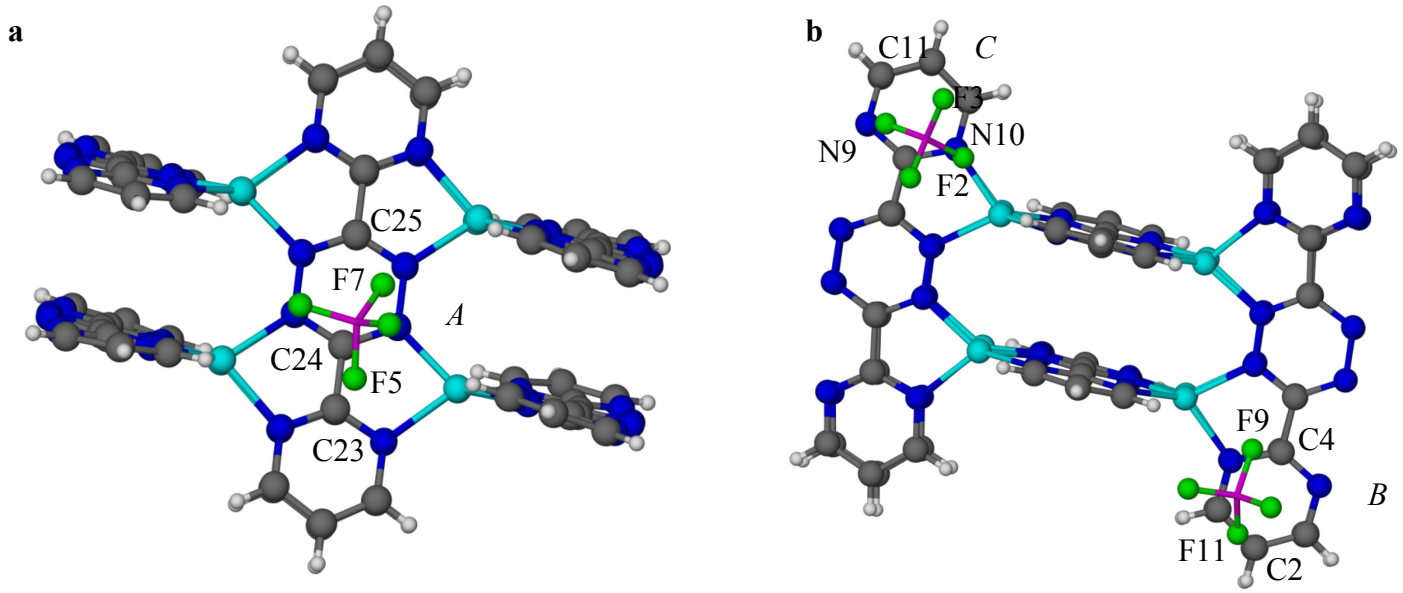

Figure 2.6. View of the structure of **1** showing the position of one of the $[BF_4]^-$ anions (*A*) over the tetrazine rings of the μ^4 bound bmtz (**a**). View of **1** showing the position of two of the $[BF_4]^-$ anions (*B*,*C*) over the pyrimidine rings of the μ^2 bound bmtz (**b**). These three anions are related to the other three anions through an inversion center in the center of the cluster. Copper atoms (teal), carbon atoms (black), nitrogen atoms (blue), hydrogen atoms (gray), phosphorus atoms (pink), fluorine atoms (green).

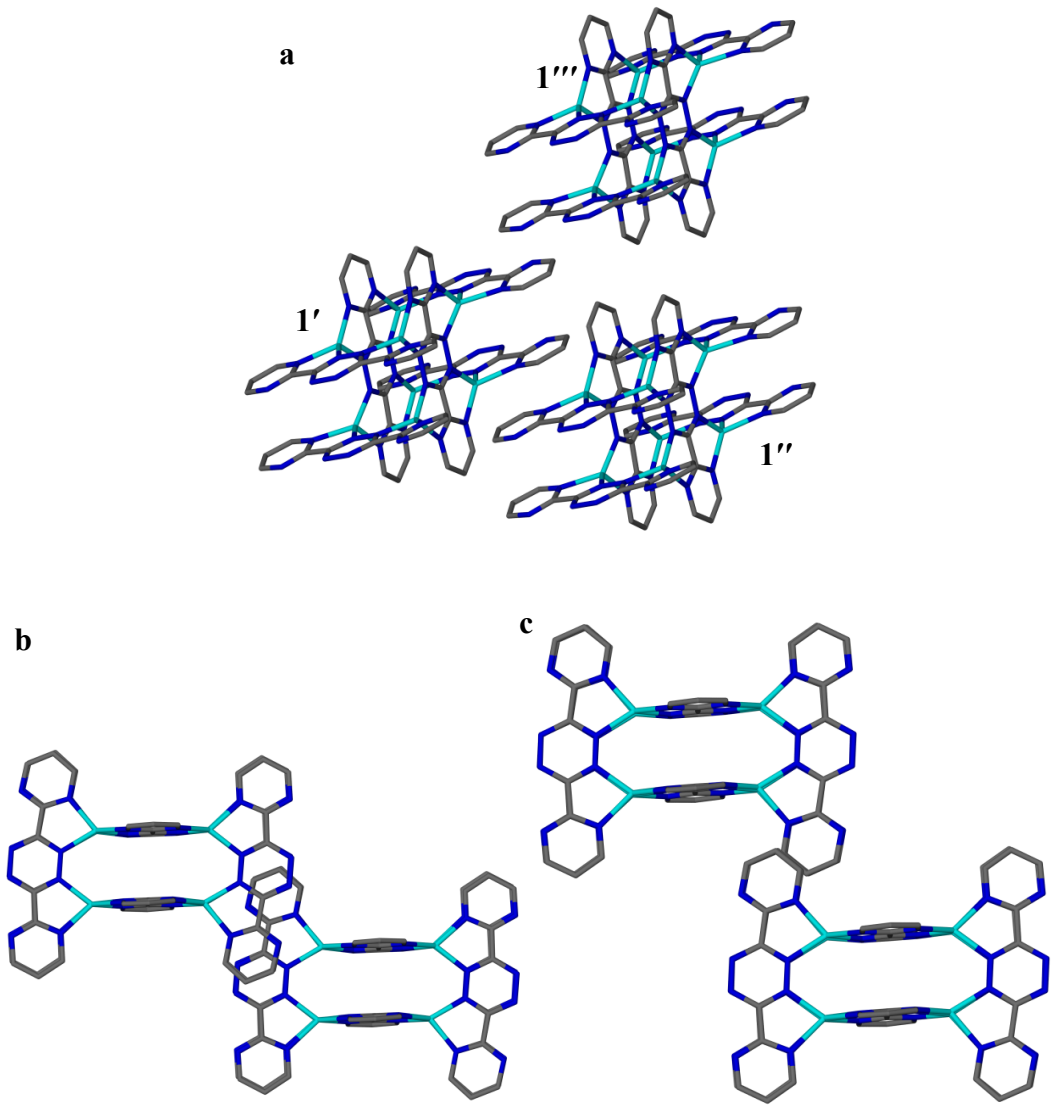

Figure 2.7. Packing diagrams demonstrating the intermolecular π-π interactions in the crystal structure of **1** (**a**). Clusters **1′** and **1″** (**b**) exhibit substantial stacking. Clusters **1′** and **1‴** (**c**) exhibit virtually no stacking. Copper atoms (teal), carbon atoms (gray), nitrogen atoms (blue).

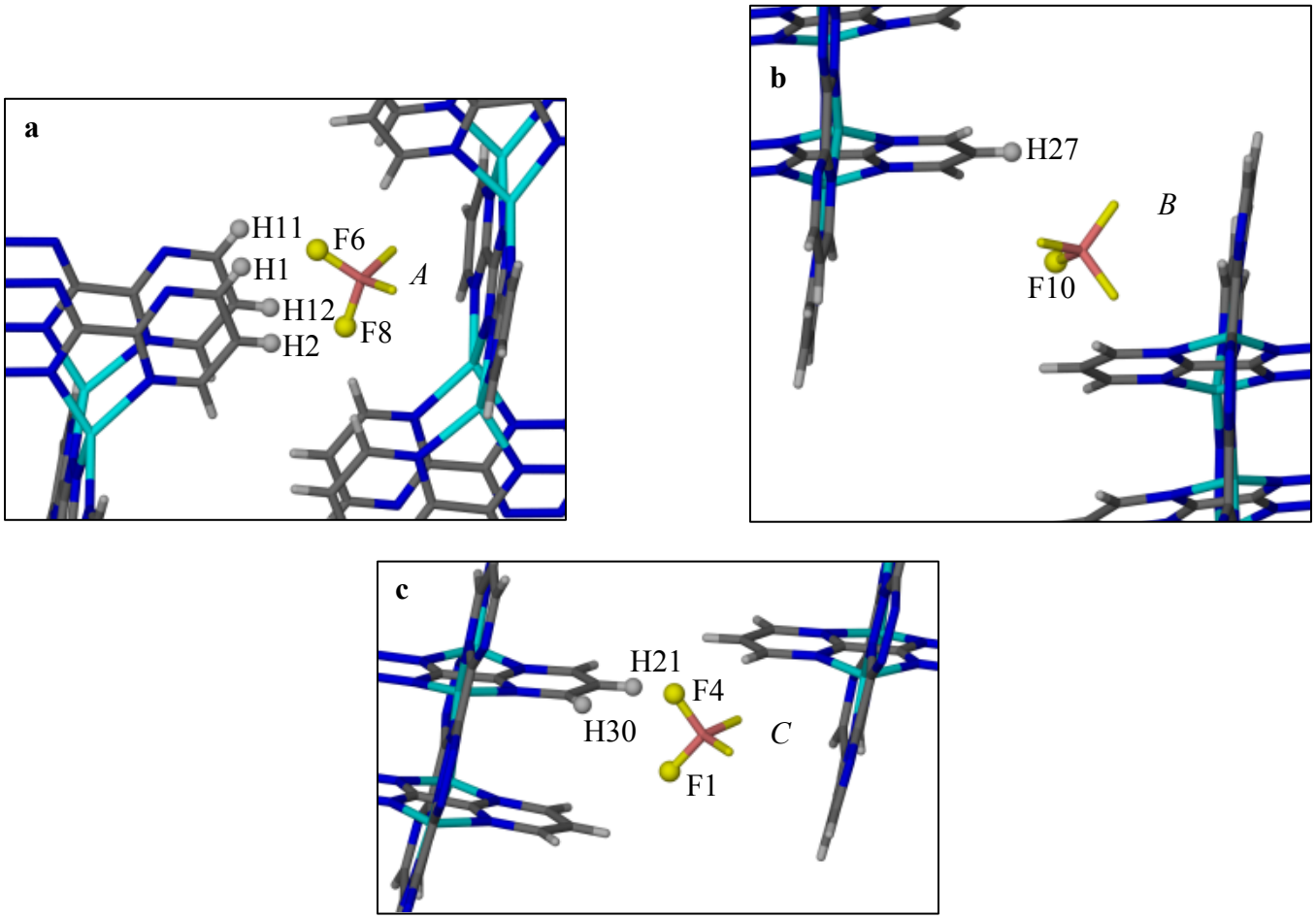

Figure 2.8. Packing diagrams depicting the $[BF_4]^-$ anions engaging in both anion-π (cluster on the right) and carbon based hydrogen bonding (cluster on the left). The interactions involving anions *A* (**a**), *B* (**b**) and *C* (**c**) are shown. Refer to Figure 2.6 for anion labels. Atoms engaging in hydrogen bonding interactions are shown as spheres. Copper atoms (teal), carbon atoms (black), nitrogen atoms (blue), hydrogen atoms (gray), phosphorus atoms (pink), fluorine atoms (yellow).

Table 2.4a. Distances observed for π-π stacking interactions. (Sum of the van der Waals radii for pertinent atoms: C+C: 3.40 Å, C+N: 3.25 Å, N+N: 3.10 Å.[95])

	Rings Involved	Distance(s) (Å)
Intramolecular	tetrazine (μ^4) - tetrazine (μ^4)	3.27
	pyrimidine (μ^4) - pyrimidine (μ^4)	3.44 - 3.80
	tetrazine (μ^2) - tetrazine (μ^2)	3.77 - 3.79
	pyrimidine (μ^2) - pyrimidine (μ^2)	3.48 - 3.71
Intermolecular	tetrazine (μ^4) - pyrmidine (μ^2)*	3.513 - 3.613
	pyrimidine (μ^2) - pyrmidine (μ^2)†	3.456

*Refer to Figure 2.7b.
†Refer to Figure 2.7c.

Table 2.4b. Distances observed for anion-π and carbon based hydrogen bonding interactions. (Sum of the van der Waals radii for pertinent atoms: F+C: 3.05 Å, F+N: 2.90 Å, F+H: 2.65 Å.[95])

	Anion Location*	Atoms†	Distance (Å)
Anion-π Interaction	tetrazine (μ^4) (*A*)	F5 - C23	2.824
		F5 - C24	3.006
		F7 - C25	3.067
	pyrimidine (μ^2) (*B*)	F9 - C4	3.054
		F11 - C2	3.439
	pyrimidine (μ^2) (*C*)	F2 - N10	3.102
		F3 - N9	3.242
		F3 - C11	3.191
CH – bonding	tetrazine (μ^4) (*A*)	F6 - H1	2.615
		F6 - H2	2.691
		F6 - H11	2.657
		F8 - H2	2.459
		F8 - H12	2.590
	pyrimidine (μ^2) (*B*)	F10 - H27	2.868
	pyrimidine (μ^2) (*C*)	F1 - H21	2.864
		F1 - H30	2.877
		F4 - H21	2.616
		F4 - H30	2.470

*Refer to Figure 2.6.
†Refer to Figures 2.6 and 2.8.

Four of the pyrimidine rings that do not participate in π-π interactions are in contact with four $[BF_4]^-$ anions (*B* and *C* as shown in Figure 2.6). The resulting anion-π interactions are near or slightly longer than the sum of the van der Waals radii of a carbon and fluorine atom (3.05 Å[95]) (Table 2.4b), indicating a weak interaction. It is interesting to note that the anions over the tetrazine rings of the μ^4-bound bmtz molecules (*A* as shown in Figure 2.6) are oriented such that the fluorine atoms of the tetrafluoroborate are directed towards the electropositive carbon atoms of the bmtz. A similar orientation is observed in two of the anions (*B*) located over the peripheral pyrimidine rings (μ^2-bound bmtz molecules), while the other two anions are oriented such that the fluorine atoms are oriented toward the two nitrogen atoms (*C)*. As expected, the anions in close-contact with the nitrogen atoms are further away than those in close-contact with the carbon atoms (Table 2.4b). In fact the *C* anions are far enough away from the pyrimidine ring that it would be unreasonable to label them as forming an anion-π interaction.

The $[BF_4]^-$ fluorine atoms that are not engaged in anion-π interactions are involved in weak hydrogen bonding interactions with the pyrimidine hydrogen atoms in the neighboring clusters. For the anions *A* and *C* (Figure 2.8), the distances between the fluorine atoms and hydrogen atoms are reasonable for an H···F interaction,[96-100] but anion *B* is not close enough to the next cluster to participate in hydrogen bonding. While some of the distances observed between anions *A* and *C* are less than 2.65 Å (the sum of the van der Waals radii for H+F and a cutoff for H-bonding interactions[96-97]), previously reported CH···F interactions (2.25-2.54 Å)[98] do tend to be shorter than most of the

distances observed in **1**. One possible explanation for this length could be the non-linear relationship between CH···F interaction (Figure 2.8). The borderline distances and non-linear relationship underscore the weakness of these H-bonding interactions. Cluster **1′′′**, as shown in Figure 2.7, is actually interacting with cluster **1′** through both *π*-*π* interactions and anion *C*.) (The packing diagram for the crystal, as seen along the **b** axis is depicted in Figure 2.9.)

Mass Spectrometry

ESI-MS for the dark powder isolated from **1** and the blue powder isolated from **2** revealed the presence of a peak at *m/z* = 342.0 (Figure 2.10a) which corresponds to the fragment $[Cu(bmtz)(NCMe)]^{+}$. The isotopic distribution for this peak is characteristic for copper and along with the obvious color change in the reaction confirms the presence of a copper-bmtz species.

Interestingly, ESI-MS also reveals two other peaks in some samples at *m/z* = 266.1 (Figure 2.10c) and *m/z* = 385.1 which correspond to the species $[Fe(bmtz)_2]^{2+}$ and $[Fe(bmtz)_3]^{2+}$, respectively. The most likely source of the iron contamination is the metal cannula used during the original reaction. The employment of a Teflon cannula eliminated these two peaks.

Electron Paramagnetic Resonance Spectroscopy

EPR spectroscopy on **2** revealed a signal at *g* = 2.022 (Figure 2.11). The breadth observed in the EPR signal could be an indication of partial delocalization of the unpaired electron between the copper center and the bmtz ligand. The position of the signal is intermediate between the *g* = 2.0040 of a bmtz radical (X-band EPR)[81] and the

previously reported values for copper(II), $g_{\perp}$= 2.057 and a $g_{\parallel}$= 2.223 (Q-band EPR).[101] Given the dark blue color of the sample, and the position of the EPR signal, it is reasonable to assume that the compound **2** contains a Cu(II) center. At X-band frequencies these two signals for copper(II) can overlap,[101] which may explain why a second signal is not observed for copper(II). No separate signal was observed at g = 2.0040 for the bmtz based radical giving further support to the idea of delocalization.

Magnetic Susceptibility Measurements

Magnetic susceptibility measurements were performed on a sample of **2** (Figure 2.12). Positive values observed in the $\chi_g T$ plot demonstrate that the sample is paramagnetic providing further evidence that a redox reaction is taking place. The actual identify of **2** has not yet been ascertained, so no definite assignments can be made.

Discussion

The pseudo tetrahedral environment of the copper atoms in the cluster indicate that in **1** the copper atoms can be assigned as copper(I).[95] While this assignment places the cluster at an 8+ charge, there are only six counter-anions in the unit cell. The remaining two electrons are assigned to coordinated bmtz molecules. Support for this assignment is found in the tetrazine N-N distances of the μ^4-bound bmtz ligands. These are similar to those reported by Glöckle, *et al*. for the compound {(bmtz)[Cu(PPh_3)$_2$]$_2$}[BF_4] which contains a bmtz radical anion (Table 2.5).[81] The deformation of the μ^2-bound bmtz ligands prevents an accurate assessment of their

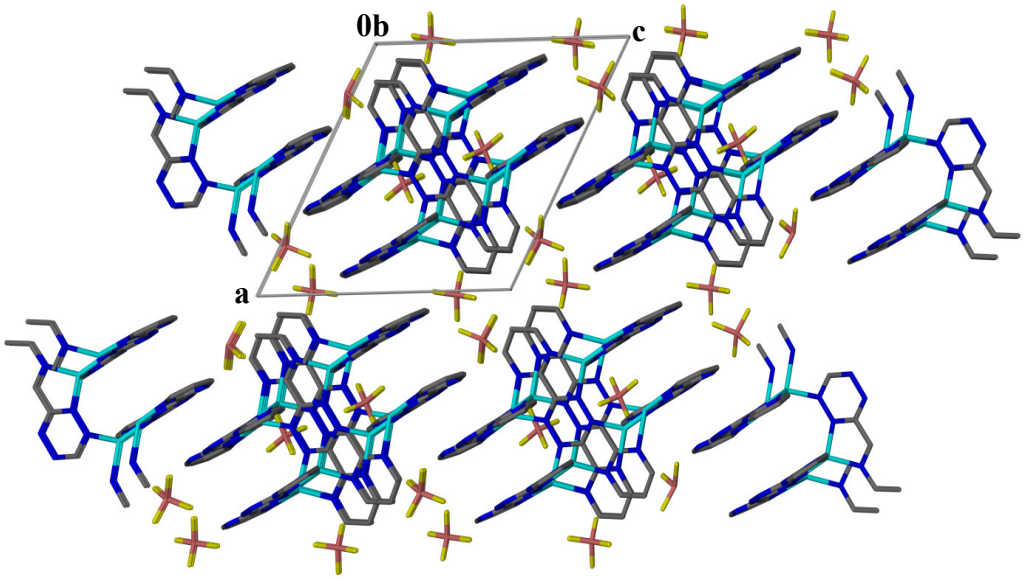

Figure 2.9. Packing diagram for **1** as viewed along the **b** axis. Hydrogen atoms and solvent molecules were omitted for the sake of clarity. Copper atoms (teal), carbon atoms (gray), nitrogen atoms (blue), phosphorus atoms (pink), fluorine atoms (yellow).

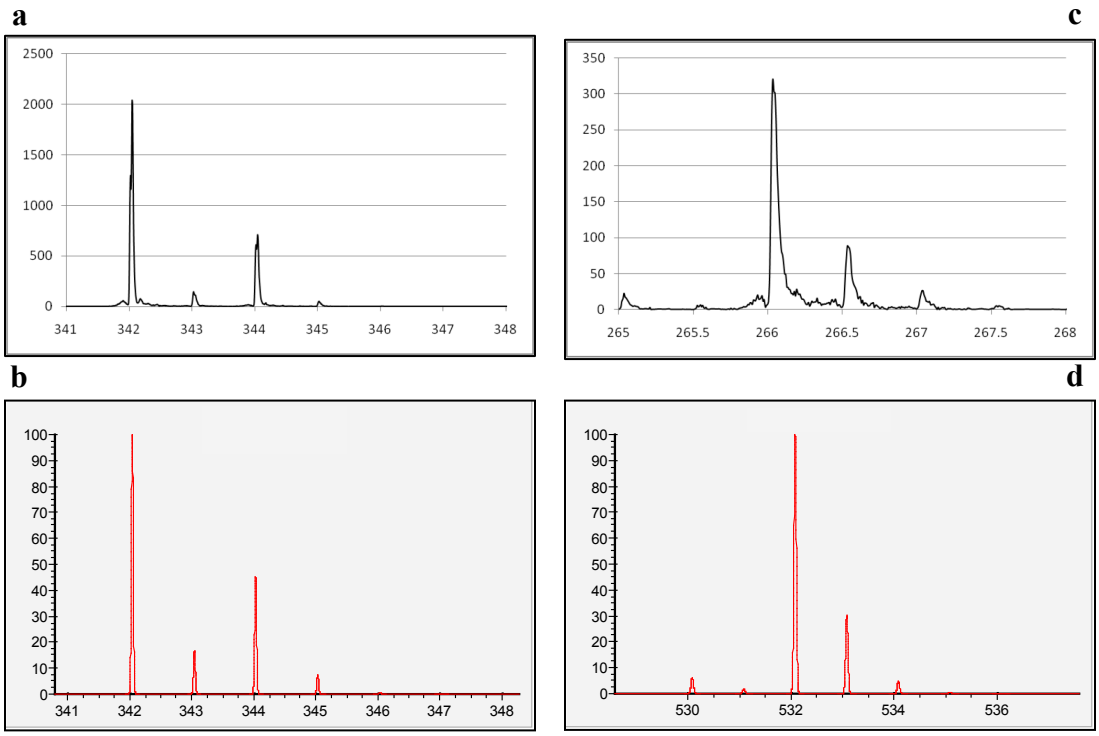

Figure 2.10. Mass spectrum showing $[Cu(bmtz)(NCMe)]^{+}$ (**a**) as observed in either a mixture of **1** and **2** or in samples of **2** and the corresponding calculated spectrum (**b**). The spectrum for $[Fe(bmtz)_2]^{2+}$ as observed in the mixture of **1** and **2** is also shown (**c**) along with the corresponding calculated spectrum (**d**). The calculated images were generated by IsoPro 3.0, which assumes all species to carry a +1 charge.

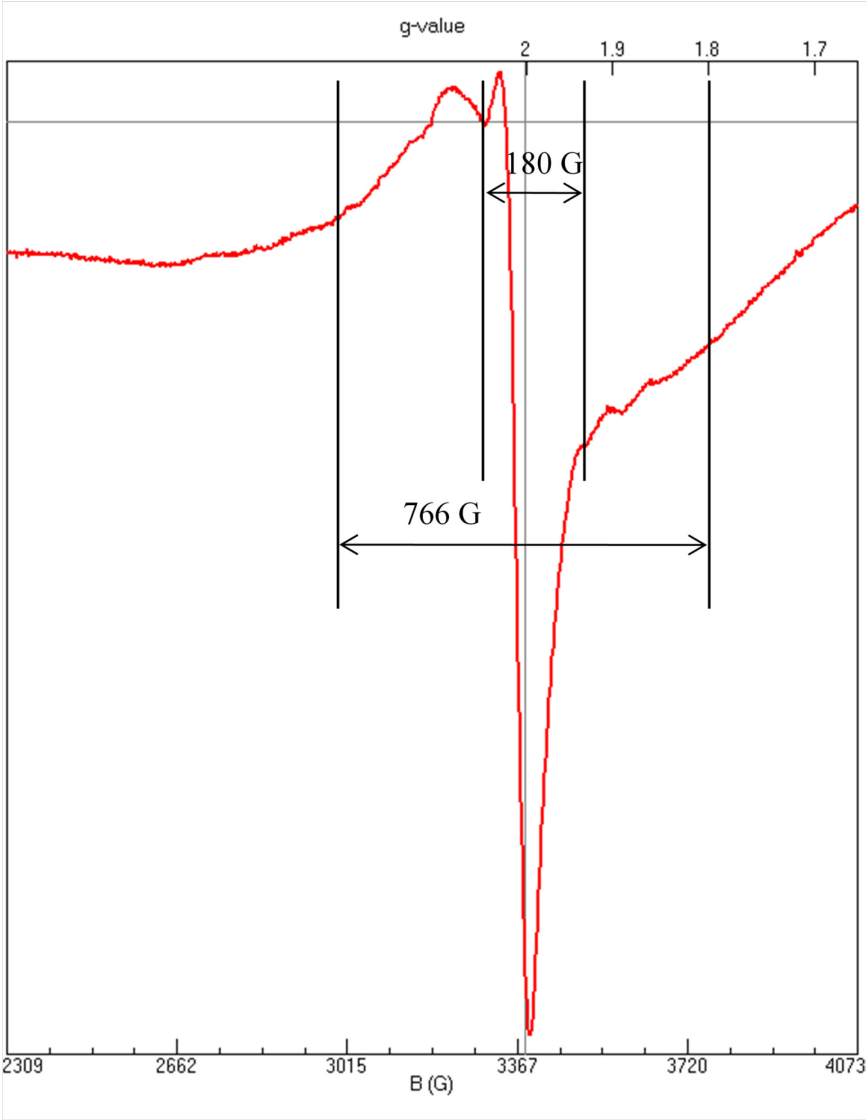

Figure 2.11. EPR spectrum for a sample of **2** performed in the solid state at 4 K.

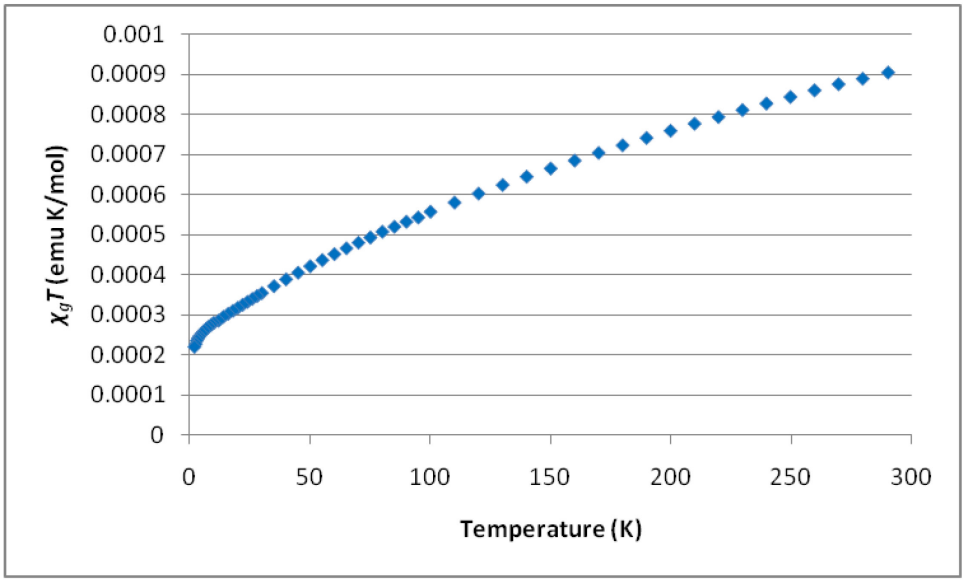

Figure 2.12. Thermal variation of the $\chi_g T$ product for the compound 2.

oxidation state by bond distances, although the N-N distances for the nitrogen atoms bound to the copper atoms are similar to those observed for neutral bmtz (Table 2.5). Since bmtz is introduced as a neutral molecule, the reduction of the ligand must occur *in situ*. The paramagnetic response observed in the magnetic susceptibility measurement and the EPR spectrum indicate the presence of unpaired electron density in **2**. The initial reaction (for either **1** or **2**) is carried out by mixing a copper(I) salt (a d^{10} metal ion) and neutral bmtz, neither of which possesses any unpaired electrons. The intense blue color of compound **2** implies that Cu(II) may be present,[95] and the fact that it is paramagnetic is clear support for the fact that a redox reaction is occurring.

The extensive conjugation of the bmtz molecule and possibility for Cu-bmtz $d\pi$-$p\pi$ interactions in **1** could lead to the delocalization of unpaired electrons throughout the entire cluster. It is also possible for cluster **1** to possess several oxidation states, ranging from $\mathbf{1}^{2+}$ to $\mathbf{1}^{8+}$ corresponding to varying numbers of reduced bmtz ligands. Since no known sample of high purity has been collected in sufficient quantities, cyclic voltammetry will not be reported. It should also be noted that the samples show low solubility in acetonitrile and dichloromethane.

Cluster **1** exhibits an interesting geometry that is reminiscent of the 2x2 grid complexes $[Ag_4(bppn)_4][SbF_6]_4$ (Figure 2.3c)[65] and $[Cu_4(bppn)_4][CF_3SO_3]_4$ (Figure 2.13).[102] The rectangular prism observed in **1** can be thought of as two 2x2 grids fused together in an "extended" cluster taking full advantage of the four binding sites on the bmtz ligand (as opposed to bppn). Exclusion of any type of capping ligand on the

Table 2.5. Comparison of the tetrazine N-N distances for bmtz$^{0/-1/-2}$ and compound **1**.

Compound	d_{N-N} (Å)	d_{Cu-N} (Å)	Charge on bmtz
*bmtz	1.33	-----	0
*{(bmtz)[Cu(PPh$_3$)$_2$]$_2$}$^+$	1.38	1.99, 2.13	-1
*{(H$_2$bmtz)[Cu(PPh$_3$)$_2$]$_2$}$^{2+}$	1.42, 1.43	2.07, 2.16	-2†
[Cu$_8$(bmtz)$_6$]$^{6+}$	1.39, 1.40 (μ^4 bmtz)	1.99 , 1.99	-1
	1.34, 1.34, 1.99, 1.99 (μ^2 bmtz)	2.05, 2.05	N/A

*Data taken from Glöckle, *et al.*[81]
†H$_2$bmtz is considered to be a reasonable model for [bmtz]$^{2-}$

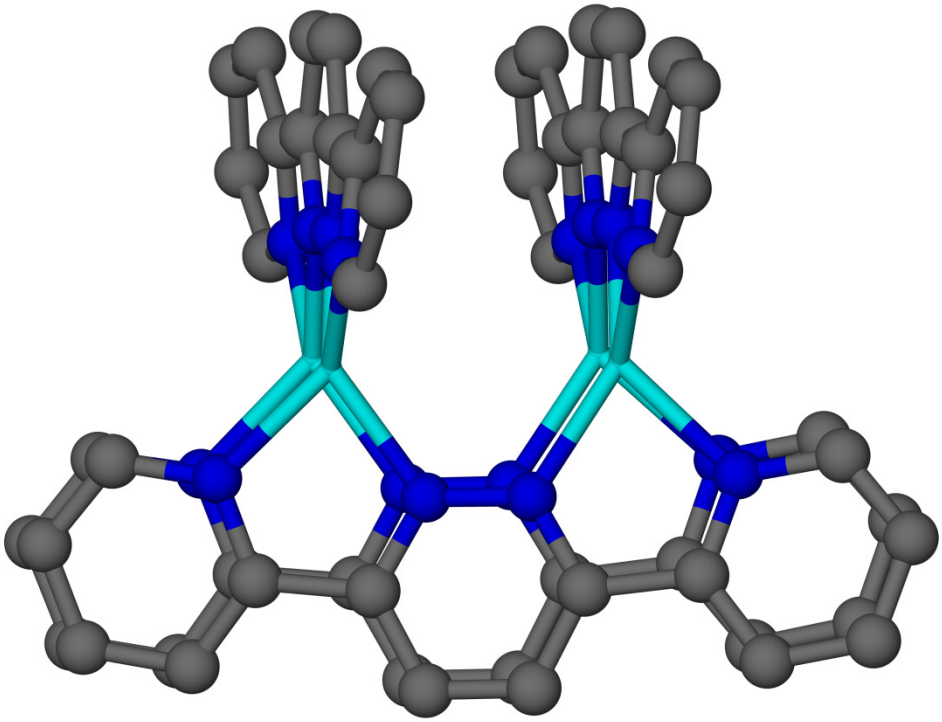

Figure 2.13. Crystal structures of the $[Cu_4(bppn)_4]^{4+}$ cation.

copper atoms, as opposed to the approach of Göckle, *et al*., allows the cluster to expand to nuclearity eight.

Conclusions

An improved synthesis for the molecules H_2bmtz and bmtz has been developed as part of our goal to investigate the molecule bmtz as a ligand capable of forming anion-π interactions similar to those observed in previous[64-65] and ongoing investigations of the ligand bptz. As a part of these investigations a new, unprecedented copper-bmtz complex, **1**, has been synthesized. X-ray data indicate that **1** contains two unpaired electrons that are associated with the bmtz ligands, but possibly delocalized across the entire cluster. As expected for the bmtz ligand, anion-π interactions are observed between the $[BF_4]^-$ anions and both the tetrazine and pyrimidine rings of the ligand. While **1** does not exhibit evidence for anion-π templation, in that there is no encapsulation of anions, further work is warranted given the possibilities for rich electrochemistry for this unique cluster. A second product, a blue species referred to as compound **2**, was also synthesized and has been shown to be paramagnetic with the EPR data indicating some copper(II) character; this material has not yet been identified and further studies will have to be performed.

CHAPTER III

COMPUTATIONAL INVESTIGATION OF THE ANION-PI INTERACTIONS BETWEEN COMPLEX ANIONS AND OLEFINS

Introduction

Anion-π interactions generally refer to the noncovalent interactions between an anion and an aromatic ring. This description completely overlooks the potential for anion-π interactions in non-aromatic, conjugated structures; olefins. There have been only a few reports dealing with this topic, specifically the work of Kim, *et al*.[56] and Rosokha, *et al*.[103]

Kim, *et al*. reported a series of computations exploring the anion-π interactions between three different types of π-systems: olefinic (tetrafluoroethylene), aromatic (hexafluorobenzne) and heteroaromatic (1,3,5-triazine). It was shown that these molecules could interact attractively not only with halides, but with cyanide, nitrate and carbonate anions as well.[56]

Experimental work by Rosokha, *et al*. demonstrated, in both solution and solid state, what are considered to be π-type charge-transfer (CT) complexes between a variety of molecules (including tetracyanoethylene (TCNE), *p*-chloranil and *o*-chloranil) and chloride, bromide and iodide anions.[103] Of particular interest is the UV/visible spectroscopic evidence for the CT between the bromide anion and TCNE. This interaction was also observed crystallographically. Subsequent reports have

demonstrated that these type of halogen-π donor-acceptor complexes[104] could be used to create molecular wires.[105-106]

A new series of computational studies was undertaken to explore the possibility of anion-π interactions between complex anions (tetrafluoroborate ($[BF_4]^-$) and hexafluorophosphate ($[PF_6]^-$) and a series of olefins. The olefins selected for this study include the aforementioned TCNE, as well as 7,7,8,8-tetracyanoquinodimethane (TCNQ), 7,7,8,8-tetracyano-1,2,4,5-tetrafluoroquinodimethane ($TCNQF_4$) and octacyanoquinodimethane ($TCNQ(CN)_4$) (Scheme 3.1).

Methods

Geometry Optimizations

All systems studied were optimized using two different methods. Density functional theory (DFT),[87] as contained in the Gaussian03[88] program suite, was employed using the Becke3 parameter hybrid exchange functional[89] and the Lee-Yang-Parr correlation function[90] (B3LYP). The second order Møller-Plesset perturbation theory (MP2),[107-108] as contained in the Gaussian03 program suite, was also employed as an *ab initio* method. Both methods were used with a Pople style double-ζ basis set with an optimized d-polarization function (6-31+G(d′)).[109]

For a given olefin-anion pair, each geometry optimization was performed three times beginning with three different starting geometries (Figure 3.1). In all cases the anion was placed outside of van der Waals contact with the olefin with one of the

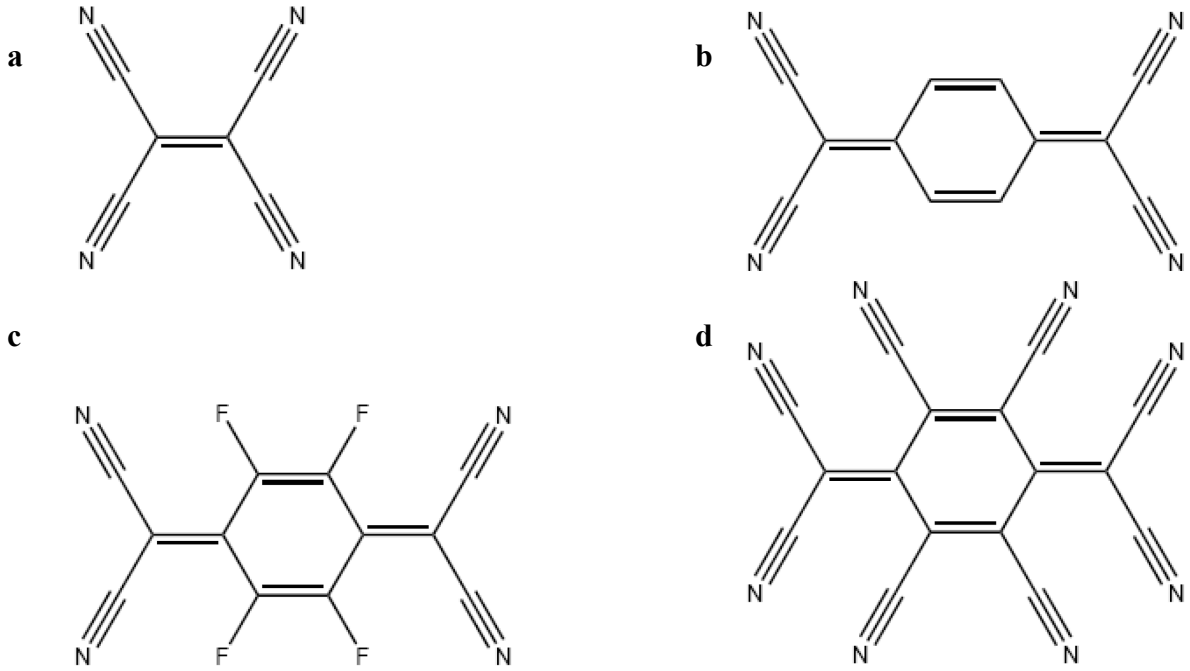

Scheme 3.1. Schematic representations of tetracyanoethylene (TCNE) (**a**), 7,7,8,8-tetracyanoquinodimethane (TCNQ) (**b**), 7,7,8,8-tetracyano-1,2,4,5-tetrafluoroquindodimethane (**c**) and octacyanoquinodimethane ($TCNQ(CN)_4$) (**d**).

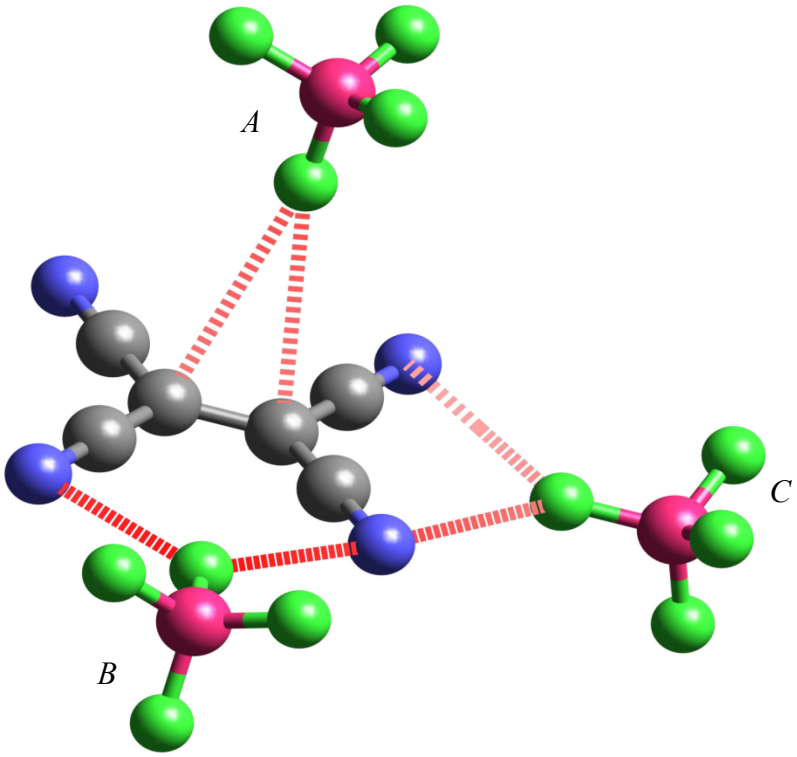

Figure 3.1. Model depicting the three different starting geometries used during both the DFT and MP2 geometry optimizations. Anion *A* is located perpendicular to the plane of the molecule, anion *B* is located in the plane of the molecule aligned with short axis (perpendicular to the C=C bond in the case of TCNE) and anion *C* is located in the plane of the molecule aligned with the long axis (along the C=C bond in the case of TCNE). Carbon atoms (gray), nitrogen atoms (blue), boron atoms (pink), fluorine atoms (green).

fluorine atoms directed toward the olefin. The lowest energy structure resulting from these three optimizations was used in all subsequent computations.

Additional geometry optimizations were performed on select systems employing B3LYP with a Pople style triple-ζ basis set with an optimized p and d-polarization functions[91-92] (6-311++G(d,p)). The olefins selected for this were TCNQ and $TCNQF_4$ with $[BF_4]^-$ and $[PF_6]^-$. Starting position *B* (Figure 3.1) was used.

Frequency computations were performed on the lowest energy optimization for each olefin-anion pair using B3LYP/6-31+G(d′).

Electrostatic Potential Maps

The electrostatic potential (ESP) maps were generated using Cerius^2 4.8[93] with an isodensity value was set at 0.02. The optimized olefin structures determined by B3LYP/6-31+G(d′) were used.

Atoms in Molecules Computations

Critical point analysis is the result of the Atoms in Molecules (AIM) theory put forward by R. F. W. Bader.[110-111] This theory correlates the critical points in the electron density (*i.e.* maxima, minima and saddle points) to chemical structures. Each of the four types of critical points (CPs) is assigned the notation (ω, σ); the rank (ω) is generally 3 for molecules at or near energetically stable conformations; and the signature (σ) is the sum of the signs of the change in electron density around that point and is indicative of the nature of the critical point.[110] Essentially, as one moves away from a given point along a Cartesian axis in three-dimensional space, the electron density will either increase (+1) or decrease (-1). The sum of *x*, *y*, and *z* terms results in the rank of the

critical point, σ. These ranks can be used to describe atoms (-3), bonds (-1), rings (1) and cages (3).

Critical point analysis was performed on the lowest energy structures for each olefin-anion pair, as determined by DFT, using the AIM 2000 program. The wavefunction file determined by DFT provided the input for AIM 2000.

Natural Bond Orbitals Computations

Natural Bond Orbitals (NBO) computations were performed with GenNBO 5.0W[112] for selected systems. The input files for GenNBO 5.0W were prepared using the internal NBO calculation, in Guassian03, on the previously obtained optimized geometries. All computations using Guassian03 were performed at the same level of theory as the optimizations.

Results

Geometry Optimizations

The geometry optimization starting in position *C* for the *ab initio* optimizations of $TCNQ(CN)_4\cdots[BF_4]^-$, $TCNQX_4\cdots[PF_6]^-$ and $TCNQ(CN)_4\cdots[PF_6]^-$ have not yet converged at the time of this writing (for $TCNQ(CN)_4\cdots[PF_6]^-$, all three starting geometries have not yet converged).

Both the DFT and MP2 results are similar for each system studied. For each olefin, the anion moved from position *A*, *B* or *C* (Figure 3.1) to a position above the centroid of the molecule positioning itself in such a way to maximize contact between the olefin π-system and the anion fluorine atoms (Figures 3.2, 3.3, 3.4, 3.5). In almost

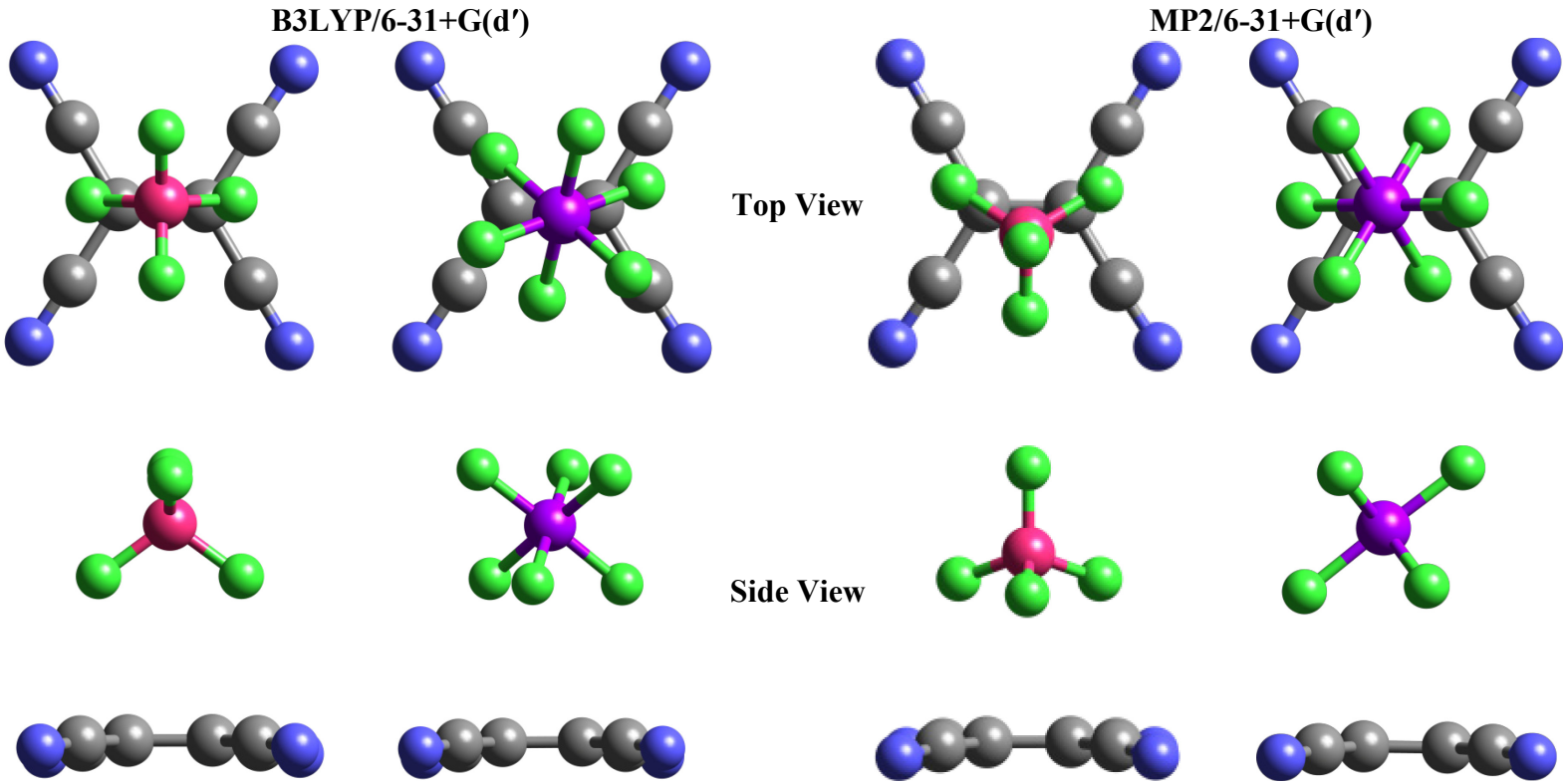

Figure 3.2. Lowest energy geometry optimized structures of TCNE···$[X]^-$ (X = BF_4, PF_6). Structures optimized using B3LYP/6-31+G(d′) are shown on the left and structures optimized using MP2/6-31+G(d′) are shown on the right. Carbon atoms (gray), nitrogen atoms (blue), boron atoms (pink), phosphorus atoms (purple), fluorine atoms (green).

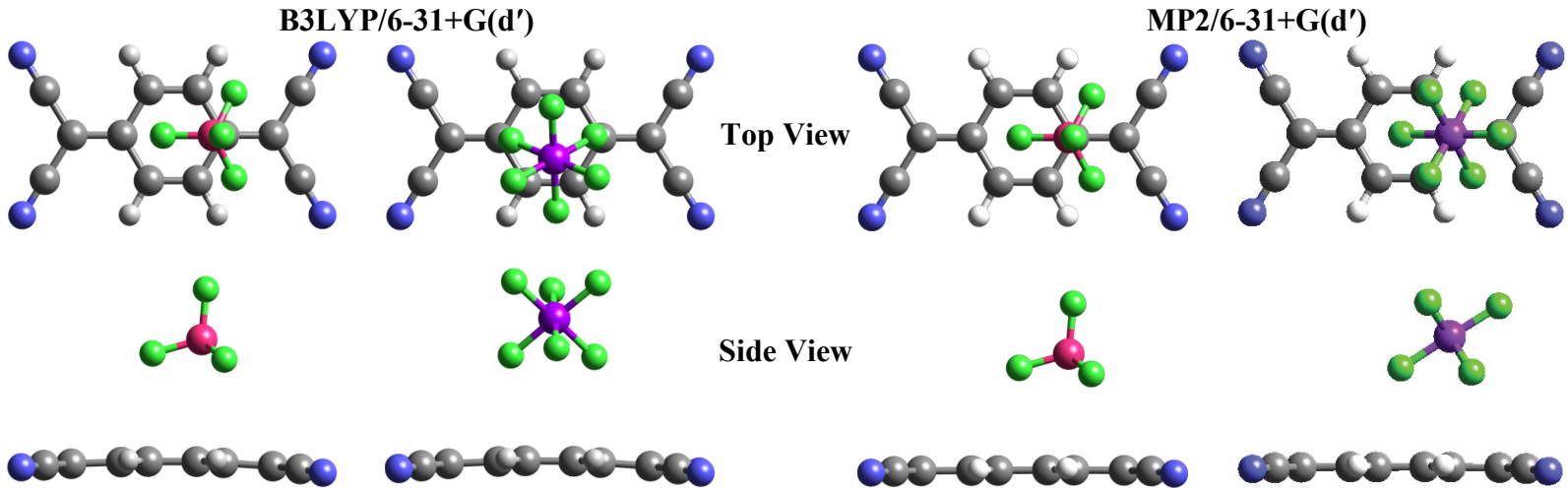

Figure 3.3. Lowest energy geometry optimized structures of TCNQ···$[X]^-$ (X = BF_4, PF_6). Structures optimized using B3LYP/6-31+G(d′) are shown on the left and structures optimized using MP2/6-31+G(d′) are shown on the right. Carbon atoms (gray), nitrogen atoms (blue), hydrogen atoms (white), boron atoms (pink), phosphorus atoms (purple), fluorine atoms (green).

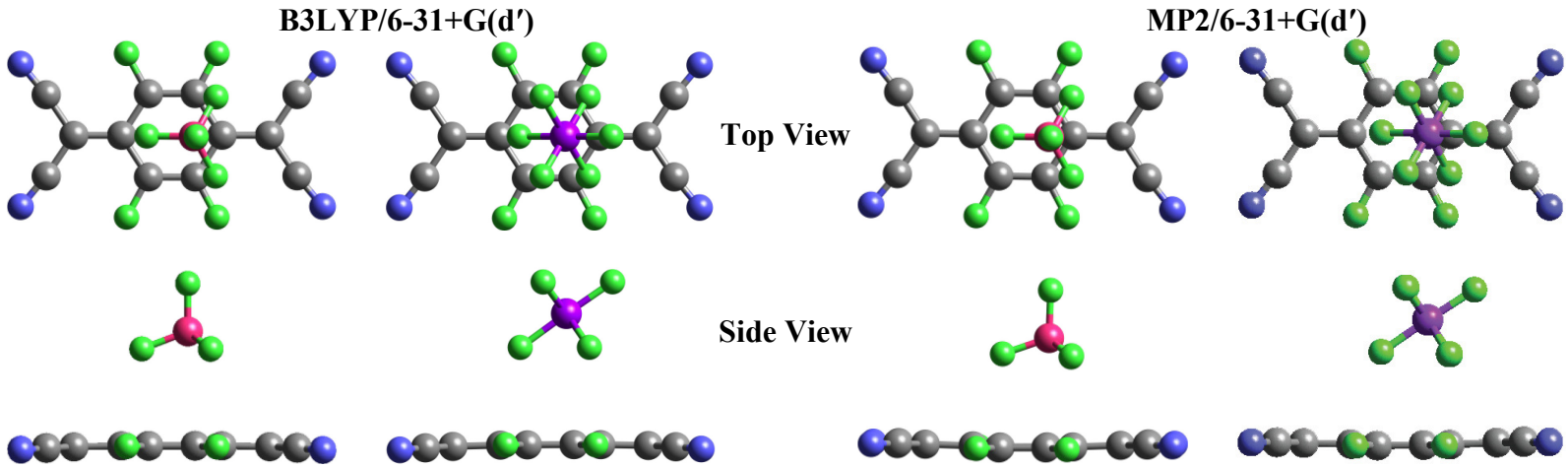

Figure 3.4. Lowest energy geometry optimized structures of $TCNQF_4\cdots[X]^-$ (X = BF_4, PF_6). Structures optimized using B3LYP/6-31+G(d′) are shown on the left and structures optimized using MP2/6-31+G(d′) are shown on the right. Carbon atoms (gray), nitrogen atoms (blue), boron atoms (pink), phosphorus atoms (purple), fluorine atoms (green).

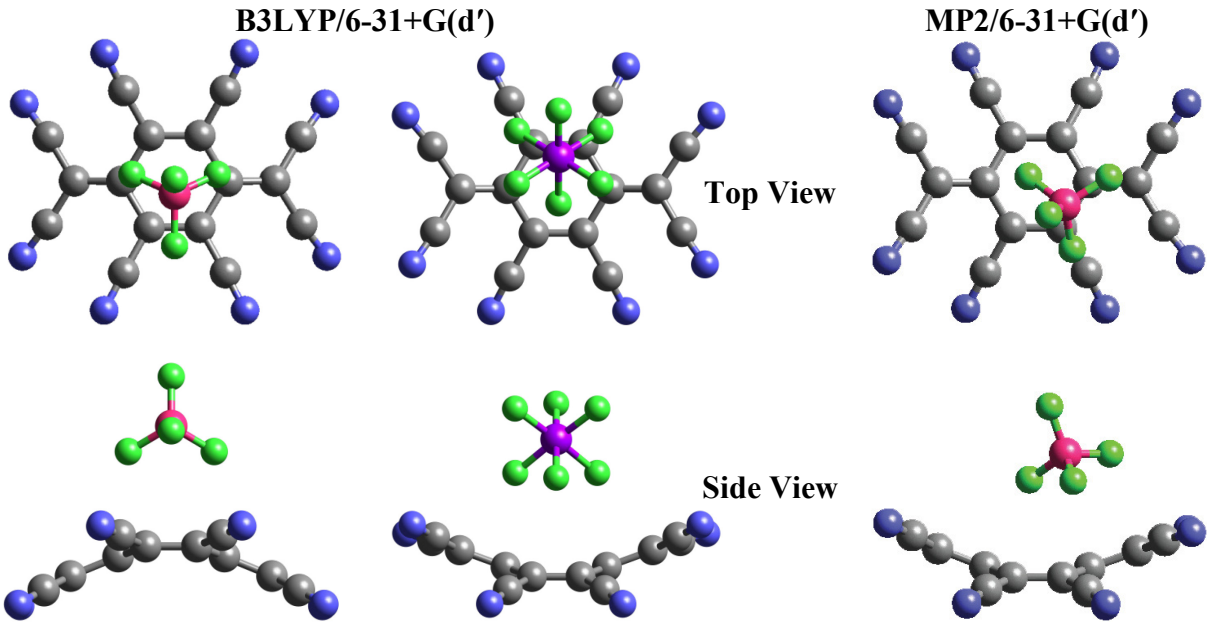

Figure 3.5. Lowest energy geometry optimized structures of $TCNQ(CN)_4\cdots[X]^-$ ($X = BF_4$, PF_6). Structures optimized using B3LYP/6-31+G(d′) are shown on the left and structures optimized using MP2/6-31+G(d′) are shown on the right. No data is presented for the MP2 optimization of $TCNQ(CN)_4\cdots[PF_6]^-$. Carbon atoms (gray), nitrogen atoms (blue), boron atoms (pink), phosphorus atoms (purple), fluorine atoms (green).

all cases the final geometries for the three optimizations were similar in energy. Ignoring the dipodal interaction observed in the DFT optimized geometry of **1a**, the anion adopted a tripodal positioning in all systems. The optimized geometry predicts, in almost all cases, that the anion will be positioned in such a way as to maintain a plane of symmetry, perpendicular to the plane of the olefin, running along either the short or long axis of the olefin. Distances observed between the anion fluorine atoms and the nearest carbon atoms of the olefins (Table 3.1) are well within the sum of the van der Waals radii, 3.05 Å for fluorine and carbon.[95]

The exceptions are in the DFT optimizations of $X\cdots[BF_4]^-$ (X = TCNE, TCNQ), systems **1a** and **2a**, respectively, and the *ab initio* optimization of $TCNQ(CN)_4\cdots[BF_4]^-$, system **4a**. For **1a**, the $[BF_4]^-$ anion adopted a tripodal positioning (similar to the MP2 result shown in Figure 3.2) for two of the three optimized geometries as opposed to the dipodal position shown for DFT in Figure 3.2. The DFT optimized geometries for **2a** were also very different from one another despite having very similar energies (Figure 3.6). This variation exhibited by the $[BF_4]^-$ anion, with respect to TCNQ, suggests that the minimum energy structure found by the DFT optimization is more likely a shallow potential well than a sharp minimum; the $[BF]_4^-$ anion can potentially interact with many points along the planar surface of the TCNQ molecule. The optimized geometry for **4a** further supports this hypothesis in that the lowest energy structure contains an anion positioned over one of the ring bonds, with a fluorine atom interacting with a nitrile group (the other structure solved contains that anion aligned with the short axis as has been previously observed).

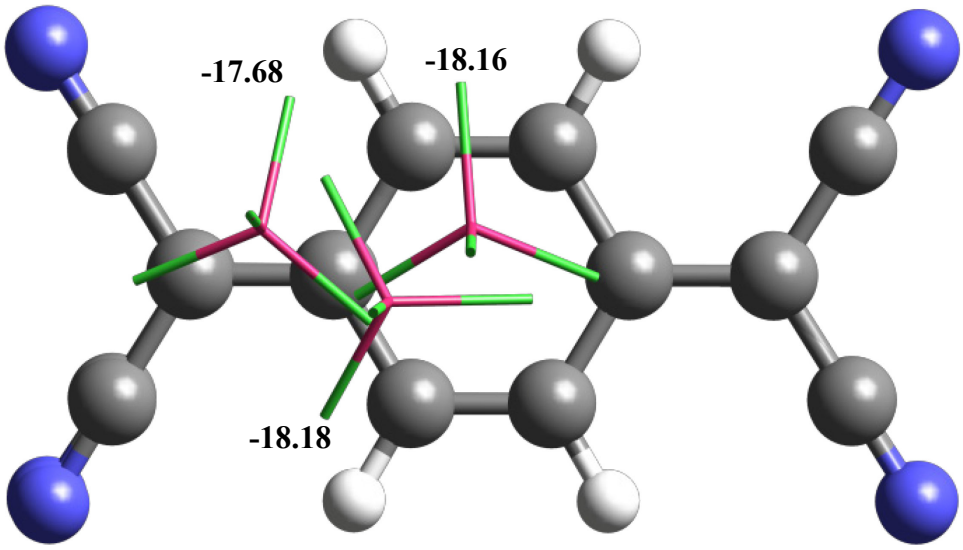

Figure 3.6. Overlaid images of the three geometry optimized structures for TCNQ···$[BF_4]^-$ (**2a**) obtained by DFT computation. Energies of interaction for these three positions are given in kcal/mol. Carbon atoms (gray), nitrogen atoms (blue), hydrogen atoms (white), boron atoms (pink), fluorine atoms (green).

Table 3.1. Results of the DFT and *ab inito* geometry optimizations.

			DFT/B3LYP/6-31+G(d')		MP2/6-31+G(d')	
System	**Olefin**	**Anion**	**d_{F-C} (Å)**	**E_t {H_t} (kcal/mol)**	**d_{F-C} (Å)**	**E_t {H_t} (kcal/mol)**
1a	TCNE	$[BF_4]^-$	2.69	-21.31 {-20.62}	2.71 - 3.01	-25.34
1b	TCNE	$[PF_6]^-$	2.86 - 2.88	-15.03 {-14.06}	2.71 - 2.90	-23.09
2a	TCNQ	$[BF_4]^-$	2.94 - 3.14	-18.18 {-17.07}	2.94 - 3.15	-23.89
2b	TCNQ	$[PF_6]^-$	2.93 - 3.62	-15.29 {-14.29}	2.99 – 3.13*	-22.72*
3a	$TCNQF_4$	$[BF_4]^-$	2.86 - 2.88	-25.69 {-24.38}	2.75 - 2.82	-33.18
3b	$TCNQF_4$	$[PF_6]^-$	2.87 - 2.91	-21.80 {-20.54}	2.75 – 2.83*	-30.85*
4a	$TCNQ(CN)_4$	$[BF_4]^-$	2.83 - 3.19	-37.22 {-34.73}	2.71 – 3.02*	-48.03*
4b	$TCNQ(CN)_4$	$[PF_6]^-$	2.98 - 2.99	-32.49 {-29.47}	------	-----

*These values were obtained by comparing the results of the optimizations with starting geometries *A* and *B* only. For all three systems, the optimization of starting position *C* encountered errors and had to be restarted. As of the time of writing this thesis, those optimizations had not converged. Based on the other

Frequency computations do not reveal the presence of any imaginary frequencies indicating that the minima found by the DFT computations are correct and are not simply local minima. Frequency computations were not performed on the *ab initio* results for reasons of both precedent and practicality. These computations are simply too large for the resources available.

Energies of interaction (E_t) were determined by subtracting from the total energy, the energies of the olefin and anion (Table 3.1). These olefin and anion energies were determined by geometry optimization under B3LYP/6-31+G(d′) and MP2/6-31+G(d′). Frequency computations provided enthalpy correction values for the DFT results, allowing enthalpies of interaction (H_t) to be determined from the E_t (Table 3.1). Basis set superposition error (BSSE), the borrowing of one molecule's basis set functions by a second non-bound molecule,[113] was not corrected. Counterpoise computations, traditionally employed to correct BSSE, are costly computations and are not generally performed with DFT results. While it is common to employ the counterpoise technique with *ab initio* methods, such as MP2, it was decided that they would not be useful in this case since our purpose in determining these E_t values was not to report them as absolute energies but to use them as a qualitative measure of the relative strengths of the interactions between the systems studied.

In order to determine if the hydrogen atoms on TCNQ would interfere with the formation of anion-π interactions by preferentially interacting with the anions, the DFT geometry optimization was repeated for **2a** and **2b** (see Table 3.1 for labels). The basis set 6-311++G(d,p) was employed because of the addition polarization functions on the *p*

orbitals that it provides; these functions will allow for more flexibility for the orbitals on the hydrogen atoms. Geometry optimization was also repeated for **3a** and **3b** to provide a point for comparison. In all four cases, only starting geometry *B* was optimized as it positions the anion near the hydrogen atoms on TCNQ. In all four cases, the anion again moved above the plane of the ring and adopted a similar position to those observed in Figures 3.3 and 3.4. Energies of interaction for these optimizations were more favorable than those reported in the original optimization (Table 3.2) due to the more diffuse basis set.

Electrostatic Potential Maps

ESP maps were generated for DFT geometry optimized structures of TCNE, TCNQ, $TCNQF_4$ and $TCNQ(CN)_4$ (Figure 3.7). The ESP maps reveal that, with the exception of TCNE, all of the carbon atoms are equally electropositive. This uniformity explains the existence of multiple orientations of a single anion over an olefin (Figure 3.6). If none of the carbon atoms is more electropositive than any others, then no preferential alignment of the anion should be observed.

Atoms in Molecules Computations

By using the results of the DFT optimizations, AIM analysis determined localized electron density between the anion fluorine atoms and olefin carbon atoms and identified this density as bond CP (Figure 3.8). Ring and cage CPs are also observed between the anion and olefin in all cases (excluding **1a** and **1b**) adding further support to the existence of electron density between the two species. Average values for this electron density are given in Table 3.3 along with average values for the electron density

Table 3.2. Comparison of the energies of interaction for the DFT optimizations performed with 6-31+G(d′) and 6-311++G(d,p) basis sets.

			6-31+G(d')	**6-311+G(d,p)**
System	**Olefin**	**Anion**	**E_t (kcal/mol)**	**E_t (kcal/mol)**
2a	TCNQ	$[BF_4]^-$	-18.18	-18.94
2b	TCNQ	$[PF_6]^-$	-15.29	-16.14
3a	$TCNQF_4$	$[BF_4]^-$	-25.69	-26.42
3b	$TCNQF_4$	$[PF_6]^-$	-21.80	-22.85

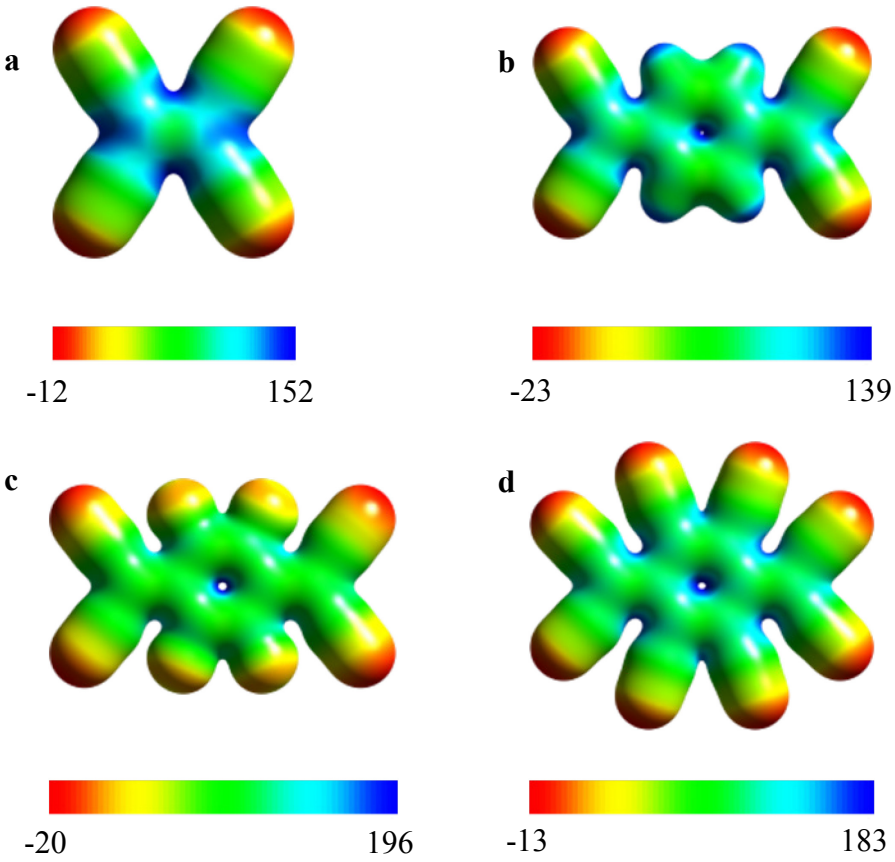

Figure 3.7. Electrostatic potential (ESP) maps for TCNE (**a**), TCNQ (**b**), $TCNQF_4$ (**c**) and $TCNQ(CN)_4$ (**d**). All energies are given in kcal/mol. The ESP maps were generated by Cerius^2 4.8 using the geometry optimized structure obtained through B3LYP/6-31+G(d′). All maps were made with an isodensity value of 0.02.

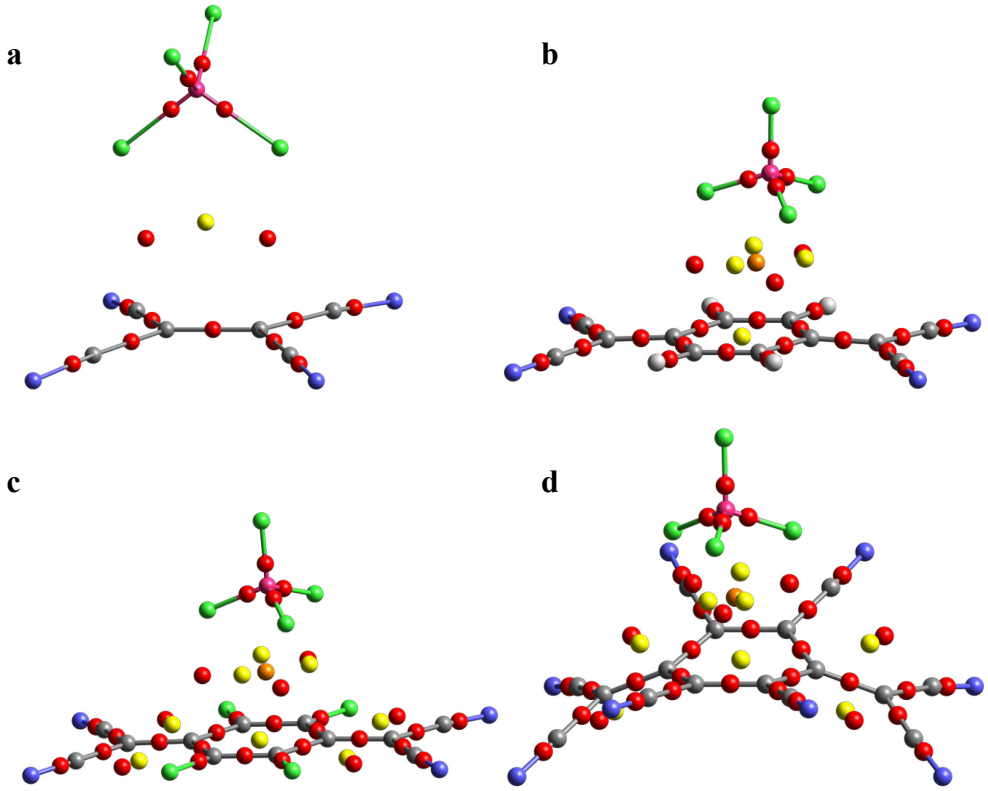

Figure 3.8. Overlay of the schematic drawings of the DFT geometry optimized structures **1a** (**a**), **2a** (**b**), **3a** (**c**) and **4a** (**d**) with the critical points (CPs) as determined by AIM. Olefin-$[PF_6]^-$ results are similar. All spheres are CPs. CPs corresponding to atoms are colored appropriately: carbon atoms (gray), nitrogen atoms (blue), hydrogen atoms (white), boron atoms (pink), fluorine atoms (green). Bond CPs (red), ring CPs (yellow), cage CPs (orange).

found in covalent bonds and in the rings of the $TCNQX_4$ (X = H, F, CN) olefins. The electron densities for the anion-π bond CPs are two orders of magnitude less than that of covalent bonds CPs. One order of magnitude separates the anion-π ring CPs and the olefin ring CPs (Table 3.3).

The CPs observed between the fluorine atoms and nitrile groups in $TCNQF_4$, and between the nitrile groups of $TCNQ(CN)_4$, are explained by the close distance between these atoms, 2.6 Å for the $TCNQF_4$ and 2.8 Å for the $TCNQ(CN)_4$ molecule. This distance is well within the sum of the van der Waals radii for these respective atoms. The presence of these CPs underscore the limitations of AIM. Critical points only give information concerning the shape and magnitude of electron density at a given point. They do not give any information regarding the factors that give rise to that electron density.

Natural Bond Orbitals Computations

The application of second order perturbation theory to the Fock matrix in the NBO basis resulted in predictions of CT interactions for all sixteen systems investigated (Table 3.4). These values are very low, ranging from 1.5 to 8.8 kcal/mol, as one would expect for donor-acceptor interactions involving the complex anions $[BF_4]^-$ and $[PF_6]^-$. Only energy contributions from fluorine lone pair orbitals to olefin anti-bonding orbitals were considered. Donations from the lone-pair orbitals into Rydberg type orbitals or into boron orbitals are not included in these values.

Interestingly, the NBO computation treated certain B-F bonds as donor-acceptor interactions and not as covalent bonds (*i.e*. the electron density normally shared between

Table 3.3. Average values for $\rho(r)$, the electron density at a given critical point between the olefin and the anion. Average values for the olefins themselves are provided.

System	Olefin	Anion	Bond CP (x10^3 a.u.)	Ring CP (x10^3 a.u.)	Cage CP (x10^3 a.u.)
1a	TCNE	$[BF_4]^-$	14.5	7.2	-----
1b	TCNE	$[PF_6]^-$	8.6	5.4	4.9
2a	TCNQ	$[BF_4]^-$	7.7	4.3	4.1
2b	TCNQ	$[PF_6]^-$	7.0	3.5	2.7
3a	$TCNQF_4$	$[BF_4]^-$	10.3	5.1	3.5
3b	$TCNQF_4$	$[PF_6]^-$	9.1	4.7	3.0
4a	$TCNQ(CN)_4$	$[BF_4]^-$	10.5	5.8	4.6
4b	$TCNQ(CN)_4$	$[PF_6]^-$	8.5	6.1	4.0
Average for the olefins			219	18.7	-----

Table 3.4. Sum of the energies predicted by NBO for the charge transfer interactions between the fluorine lone pairs and the antibonding orbitals of the olefins.

System	Olefin	Anion	NBO (kcal/mol) (B3LYP)	NBO (kcal/mol) (MP2)
1a	TCNE	$[BF_4]^-$	5.73*	8.79
1b	TCNE	$[PF_6]^-$	3.10	6.64
2a	TCNQ	$[BF_4]^-$	2.28	3.32*
2b	TCNQ	$[PF_6]^-$	1.52	2.89*
3a	$TCNQF_4$	$[BF_4]^-$	3.40	5.83*
3b	$TCNQF_4$	$[PF_6]^-$	2.22	5.19*
4a	$TCNQ(CN)_4$	$[BF_4]^-$	6.05*	8.55*
4b	$TCNQ(CN)_4$	$[PF_6]^-$	2.83	-----

*Some of the B-F bonds were treated as donor-acceptor interactions in these systems.

the boron and fluorine atoms is localized to a fluorine atom lone-pair and is being donated into an empty orbital on the boron atom. This behavior has been previously observed,[114] and can be taken as an indication of a weakened bond between the boron and fluorine atoms. In fact, correlation between the B-F bond distance (as determined by geometry optimization) and donor-acceptor behavior (as determined by NBO) can be observed for the DFT and *ab inito* results (Table 3.5). For the *ab initio based* **2b** and **3b** structures, NBO treated the P-F systems as donor-acceptor interactions as well, showing similar correlation as observed in Table 3.5. In general, above a certain bond length, NBO will treat the X-F bond as a donor acceptor interaction.

Discussion

The geometry optimized structures support the contention that anion-π interactions occur between the complex anions $[BF_4]^-$ and $[PF_6]^-$ and the olefins TCNE, TCNQ, $TCNQF_4$ and $TCNQ(CN)_4$; both the short F-C distances and favorable energies and enthalpies of interaction support this conclusion (Table 3.1). Further computations demonstrated that the possibility of CH-bonding (through the TCNQ hydrogen atoms) was not a concern; the anion preferred the anion-π interaction over the CH-bond. Since *ab inito* methods are known to overestimate interactions between non-bonded species[113] and DFT methods have been shown to underestimate the same interactions,[77] we feel it is reasonable to assume that the energy of the interactions for these systems are between the values determined by the B3LYP and MP2 methods. Since the order of interaction

Table 3.5. B-F bond distances observed in the geometry optimizations.

System	Olefin	Anion	d_{B-F} (Å) (B3LYP)*	NBO Treatment	d_{B-F} (Å) (MP2)*	NBO Treatment
-----	-----	$[BF_4]^-$	1.420	-----	1.422	-----
1a	TCNE	$[BF_4]^-$	1.434, 1.434 1.398, 1.399	$[F\cdots BF_2\cdots F]^-$	1.423, 1.430, 1.430 1.340	$[BF_4]^-$
2a	TCNQ	$[BF_4]^-$	1.424, 1.426, 1.424 1.401	$[BF_4]^-$	1.425, 1.429, 1,429 1.402	$[F,F\cdots B\cdots F,F]^-$
3a	$TCNQF_4$	$[BF_4]^-$	1.425, 1.425, 1.431 1.394	$[BF_4]^-$	1.428, 1.429, 1.432 1.395	$[F,F\cdots B\cdots F,F]^-$
4a	$TCNQ(CN)_4$	$[BF_4]^-$	1.405, 1.436, 1.436 1.385	$[F\cdots BF_2\cdots F]^-$	1.420, 1.429, 1.432 1.389	$[F,F\cdots BF\cdots F]^-$

*The first line of values denotes the B-F distances that correspond to those fluorine atoms interacting with the olefin. The numbers in red correspond to the B-F distances that correspond to the F→B interactions.

energies is consistent for both series of computations, the observed trend in the E_t values should hold true experimentally.

For the $TCNQX_4$ molecules (X = H, F, CN), E_t (**4a**) > E_t (**4b**) > E_t (**3a**) > E_t (**3b**) > E_t (**2b**) > E_t (**2b**), a consequence of the fact that as you add electron withdrawing substituents to the base ring, the energy of interaction becomes more favorable. The relative large energies of interaction, particularly for **4a** and **4b**, are unexpected. These data seem to support the conclusion of Kim, *et al*. that anion-π interactions should be energetically comparable to cation-π interactions.[56] It is more likely that these are not simply electrostatic interactions, but that they include some element of CT, as Roskha, *et al*. demonstrated between TCNE and bromide anion.[103] Another likely mechanism of interaction between the olefins and the complex anions is the charge-dipole interaction described by Wheeler, *et al*.[38] The electron withdrawing nitrile and fluoro groups added to these olefins will transfer electron density along the σ-bonding framework resulting in dipoles with which the anion can interact. What is not clear is whether or not the π orbital conjugation between the nitrile and the olefin will result in a π-acidic environment. Conjugation, in this case, allows for the possibility of anion-π and π-type CT interactions to occur.

The dissociation of $[BF_4]^-$ aside, NBO computations predict donor-acceptor interactions between the fluorine lone pair electrons and the π^* orbitals on the olefins. These interactions, shown in Table 3.4, follow the same trends observed in the E_t values determined by geometry optimization (Table 3.1). In all cases, favorable energies are observed with the energies of the structures determined from *ab inito* methods being

more favorable than those of structures determined by DFT, interactions with $[BF_4]^-$ are more favorable than interactions with $[PF_6]^-$, and for the series of $TCNQX_4$ (X=H,F,CN), the interactions involving $TCNQ(CN)_4$ are the most favorable and TCNQ the least. Parallels exits between the ordering of the energies observed by the geometry optimizations and NBO computations and the electron densities determined for the bond CPs by AIM. The trend is not so pronounced in the ring and cage critical points. The electron density of a critical point can be taken as a measure of the strength of the interaction.

Conclusions

DFT and *ab initio* geometry optimizations provide evidence for anion-π interactions between the olefins TCNE, TCNQ, $TCNQF_4$ and $TCNQ(CN)_4$ and the anions $[BF_4]^-$ and $[PF_6]^-$. AIM analysis provides further evidence for electron density between the fluorine atoms of the anions and the nearby carbon atoms of the olefin molecules. This shared electron density is most likely due to the donor-acceptor interactions identified by NBO computations. The energies determined by NBO lend further support to trends observed in the geometry optimizations. Further experiments, particularly UV/visible solution studies, will be required to determine if the interactions predicted by NBO are observable.

CHAPTER IV

COMPUTATIONAL INVESTIGATION OF THE ANION-PI INTERACTIONS BETWEEN HALIDES AND 1,4,5,8,9,12-HEXAAZATRIPHENYLENE-HEXACARBONITRILE

Introduction

The molecule 1,4,5,8,9,12-hexaazatriphenylene (HAT) was first suggested as an anion-π receptor in a computational study by Garau, *et al*. in 2005.[61] That same year, Furukawa, *et al*. reported anion-π interactions for two copper structures containing the HAT derivative, 1,4,5,8,9,12-hexaazatriphenylene-hexacarbonitrile ($HAT(CN)_6$) (Scheme 4.1).[115] Hexafluorophosphate, the anion reported to interact with $HAT(CN)_6$ by Furukawa, *et al*.,[115] was also shown to engage in anion-π interactions with another HAT derivative, 2,3,8,9,14,15-hexamethyldiquinoxoalino[2,3-*a*:2′,3′-*c*]phenazine ($HATNMe_6$) which is a derivative of 1,6,7,12,13,18-hexaazatrinaphthylene; tetrafluoroborate anion was also observed to interact.[116] In this case, the $HATNMe_6$ was part of a titanium complex reported by Piglosiwicz, *et al*.[116]

It can be argued that the anion-π interactions observed by Furukawa, *et al*. and Piglosiwicz, *et al*. are due to the presence of three transition metal cations bound to the HAT based ligands and not necessarily an interaction inherent to the ligands themselves. This argument, however, overlooks an earlier report by Dunbar and co-workers who observed neutral, uncoordinated, $HAT(CN)_6$ engaged in anion-π interactions with the iodide and hexafluorophosphate anions.[73] Co-crystallization of $HAT(CN)_6$ molecules

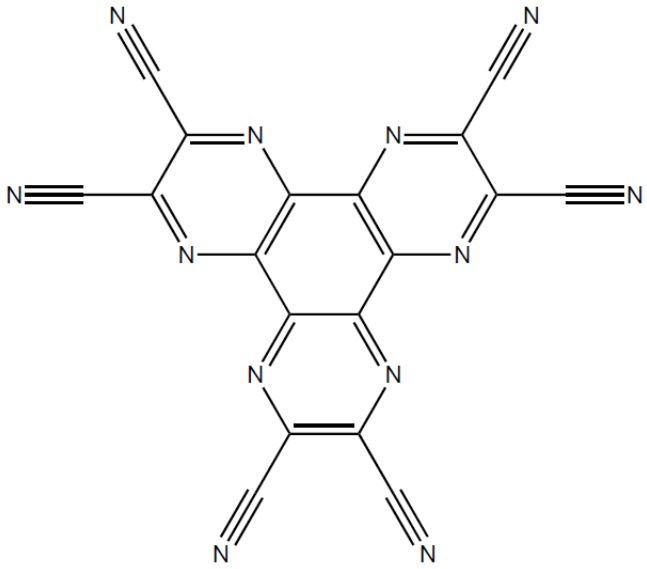

Scheme 4.1. Schematic representation of 1,4,5,8,9,12-hexaatatriphenylene-hexacarbonitrile ($HAT(CN)_6$).

with tetra-*n*-butylammonium iodide ([*n*-Bu_4][I]) or cobaltocenium hexafluorophosphate resulted in the formation of {([*n*-Bu_4N][I])$_3$[HAT(CN)$_6$]$_2$}·3C_6H_6 (Figure 4.1a) and {[$CoCp_2$][PF_6]}$_3$[HAT(CN)$_6$] (Figure 4.1b), respectively. In both of these compounds (abbreviated HAT(CN)$_6$[I]$_3$ and HAT(CN)$_6$[PF_6]$_3$), alternating layers of HAT(CN)$_6$ and anions result in infinite "chains". In the case of HAT(CN)$_6$[I]$_3$, an ABCD type of stacking is observed (Figure 4.1a). The three iodide anions are disordered over four crystallographic positions; one of the positions is located directly above the centroid of the HAT(CN)$_6$ molecule (the central, or "anion-π" position) (Scheme 4.2a) while the other three positions are located on the opposite face of the HAT(CN)$_6$ over the peripheral pyrazinyl carbon-carbon bonds (the outer, or "charge-transfer" (CT) position) (Scheme 4.2b). This disorder is not observed in the HAT(CN)$_6$[PF_6]$_3$ structure, which exhibits a simpler AB stacking, with the three hexafluorophosphate anions occupying the three outer positions. It should be noted that the structure {([*n*-Bu_4N][Br])$_3$[HAT(CN)$_6$]$_2$}·3C_6H_6 (HAT(CN)$_6$[Br]$_3$) has also been determined and it is structurally identical to the HAT(CN)$_6$[I]$_3$ structure.[51]

The dark color of the crystals of the HAT(CN)$_6$[X]$_3$ (X=Br, I) as well as the unprecedented finding of two distinct anion···arene interactions with one ring (in the solid state), led Dunbar and Chifotides, *et al*. to investigate these interactions in solution (UV-Vis, ^{13}C-, ^{35}Cl-, ^{81}Br- and ^{127}I-NMR) and in the gas-phase (ESI-MS).[51] For solutions of HAT(CN)$_6$ and [*n*-Bu_4N][X] (X = Cl, Br, I), evidence for the existence of the CT complex, {[HAT(CN)$_6$]$_2$[X]$_3$}$^{3-}$ (X = Cl, Br, I), was obtained. The spectroscopic data also indicate that the three anions are positioned in the "outer" positions of the

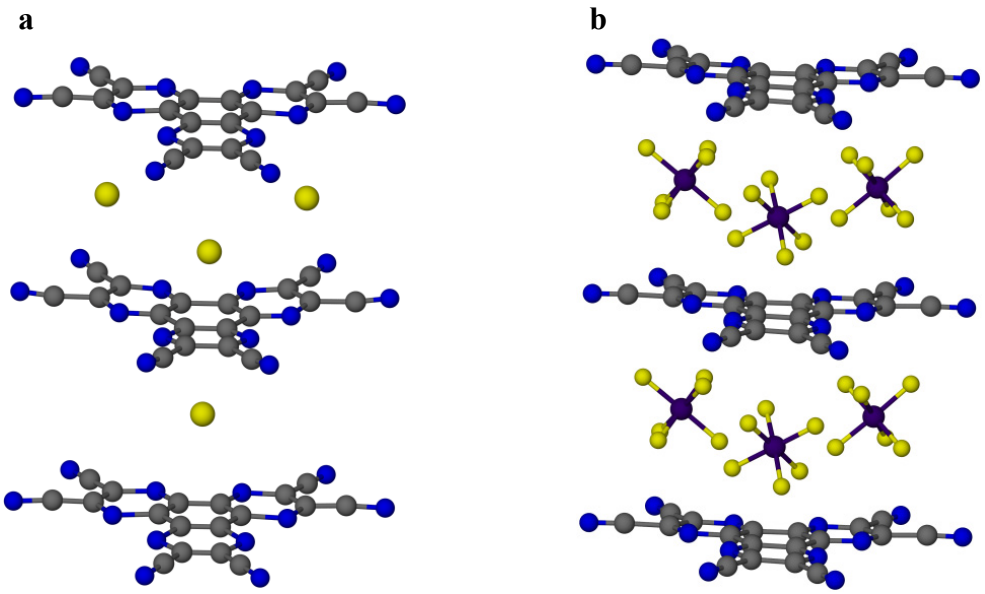

Figure 4.1. Packing diagrams for $\{([n\text{-}Bu_4N][I])_3[HAT(CN)_6]_2\}\cdot 3C_6H_6$ (**a**) and $\{[CoCp_2][PF_6]\}_3[HAT(CN)_6]$ (**b**). All solvent molecules and cations are omitted for the sake of clarity. Carbon atoms (gray), nitrogen atoms (blue), phosphorus atoms (purple), iodide anions and fluorine atoms (yellow).

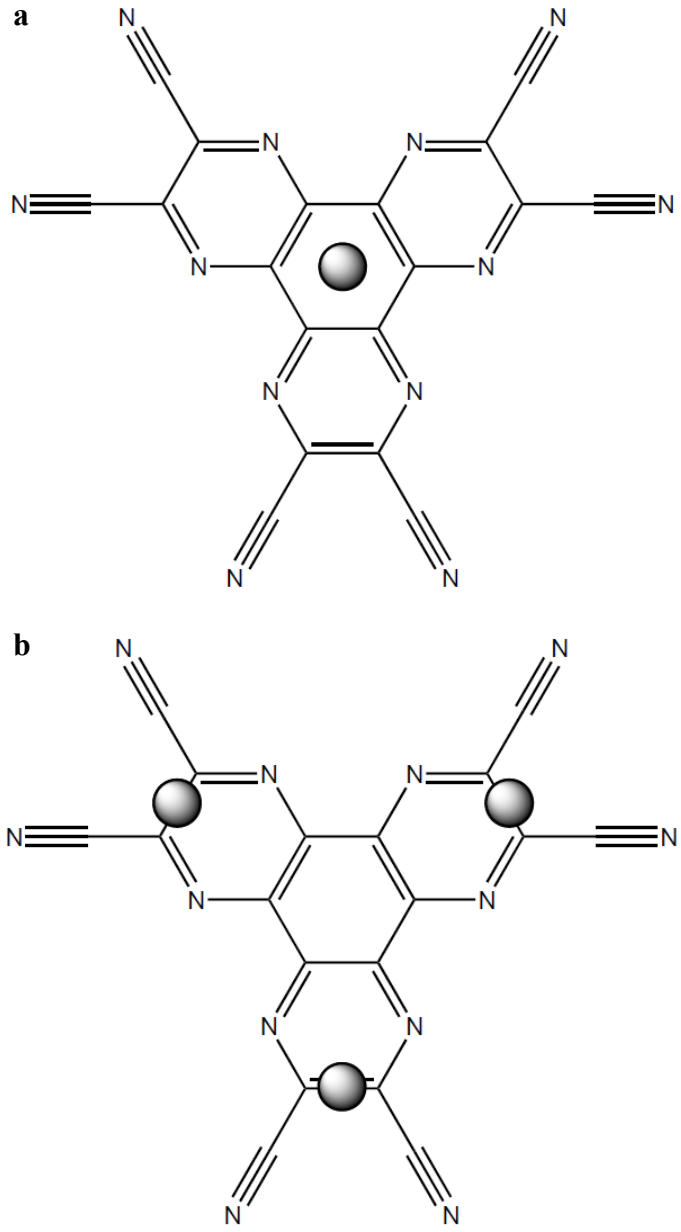

Scheme 4.2. Schematic representations of the "central" (**a**) and "outer" (**b**) positions on $HAT(CN)_6$. Gray spheres are used to denote these positions.

$HAT(CN)_6$ molecules in an η^2-η^2 fashion as found in the $HAT(CN)_6[I]_3$ and $HAT(CN)_6[Br]_3$ crystal structures. It is also worth mentioning that the interactions persist in the gas phase as evidenced by the observation of mass cluster peaks attributable to species $\{HAT(CN)_6[X]\}^-$ (X = Cl, Br, I).

Computational studies were undertaken in order to further understand these systems in general. More specifically the differences between the interactions at the "central" and "outer" positions were investigated.

Methods

Geometry Optimizations

All optimizations were performed using density functional theory (DFT)[87] as contained in the Gaussian03[88] program suite. The Becke3 parameter hybrid exchange functional[89] and Lee-Yang-Parr correlation function[90] (B3LYP) was also used. Given the presence of heavier atoms (beyond the second period), namely chlorine and bromine, a mixed basis set was employed; a Pople style double-ζ basis set with an optimized d-polarization function (6-31+G(d′))[109] was used for carbon, nitrogen and fluorine atoms. For the sake of convenience, electrostatic core potentials (ECPs) were employed using the Las Alamos National Laboratories double-ζ basis set (lanl2dz) for the chlorine and bromine atoms.[117-118] It should be noted that all calculations were performed in the gas phase.

Prior to the geometry optimizations of any $HAT(CN)_6 \cdot\cdot [X]^-$ systems, $HAT(CN)_6$ itself was optimized. This model of $HAT(CN)_6$ was then used for all subsequent

optimizations. In all cases the anion of interest was placed approximately 4 Å away from the plane of the $HAT(CN)_6$ molecule. As previously described, the structures $HAT(CN)_6[X]_3$ (X = Br, I) exhibit two distinctive crystallographic positions for the anions with respect to the $HAT(CN)_6$ molecules (the central and outer positions as shown in scheme 4.2). In order to probe the differences in the anion-π interactions of these two positions, a series of optimizations was carried out for each anion of interest (Cl^-, Br^-). Two separate single anion optimizations were carried out – one optimization involving a single anion positioned over the central position (**1a** and **2a**, chloride and bromide ion respectively) and a second one with an anion positioned over the outer position (**1b** and **2b**, chloride and bromide ion respectively).

A symmetry constrained geometry optimization was also performed. By using the same starting geometries and conditions as in **1b** and **2b**, the optimization was repeated under the constraint of C_s symmetry (**1b*** and **2b***, chloride and bromide ion respectively).

Natural Bond Orbitals Computations

Natural Bond Orbitals (NBO) computations were performed with GenNBO 5.0W[112] for selected systems. The input files for GenNBO 5.0W were prepared using the internal NBO calculation in Guassian03, on the previously obtained optimized geometries. All computations using Guassian03 were performed at the same level of theory as the optimizations. The resulting orbital diagrams were created using NBOView.[119]

NBO computations were performed on systems **1a**, **1b***, **2a**, **2b***. In order to properly account for the resonance in the $HAT(CN)_6$ molecule, the orbital occupancy threshold had to be lowered from 1.90 *e* to 1.50 *e* (for **1b*** and **2a**) and 1.40 *e* (for **1a** and **2b***). If this is not done, the resulting model has lone pairs of electrons localized to some of the C atoms of the central phenylene ring of $HAT(CN)_6$.

Results

Geometry Optimizations

For the single anion calculations, the central anions and outer anions behaved similarly in both cases (Figure 4.2a,b,d,e). The central anion remained over the centroid of the molecule whereas the outer anion "attacked" one of the carbon atoms in the pyrazinyl ring, forming the aforementioned σ-type CT complex.[40] This behavior is reflected in the C-X distances listed in Table 4.1. The outer position distances are much closer to the $HAT(CN)_6$ molecule than the central position, possibly indicating a greater degree of orbital overlap at the outer position. Since **1b** and **2b** did not accurately model the η^2 behavior observed in the crystal structures $HAT(CN)_6[X]_3$ (X = Br, I), the computations were repeated employing a C_s symmetry constraint. These computations, **1b*** and **2b*** reproduced the η^2 behavior (Figure 4.2c,f) and the distances are intermediate between those seen in **1&2a** and **1&2b** (Table 4.1), which would be expected for the π-type CT observed in the previous experimental work.[51,73] All the calculated distances fall within the sum of the van der Waals radii for the respective

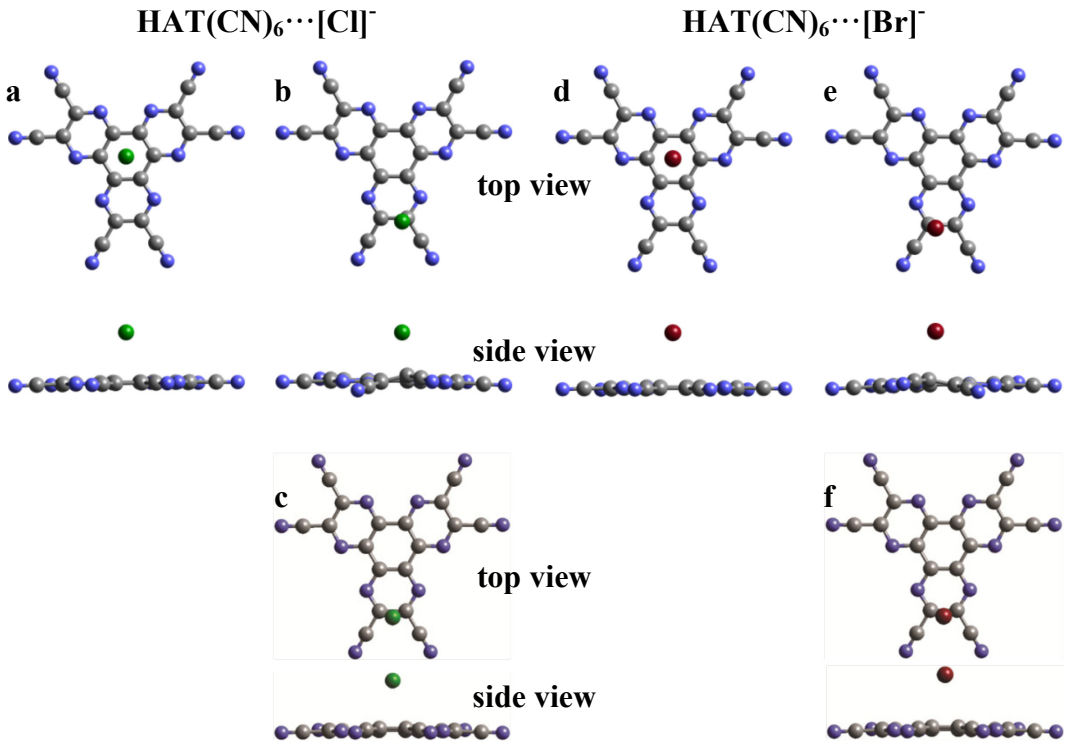

Figure 4.2. Geometry optimized structures computed for $HAT(CN)_6\cdots[X]^-$. Anion located over the central position (**a** & **d**), anion located in the outer position, without symmetry constraint (**b** & **e**), anion located in the outer position, with the symmetry constrained to C_s (**c** & **f**). Carbon atoms (gray), nitrogen atoms (blue), chloride anion (green), bromide anion (red).

Table 4.1. Distances observed in the $HAT(CN)_6\cdots[X]^-$ DFT geometry optimizations.

System	Anions	Distance (central) (Å)	Distance (outer) (Å)	Sum of the van der Waals radii, C-X (Å)
1a	1 Cl (central)	3.06 - 3.09	**-----**	3.50
1b	1 Cl (outer)	**-----**	2.34	
1b*	1 Cl (outer)	-----	2.72	
2a	1 Br (central)	3.29 - 3.33	**-----**	3.60
2b	1 Br (outer)	**-----**	2.68	
2b*	1 Br (outer)	-----	2.94	

atoms indicating the presence anion-π interactions between the $HAT(CN)_6$ molecule and the anions.

Favorable energies of interaction (E_t) were observed for systems **1a**, **1b***, **2a** and **2b***. Energies of interaction (E_t) were determined by subtracting from the total energy, the energies of the $HAT(CN)_6$ molecule and anion (Table 4.2). The energy for $HAT(CN)_6$ was determined by geometry optimization under B3LYP/6-31+G(d′) and the anion energies were determined by geometry optimization under B3LYP/lanl2dz using the appropriate ECPs.

Natural Bond Orbitals Computations

While all four systems are predicted, by NBO, to exhibit some degree of charge-transfer, **1b*** and **2b*** are predicted to engage in stronger charge-transfer interactions then **1a** and **2a**, respectively (Table 4.2). This result is not surprising given the positions of the anions relative to the $HAT(CN)_6$ molecule. In **1a** and **2a**, the anion is positioned over the centroid of the molecule; a location at which one would expect minimal orbital density from the surrounding atoms. In contrast, **1b*** and **2b*** are cases in which the anion is positioned directly over a C-C bond; a location of significant orbital density. The increased orbital overlap in **1b*** and **2b***, relative to **1a** and **2a** is readily apparent in the contour plots shown in Figure 4.3. For the purposes of this study, the only CT interactions considered are those between the lone pairs on the halide ions and the antibonding orbitals on the $HAT(CN)_6$ (Figures 4.3 and 4.4); CT interactions into Rydberg type orbitals were not included. Closer inspection of the data from the NBO

Table 4.2. Sum of the energies determined by NBO for the charge transfer interactions between the halide lone pairs and the antibonding orbitals of $HAT(CN)_6$ and the energies of interaction determined by DFT computations.

System	ΔE_{CT} (kcal/mol) (NBO)	E_T (kcal/mol) (DFT)
1a	7.61	-46.08
1b*	25.66	-37.75
2a	12.58	-33.78
2b*	19.97	-25.93

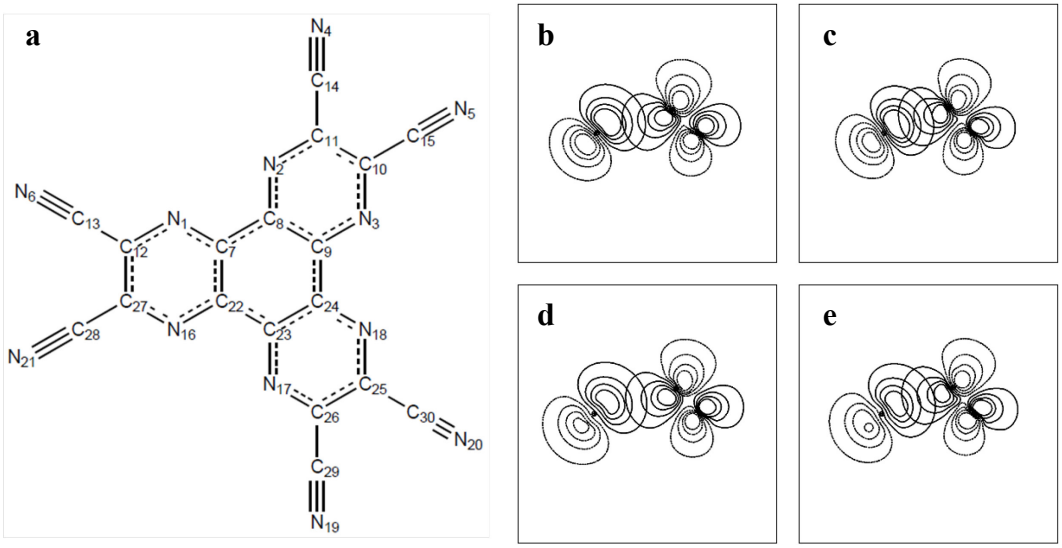

Figure 4.3. Representative contour plots for halide p_z orbital and C-N antibonding orbitals generated by NBOView. Schematic of $HAT(CN)_6$ with atoms labeled (**a**). System **1a**, Cl···C_{24}-N_{18} (**b**). System **1b***, Cl···C_{11}-N_2 (**c**), System **2a**, Br···C_{24}-N_{18} (**d**). System **2b***, Br···C_{11}-N_2 (**e**).

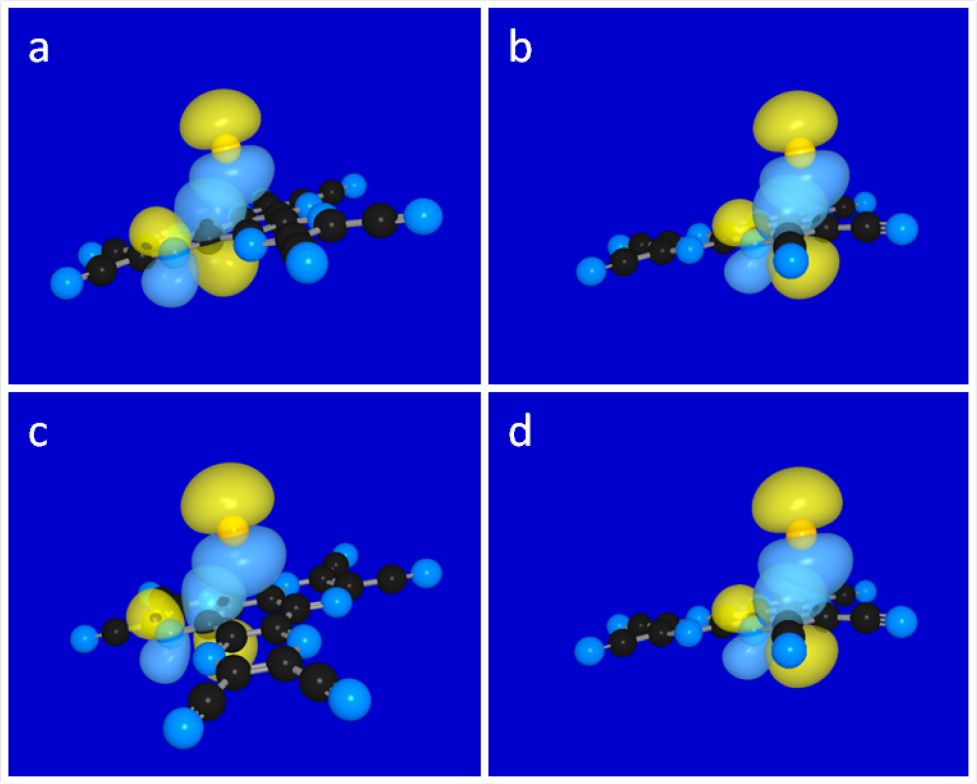

Figure 4.4. Representative orbital diagrams for halide p_z and C-N antibonding orbitals generated by NBOView. System **1a**, Cl···C_{23}-N_{17} (**a**). system **1b***, Cl···C_{11}-N_2 (**b**), system **2a**, Br···C_{23}-N_{17} (**c**), system **2b*** Br···C_{11}-N_2 (**d**).

computation reveals that all four lone-pairs of the Cl^- or Br^- contribute some density to stabilization energy to the final structure. In both computations these orbitals are NBOs 97, 98, 99 and 100. If we defined a Cartesian coordinate system such that the $HAT(CN)_6$ molecule lies in the xy plane then NBO 97 is predominately an *s* orbital, NBOs 98 and 99 are the p_x and p_y orbitals and 100 is predominately the p_z orbital. It should be noted that there is some mixing of the *s* and p_z orbitals observed in NBOs 97 and 100, but it is miniscule in all cases. The majority of the stabilization resulting from the CT interactions arise from the donation of charge from NBO 100, the p_z orbital, to the nearby C-N antibonding orbitals on $HAT(CN)_6$ (Table 4.3).

Discussion

The computational data support the conclusion that anion-π interactions occur between chloride and bromide anions and the $HAT(CN)_6$ molecule. The geometry optimizations demonstrated that, in all cases, the distances observed between the anion and the closest carbon atoms is less than the sum of the van der Waals radii for the respective atoms (a strong indication of supramolecular interactions). A comparison of the distances observed for the $HAT(CN)_6\cdots[Br]^-$ interactions in the solid state with the computational data demonstrates that the computational data overestimates the C-Br distances in both the outer and central positions by 0.2-0.3 Å (Table 4.4). This overestimation may simply be due to the fact that there are two $HAT(CN)_6$ molecules sandwiching Br^- in the crystal structure whereas there is only one $HAT(CN)_6$ molecule in the computation. The fact that the DFT computation takes place in the gas phase can

Table 4.3. Contributions to the total ΔE_{CT} from each of the individual X^- NBOs.

System	NBO 97 (%)	NBO 98 (%)	NBO 99 (%)	NBO 100 (%)
1a	4.68	28.25	12.88	54.01
1b*	7.17	5.07	14.89	72.88
2a	4.69	14.71	14.94	65.66
2b*	6.81	4.46	13.67	75.06

Table 4.4. Comparison of the X-C distances observed in the $HAT(CN)_6\cdots[Br]^-$ interactions for the crystal structure and computational model.

	Central (Å)	**Outer (Å)**
Crystal Structure	3.53-3.64	3.24-3.38
Computation	3.29-3.33	2.94*

*This is the value of the symmetry constrained computation.

also lead to stronger interactions than would normally be observed. It is possible to infer, from the computations, that the presence of two $HAT(CN)_6$ molecules is necessary to stabilize the π-type CT interaction. Since a σ-type CT interaction occurs without symmetry constraint (as opposed to the η^2 behavior), it is reasonable to propose that the presence of the two molecules, allowing for η^2-η^2 behavior, stabilizes the π-type CT. (It has been previously shown that numerous weaker interactions can be favored over one stronger interaction.[120]) It should be noted that this inference is not certain given uncertainty in the accuracy of the computed results. Despite the overestimation of the X-C distances in this system, the relative positioning of the Br^- with respect to the $HAT(CN)_6$ is consistent with the experimental evidence so it can be assumed that the orbital arrangement observed in the NBO computations is similar and that the predicted trends are accurate.

It is evident from the NBO computations that the CT interactions in the outer position (**1b*** and **2b***) are stronger than those observed for the central position (**1a** and **2a**). (The presence of any CT interaction in the center position is most likely due to the overestimation of the interaction in the geometry optimization.) This is in agreement with the solution studies, in which the anions were detected spectroscopically in the outer positions wheras no anion was observed to be present in the central position.[51] The lack of evidence for a centrally located anion in solution indicates that the interaction is either too weak to be detected or is too weak to exist in solution. In either case, the solution studies explicitly demonstrate that the π-type CT interaction is stronger than the anion-π interaction. The previous studies in our laboratories also clearly demonstrated

that the $HAT(CN)_6\cdots[Cl]^-$ interaction is stronger than the analogous interaction with the bromide anion. The computational data support this observation in both the geometry optimization (the C-Cl distances are shorter than the C-Br distances, Table 4.1) and the NBO computations (the energies of interaction are more favorable in both **1a&b*** than in **2a&b***, Table 4.2).

Although the E_t values obtained by the DFT computations are favorable, the trends predicted by DFT do not agree with the NBO results (Table 4.2). Specifically, the DFT computations predict that the energy of the central position (**1a** and **2a**) is more favorable than the energy of the outer position (**1b*** and **2b***). This is in direct contrast to both the NBO computations and the previously reported spectroscopic data.[51] This difference is readily explained by the fact the E_t values determined by DFT consider all energies whereas the energies determined by NBO are limited to the CT interaction. The DFT computation indicates that other interactions, aside from those of the CT type, are present in the $HAT(CN)_6\cdots[X]^-$ (X = Cl, Br). The anion-π interaction is the most likely explanation.

Conclusions

A series of DFT and NBO computations have been performed on the molecule $HAT(CN)_6$ in the presence of chloride or bromide anion. In the case of the center, or anion-π interaction, positioning of the anion with respect to the crystal structure is probed by the geometry optimization. Accurate positioning was not accomplished, without symmetry constraint, for the outer, or π-type CT interaction. Despite

overestimation of the interaction by DFT, the computational results are in agreement with the previously reported solid state[73] and solution[51] results. The computational results provide evidence for the stabilization of the π-type CT by both interacting $HAT(CN)_6$ molecules and point to the C-N π antibonding orbitals on the $HAT(CN)_6$ molecule as the electron density acceptors for the CT interactions.

CHAPTER V

SEARCHING FOR POTENTIAL ANION-PI INTERACTIONS IN THE PROTEIN DATA BANK

Introduction

One intriguing question for the anion-π community is whether anion-π interactions play a role in biological systems.[6-7] While there are currently few reports addressing this question, there is experimental evidence that anion-π interactions could occur biologically. The report of Garcia-Rosa, *et al*. demonstrates that anion-π interactions can occur between tetrachloromercurate(II) and tetrachlorozincate(II) anions and bisadenine derivatives,[121] and a copper-cytosine complex reported by García, *et al*. exhibits an interaction between the aromatic ring of the cytosine and the nearby perchlorate anion.[122] These reports support the notion that the aromatic rings in nucleotides can interact attractively with anions. In light of this, albeit, limited evidence, researchers are beginning to consider anion-π interactions in their synthetic designs of derivatives[123] and models.[67,124]

An ongoing example of incorporation of anion-π interactions into model compounds of biological systems is the previously mentioned "anion-π slide" (Figure 5.1) first reported by Gorteau, *et al*.[67] The slide is an artificial trans-membrane channel utilizing anion-π interactions to selectively transport chloride anions across a lipid bilayer. Research on this compound has continued[125-126] ultimately resulting in what the

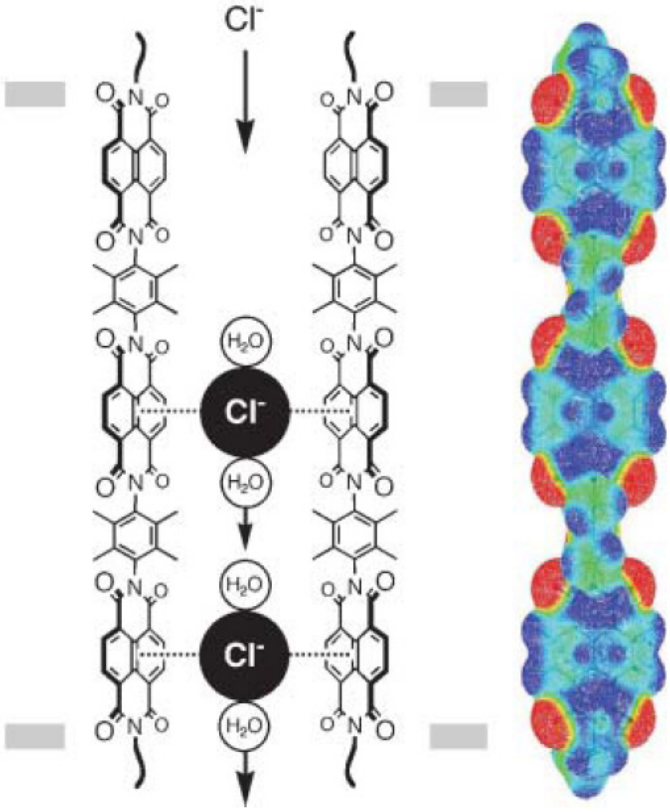

Figure 5.1. Schematic diagram of the synthetic chloride anion channel prepared by Matile, *et al.* (left) and an electrostatic potential map of the same (right). (Adapted with permission Matile, *et al*.[67])

authors refer to as, "…unequivocal, clear-cut, experimental evidence for the functional relevance of anion-π interactions…"[127]

As interesting as all of these reports are, there has yet to be any direct evidence for an anion-π interaction occurring in a biological system. One simple way to ascertain whether or not anion-π interactions occur in proteins, for example, is to systematically search the Protein Data Bank (PDB). While searches of the Cambridge Structural Database for anion-π interactions have been performed numerous times,[33,35,40,42-43,61,128-135] only two reports have appeared that involve searches of protein structures.[57,136]

Jackson, *et al*. investigated the interactions between the anionic side chains of aspartate (Asp) and glutamate (Glu) (Scheme 5.1) and the aromatic side chains of phenylalanine (Phe), tyrosine (Tyr) and tryptophan (Trp) (Scheme 5.1).[136] The data garnered from the PDB revealed that, while the anions could be positioned at all angles between 0° (in the plane of the ring) and 90° (above the centroid of the ring), the preference is clearly for what Jackson, *et al*. refer to as the edgewise interaction (angles less than 10°) with interactions at higher angles (greater than 20°) occurring less than would be expected (Figure 5.2). This report indicates that anion-π interactions most likely do not occur for between these amino acids.

The results of Jackson, *et al*.[136] can be contrasted with a report from Marsili, *et al*., wherein a PDB search was used to help determine the thermodynamic contributions to protein stability from arene···X interactions, where X is either an arene, anion or cation.[57] The arene···anion interactions studied were found to be favorable, but less stable than the arene···arene and arene···cation interactions considered. It should be

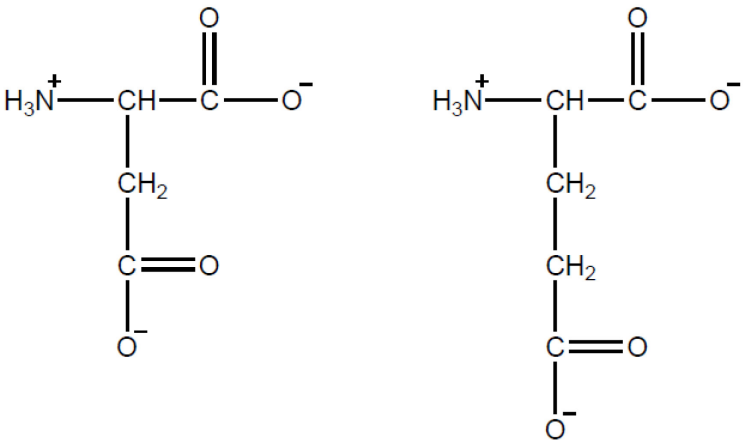

Asp Glu

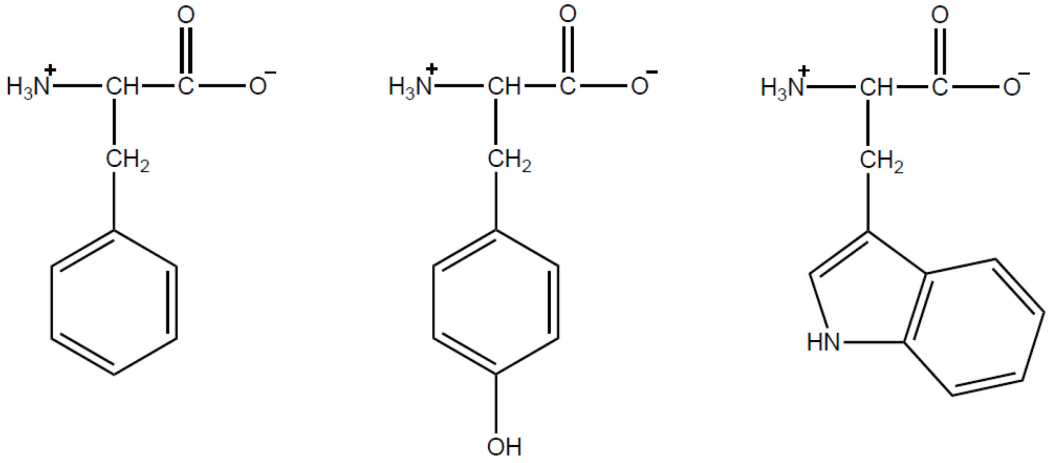

Phe Tyr Trp

Scheme 5.1. Schematic representations of Aspartate (Asp), Glutamate (Glu), Phenylalanine (Phe), Tyrosine (Tyr) and Tryptophan (Trp).

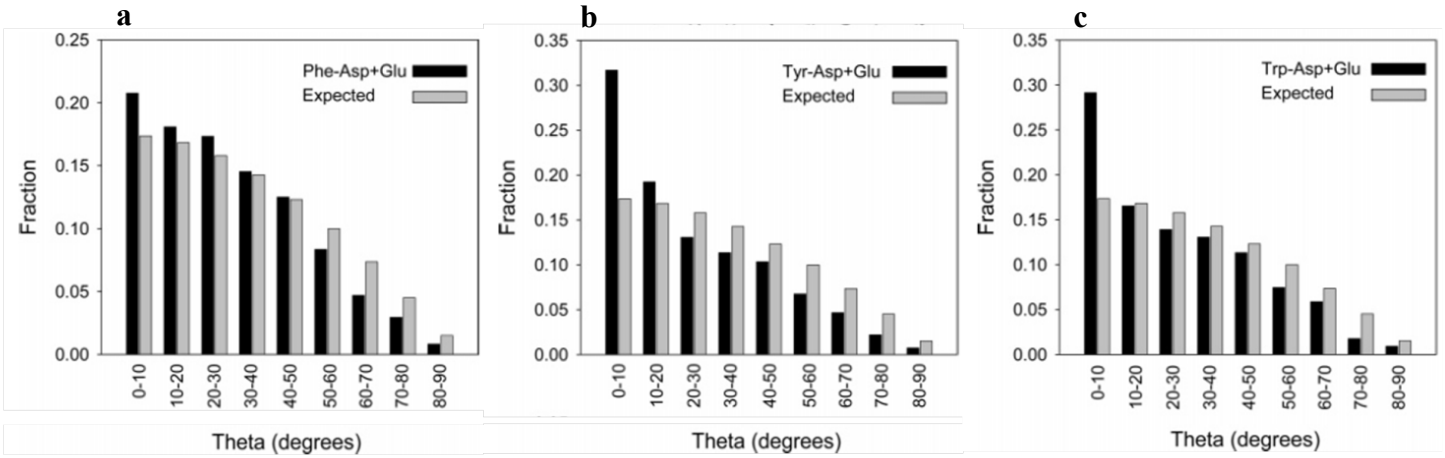

Figure 5.2. The results of the PDB search performed by Jackson, *et al*. Graphical distributions are shown for the cases of Phe (**a**), Tyr (**b**) and Trp (**c**). Expected values refer to the statistical population of anion···arene pairs within a sphere. (Adapted with permission Jackson, *et al*.[136])

noted that, like Jackson, *et al.*, Marsili, *et al.* only considered interactions between amino acids.

From the work of Garcia-Rosa, *et al*.[121], García, *et al*.[122] and Dawson, *et al*.[127] the potential for anion-π interactions in biological systems is clear. The reports of Jackson, *et al*.[136] and Marsili, *et al*.[57], while failing to show clear evidence for anion-π interactions, underscore that these type of supramolecular interactions are of interest in biologically relevant systems. Marsili, *et al*. lend further support to the biological occurrence of anion-π interactions. While the biological relevance of anion-π interactions is not yet clear, what is clear is the need for more research in this area. All research to date point to anion-π interactions having a low occurrence in biological systems, but the role that these interactions play is still unclear and as stated above, there are no definitive functional examples of this interaction in a biological system. In an effort to find examples of anion-π interactions in protein structures, new searches of the PDB were designed and carried out. Instead of focusing on the anionic side chains of amino acids incorporated into the protein itself[57,136], these new searches focused on the chloride and iodide anion.

Methods

All data were obtained by searching the Protein Data Bank (PDB) by using both the internal search engine of the site and a specially written script. The scripts were written in the open access language python, version 2.5.2, using the IDLE 1.2.2 graphic user interface.

Contacts-Cl.py

This script is a modification of one originally written by Dr. Thomas Ioerger (Department of Computer Science and Engineering, Texas A&M University) to search for close contacts between silver atoms and any other atom within a particular protein structure as described by a .pdb file (the file type used by the PDB). This script was modified by changing the search parameter from silver atoms to chlorine atoms (*line[12:14]=="AG"* to *line[12:14]=="CL"*) and setting the distance constraint to 4.0 Å (*if d<4.0:print...*). This script includes functionality enabling it to retrieve the Cartesian coordinates for any particular atom as listed in the .pdb file, calculate the distance between two points given those coordinates, identify any particular chlorine atom within a protein structure and search for all atoms within 4.0 Å of the identified chlorine atom. Atoms belonging to water molecules were excluded from this search. Information provided by this script included the name of the particular .pdb file, the identities of any substrate molecules included in the structure and the identity and coordinates of any chlorine atom(s) found within the structure listed with the corresponding close contact atoms.

This script was run on .pdb files downloaded from the PDB using the internal search engine to identify any and all protein structures possessing chlorine atoms.

Protein-Cl_Full+.py

This script was written using the script *Contacts-Cl.py* as a base. The primary reason for writing this second script was to make the search parameters specific to chloride ions (*Contacts-Cl.py* did not differentiate between atoms and ions) and the

aromatic rings on the amino acids phenylalanine (Phe), tryptophan (Trp) and tyrosine (Tyr). The script was also written to provide more detailed information regarding the close contacts in the output.

In order to accomplish these goals, functions were written enabling the script to calculate the Cartesian coordinates for the centroid of a 5-membered ring, 6-membered ring and fused 5 and 6-membered rings (as observed in the side chain of Trp). A function for the calculation of the angle formed by the line between the ring centroid and the chloride ion and the line between the ring centroid and a ring atom within 4.0 Å of the chloride ion was also written. Given the improved specificity of this script with respect the original *Contacts-Cl.py*, the coding preventing water molecules from being considered as close contacts was removed. Additional coding was added to the search function enabling the script to search for specified cations within 5.0 Å of the ring atoms belonging to aromatic rings previously identified as being within 4.0 Å of a chloride ion. This secondary search was facilitated by coding that allowed for the creation of a list containing all the aromatic rings identified as being within close contact to a chloride ion in a specific .pdb file. The cations specified for this search included the alkali metal, magnesium, calcium, zinc, ammonium, tetraethylammonium and hexaamminecobalt (charge was not specified) cations. These species were identified as cations contained in the .pdb files to be search using the script *HETNAM_search.py*.

Output from this script included the filename of the .pdb file, the resolution of the protein structure, the identities of any substrates within the protein structure and the identities and coordinates of all chloride ions within the structure along with the

identities and coordinates for any ring atoms within close-contact and the corresponding distances (chloride ion to ring atom and chloride ion to centroid) as well as the aforementioned angle. The script would then print the identities and coordinates for any cations identified as being in close-contact with one of the previously identified aromatic rings along with the pertinent distances and angle (this section was written to mirror the output for the chloride ions). At the end of the output file the script prints all identities and coordinates for all the atoms for each aromatic ring identified by the script for that protein structure.

This script was run on the .pdb files identified using the same search parameters as the *Contacts-Cl.py* script.

Protein-Cl_Basic+.py

This script was created by modifying the *Protein-Cl_Full+.py* script. The functionality of the *Protein-Cl_Full+.py* script was unchanged in the *Portein-Cl_Basic+.py* script. The "basic" script was written to provide a more simplistic output to facilitate reading the data. The output from the "basic" script was limited to the filename, resolution, the identity of any chloride ions found with the identities of any aromatic ring atoms in close-contact, the ratio between the chloride anion to ring atom distance and the chloride atom to centroid distance, the ratio between the chloride ion to centroid to ring atom angle and 90° and the existence of any cations within close contact of the identified aromatic rings.

This script was used on the same files searched by the corresponding "full" script.

Protein-I_Full+.py

This script is identical to the *Protein-Cl_Full+.py* script except that it was modified to search for iodide ions instead of chloride ions. This was accomplished by changing the code *line_i[17:20]==" CL"* to *line_i[17:20]=="IOD"* instructing the script to search for the atom iodine instead of chlorine. The larger van der Waals radius of the iodine atom, with respect to the chloride ion was accommodated by changing the variable VDW from 4.0 to 4.2.

This script was run on .pdb files downloaded from the PDB using the internal search engine to identify any and all protein structures possessing iodide atoms.

Protein-I_Basic+.py

This script is identical to the *Protein-Cl_Basic+.py* script except that it was modified to search for iodide ions instead of chloride ions. This was accomplished by changing the code *line_i[17:20]==" CL"* to *line_i[17:20]=="IOD"* instructing the script to search for the atom iodine instead of chlorine. The larger van der Waals radius of the iodine atom, with respect to the chloride ion was accommodated by changing the variable VDW from 4.0 to 4.2.

This script was used on the same files searched by the corresponding "full" script.

Results

Contacts-Cl.py

The nonspecific nature of this script rendered the results of this particular search to be too general to be convenient for further analysis. Given that analysis of any data collected via this script would require all $[Cl]^{-}\cdots X$ interactions, where X was not a ring atom of PHE, TRP or TYR, to be isolated and removed before any potential anion-π interactions could be analyzed, it was decided to write a script containing a higher degree of specificity.

Protein-Cl_Full+.py

On December 4, 2007, the internal search engine of the PDB was used to identify and download 2,517 .pdb files containing one or more chloride anions. The script *Protein-Cl_Full+.py* was executed on these files identifying 620 protein structures exhibiting one or more close contacts between a chloride ion and one of the ring atoms in PHE, TRP or TYR; a total of 1,203 distinct chloride anion – ring pairs were identified. An excerpt of the results of this search is given in Figure 5.3. (Colors given in parentheses refer to the highlighted areas in Figure 5.3). Protein 1MWQ[137] had a resolution of 0.99 Å (yellow), contained multiple substrates (green), contained two separate cases of close-contact between chloride ions and aromatic ring atoms (pink), and one close-contact between a zinc ion and an aromatic ring atom (teal). It should be noted that the bulk of this information was directly taken line by line from the .pdb file by the script and compiled into this format adding calculated distances and angles as appropriate.

```
678 1MWQ.pdb
1MWQ.pdb
REMARK   2 RESOLUTION. 0.99 ANGSTROMS.
HETNAM     MSE SELENOMETHIONINE
HETNAM      ZN ZINC ION
HETNAM      CL CHLORIDE ION
HETNAM     CAC CACODYLATE ION
HETNAM     1PE PENTAETHYLENE GLYCOL
HETNAM     PEG DI(HYDROXYETHYL)ETHER
HETATM 1712 CL    CL A 305      21.798   6.406   5.084  1.00 11.17          CL
HETATM 1713 CL    CL A 306      20.934   9.069   7.648  1.00 13.69          CL
CE1 PHE B  98
            Distance to closest contacts = 3.98
            Distance to centroid = 5.19
            The angle of the anion-centroid axis with the plane of the ring = 23.86
HETATM 1714 CL    CL A 307      24.198   7.520   7.579  1.00 11.36          CL
HETATM 1715 CL    CL B 308      13.493 -11.971   5.627  1.00  8.61          CL
HETATM 1716 CL    CL B 309       9.972 -12.751   4.463  1.00 10.40          CL
HETATM 1717 CL    CL B 310      12.885 -14.075   2.700  1.00  9.61          CL
CE2 TYR B  80
            Distance to closest contacts = 3.98
            Distance to centroid = 5.34
            The angle of the anion-centroid axis with the plane of the ring = 10.05
++++++++++++++++++++++++++++++++++++++++
CE2 TYR B  80
HETATM 1709 ZN    ZN B 302      12.073 -13.467   4.770  1.00  8.08          ZN
            Distance to cation = 4.80
            Cation to centroid = 1.39
            The angle of the cation-centroid axis with the plane of the ring = 25.93
Cartesian coordinates for the above mentioned amino acids:
ATOM   1557  CG  TYR B  80      15.155 -19.224   4.722  1.00  7.53           C
ATOM   1558  CD1 TYR B  80      14.359 -20.357   4.472  1.00  8.53           C
ATOM   1559  CD2 TYR B  80      14.653 -18.021   4.297  1.00  7.72           C
ATOM   1560  CE1 TYR B  80      13.168 -20.279   3.820  1.00  8.79           C
ATOM   1561  CE2 TYR B  80      13.442 -17.912   3.599  1.00  8.08           C
ATOM   1562  CZ  TYR B  80      12.710 -19.064   3.388  1.00  8.53           C
ATOM   1700  CG  PHE B  98      15.443   9.737   7.523  1.00  9.39           C
ATOM   1701  CD1 PHE B  98      16.837   9.811   7.515  1.00  9.23           C
ATOM   1702  CD2 PHE B  98      14.736  10.883   7.256  1.00 11.43           C
ATOM   1703  CE1 PHE B  98      17.477  10.988   7.229  1.00 10.31           C
ATOM   1704  CE2 PHE B  98      15.388  12.064   6.963  1.00 12.03           C
ATOM   1705  CZ  PHE B  98      16.768  12.131   6.972  1.00 11.73           C
```

Figure 5.3. A sample of the output from the script *Protein_Cl-Full+.py*. Highlighting was added to correspond to the lines mentioned in the **Results** section of Chapter V (page 107). All lines beginning with "HETATM" or "ATOM" are space delimited lines that can be read as follows: Atom #, Atom type, Residue, Protein chain, residue number, Cartesian coordinate (x), (y), (z), occupancy factor, temperature factor, element. A line in all capital letters is a line taken verbatim from the .pdb file).

Protein-Cl_Basic+.py

The script *Protein-Cl_Basic+.py* was run on the same 2,517 .pdb files that were searched using the script *Protein-Cl_Full+.py*. As was stated previously, the "basic" search was written to facilitate reading with respect to the "full" search. An example of the sample output for the "full" search was given using the data for protein 1MWQ[137]; sample output for the "basic" search for 1MWQ is shown in Figure 5.4. (Colors given in parentheses refer to the highlighted areas in Figure 5.4). Reported data include a resolution of 0.99 Å (yellow), two separate cases of close-contact between chloride ions and aromatic ring atoms (pink), and one close-contact between a cation and an aromatic ring atom (teal). Notably absent are the detailed coordinate data for each atom, the particular distances and angles (replaced by the aforementioned ratios, see **Methods**, page 105) and all of the specific data pertaining to the cation close contact.

Protein-I_Full+.py

On Dec. 8, 2008, the internal search engine of the PDB was used to identify and download 187 .pdb files containing 1 or more iodide anions. The script *Protein-I_Full+.py* was executed on these files identifying 108 protein structures exhibiting one or more close contacts between an iodide anion and one of the ring atoms in PHE, TRP or TYR; a total of 353 distinct iodide anion – ring pairs were identified. The output format for this script is identical to that of the *Protein-Cl_Full+.py* script.

```
678 1MWQ.pdb
=====================================
REMARK   2 RESOLUTION. 0.99 ANGSTROMS.
CL    CL A 306
CE1 PHE B  98
            Atom/Centroid Distance Ratio = 0.77
            Atom/Centroid Angle Ratio = 0.27
CL    CL B 310
CE2 TYR B  80
            Atom/Centroid Distance Ratio = 0.74
            Atom/Centroid Angle Ratio = 0.11
Possible cation-pi interaction-
```

Figure 5.4. A sample of the output from the script *Protein_Cl-Basic+.py*. Highlighting was added to correspond to the lines mentioned in the **Results** section of Chapter V (page 109). Any line in all capital letters is a line verbatim from the .pdb file).

Protein-I_Basic+.py

The same 187 .pdb files that were downloaded for the *Protein-I_Full+.py* script were searched using the "basic" script. The output format for this script is identical to that of the *Protein-Cl_Basic+.py* script.

Discussion

General Discussion for the PDB Search

As stated previously, the maximum allowed distance between any particular chloride anion and an aromatic ring atom was 4.0 Å. It was decided to increase this cutoff distance from 3.5 Å, the sum of the van der Waals radii for a carbon atom and chlorine atom,[95] in order to take the resolution of the protein structures, on average 2.00 Å for this search, into account. Another reason to increase the cutoff distance to 4.0 Å originates in the methodology used when solving protein crystal structures. Manual displacement of non-bonding atoms in van der Waals contact within the protein crystal structure can occur if the contact is believed to be erroneous.[138-139] Given that anion-π interactions are relatively new concepts in the literature and are, in general, counter-intuitive, it is not difficult to presume that any close contacts between anions and the π face of an aromatic ring would be thought to be erroneous and thus "corrected". For these same reasons the 5.0 Å cutoff for potential cation-π interactions was rounded up from 4.4 Å, the sum of the van der Waals radii between a carbon atom and cesium atom.[95] Using distances larger than the sum of van der Waals radii for the atoms under consideration is not unprecedented when dealing with weak interactions in protein

crystal structures. The previously cited paper by Jackson, *et al.* used a cutoff of 7 Å in their search of the PDB,[136] and in their study of cation-π interactions Gallivan, *et al.* use a cutoff of 6 Å.[72]

For each chloride anion – aromatic ring atom contact identified in the search, three different values were reported by the "full" script: the distance between the chloride anion and the aromatic ring atom (d), the distance between the chloride anion and ring centroid (d_c), and the angle between the anion – centroid vector and the plane of the aromatic ring (θ) (Figure 5.5). In order to simplify the search criteria, these values were normalized, giving rise to only two parameters per anion – ring atom contact instead of three. This normalization was accomplished via the "basic" script. The first parameter is the ratio $d:d_c$. In an idealized anion-π interaction, the anion is positioned directly above the ring centroid meaning that the d_c distance will be shorter than d distance and the ratio $d:d_c$ will be greater than one. The second parameter is the ratio θ:90°. Again the anion would be positioned directly above the ring centroid in an idealized anion-π interaction, making the angle θ equal to 90°. In this case, the θ:90° ratio would become equal to one.

A plot of the ratio θ:90° against the ratio $d:d_c$ (Figure 5.6a) demonstrates that the overwhelming majority of the contacts identified are not near the idealized anion-π interaction. This result is not unexpected and fits with the results presented by Jackson, e*t al* (Figure 5.2).[136] Although the authors considered a different anion (the anionic side chain of Asp or Glu instead of chloride anion) and employed a different cutoff distance (6 Å instead of 4 Å) than was considered in the present search, two useful comparisons

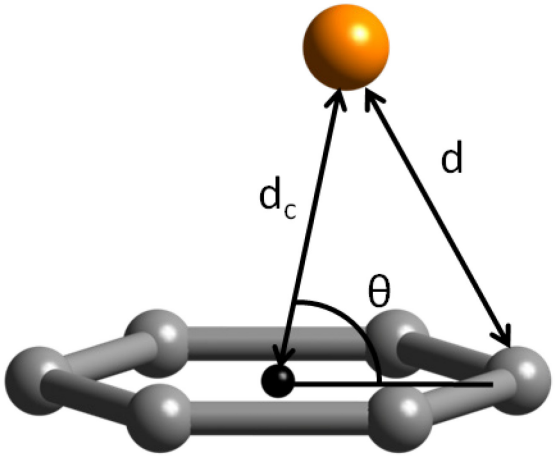

Figure 5.5. Depiction of the parameters for the distance (d) between an anion (orange) and an aromatic ring atom (gray), the distance (d_c) between an anion and the ring centroid (black), and the angle (θ) between the anion – ring centroid vector and the plane of the aromatic ring.

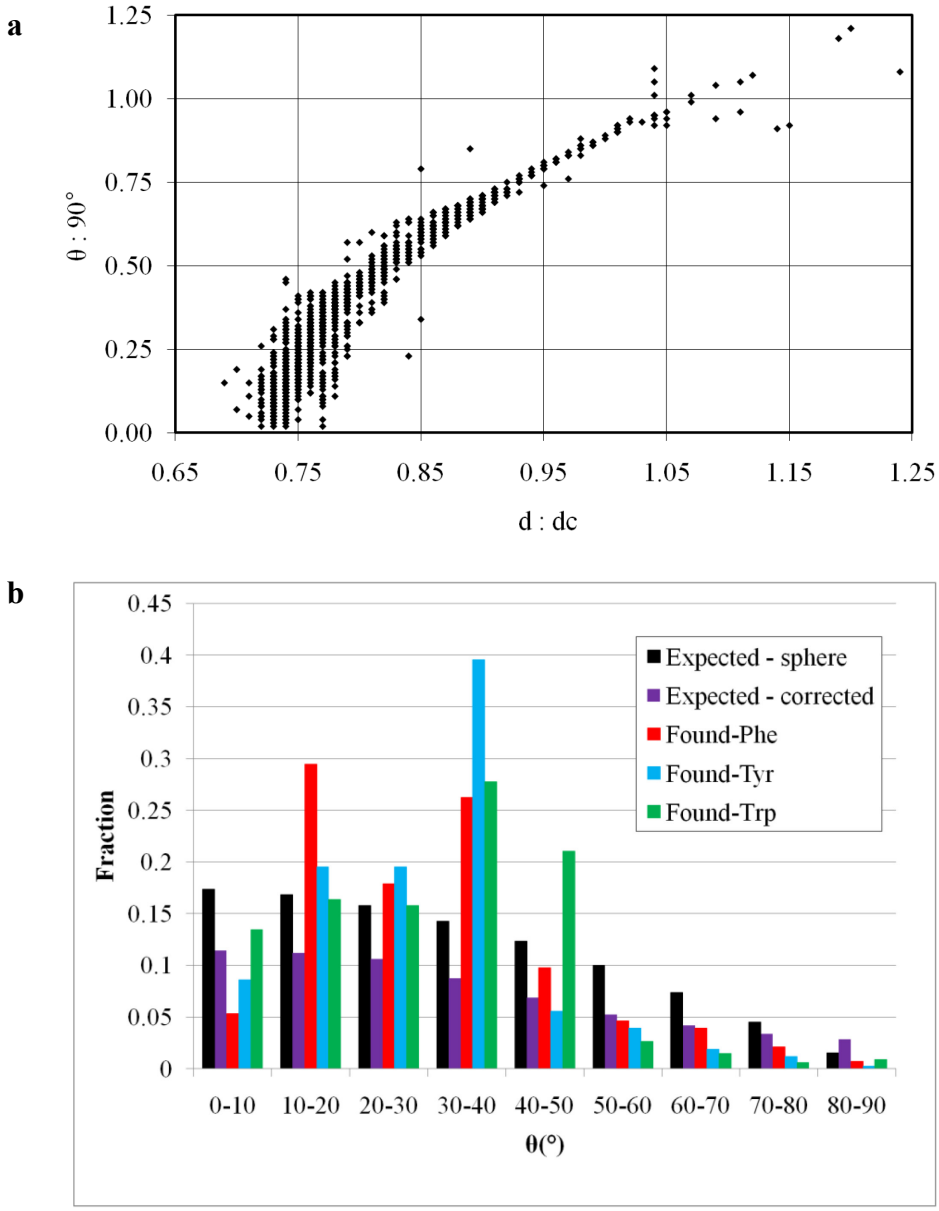

Figure 5.6. Graph depicting the contacts determined by the script *Protein-Cl_Basic+.py*. Points in the regions where $d:d_c \geq 1$ and $\theta:90° \approx 1$ represent likely candidates for anion-π interactions (**a**). Graphical distribution of the data found by the script *Protein-Cl_Basic+.py*. The *expected – sphere* values shown are derived from the appropriate volumes inside of a sphere and the *expected – corrected* values are derived from a sphere around a benzene molecule. This graph takes into account that no anion can exist within the atomic radius of a carbon or hydrogen atom. These values were determined by the script *Expected_Distribution_2.py* (**b**).

can be made between the two sets of results. The first one is that in the 80-90° region (Figure 5.6b), the region where one would expect to see ideal anion-π interactions, the fraction of contacts observed is less than what is statistically expected in both cases. These results suggest that the anion-π interaction does not occur with any significant frequency in the proteins considered with the script and criteria used. The second region of note is the range 30-40° (Figure 5.6b). Whereas Jackson, *et al.* observe only expected behavior in that region for the carboxylate anions, the high frequency of contacts in this range indicate that this position is the preferred point of interaction for chloride anions with aromatic rings in protein structures. Similar results are observed for the script *Protein-I_Basic+.py* (Figure 5.7) with the notable exception that no interactions are observed in the 80-90° region.

The generally poor R-values and resolutions observed in protein structures (Table 5.1) can make it difficult to accurately identify single unbound atoms, or in this case chloride anion. As was also previously discussed, a practice for protein crystallographers is to adjust the position of anions so that they are not in van der Waals contact with other atoms.[138-139] It is also possible to misidentify chloride anions as water molecules and vice versa.[140] In general this means the chloride anions are a challenging candidate for a search such as this one. The larger iodide anion is able to avoid many of these problems, but as evidenced in Figure 5.7b, no iodide anion···arene interactions were observed in the 80°-90° range.

It must be made clear at this point that the data reported in Figures 5.6 and 5.7 do not represent the number of anion – arene contacts found by the search, but the number

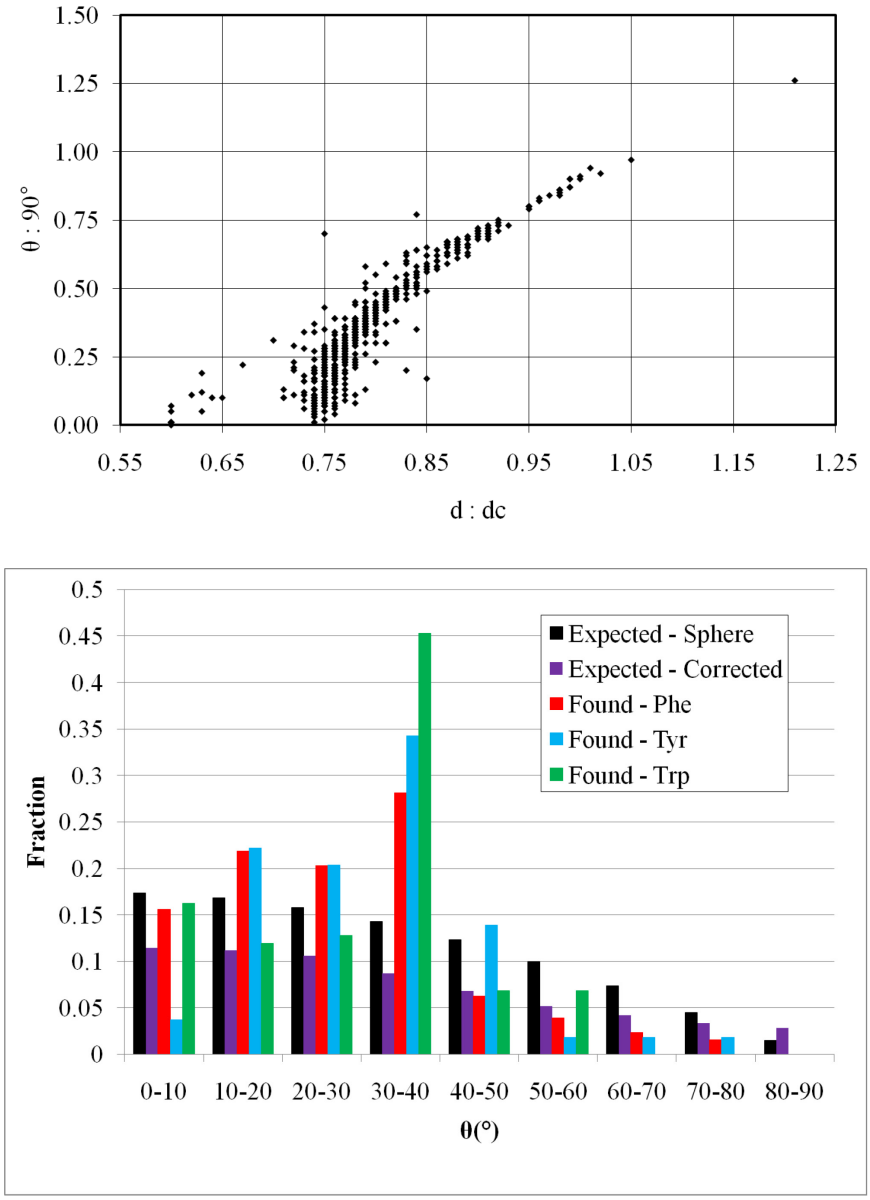

Figure 5.7. Graph depicting the contacts determined by the script *Protein-I_Basic+.py*. Points in the regions where $d:d_c \geq 1$ and $\theta:90° \approx 1$ represent likely candidates for anion-π interactions (**a**). Graphical distribution of the data found by the script *Protein-I_Basic+.py* (**b**). The *expected* data were determined using the same methods as in Figure 5.6b.

Table 5.1. Resolutions and R-values for all protein structures found by *Protein-Cl_Basic+.py* to contain angles above 60°*. The resolution is from the .pdb file, as reported by the script. The R-values were retrieved from the PDB (http://www.pdb.org) directly on September 26, 2010.

Protein	Resolution (Å)	R-Value	Angle, θ† (°)	Protein	Resolution (Å)	R-Value	Angle, θ† (°)
1GKZ	2.20	0.237 (obs.)	89	2FPU	1.80	0.185 (obs.)	68
2OWR	2.30	0.255 (obs.)	88	1IS9	1.03	0.131 (work)	67
1FP8	2.30	0.197 (obs.)	79	1J07	2.35	0.199 (obs.)	66
2AZT	2.70	0.239 (obs.)	76	1H6G	2.20	0.193 (obs.)	65
2IW5	2.57	0.204 (obs.)	75	1HKX	2.65	0.246 (obs.)	64
1V3Z	1.72	0.169 (obs.)	72	2NRT	1.50	0.187 (obs.)	64
2DHO	1.60	0.173 (work)	72	1O1H	1.40	0.156 (obs.)	63
2GFG	2.12	0.277 (obs.)	71	2GHW	2.30	0.251 (obs.)	62
1T6H	2.01	0.160 (obs.)	70	2GO7	2.10	0.173 (obs.)	61
1ZSV	2.30	0.197 (obs.)	70	2IGA	1.95	0.185 (work)	61
2OU3	1.85	0.163 (obs.)	69	2QML	1.55	0.181 (obs.)	61
2O79	1.80	0.150 (obs.)	68				

*Please note that 60° was an arbitrary cutoff.

†The angle, θ, refers to the angle between the anion – ring centroid vector and the anion – ring atom vector. If multiple anion – ring atom contacts (d < 4.0 Å) were observed for a given anion – arene pair, the average value is given here.

of anion – ring atom contacts. Given this fact, a particular anion···arene interaction may give rise to several anion – aromatic ring atom contacts under the script used in this search. It may be possible to correct this redundancy in the data by defining the angle θ by using the vector normal to the plane of the ring (a unique vector defining the ring) and the ring centroid – anion vector. The current script uses the ring centroid – ring atom vector to define this angle, giving rise to a unique angle to each anion – ring atom contact. It should also be possible to write a function to prevent the script from considering ring atoms belonging to previously identified aromatic rings. This should be done in the future in order to render this exercise useful for future considerations of where to look for anion-pi contacts in proteins.

Specific Examples of Potential Anion-π Interactions Found by the PDB Search

Only three structures, 1GKZ[141], 2OWR[142], and 1FP8[143] will be discussed, as these three structures are the ones exhibiting the most favorable θ values for the anion···arene interaction, 89°, 88° and 79°, respectively. The next structure to consider would be 2AZT[144] with a θ value of 76° (Table 5.1).

1GKZ (Figure 5.8a) is a branched-chain alpha-ketoacid dehydrogenase kinase complexed with ADP published by Machius, *et al*.[141] Phe 234 A was found to be in close contact with Cl 502 A (Figure 5.8b) averaging 3.9 Å between the chloride anion and the five carbon atoms in close-contact (less than 4.0 Å) with the anion (Table 5.2). While the distances are further than the aforementioned 3.5 Å, the position of the chloride ion makes 1GKZ are good example of a potential anion-π interaction.

An even better example than 1GKZ is 2OWR (Figure 5.9a). Reported by Schormann, *et al*., 2OWR is a vaccinia virus uracil-DNA glycosylase.[142] In this case Trp 119 C was observed to be in close-contact with Cl 600 (Figure 5.9b). In addition to the well positioned chloride anion, the average distance between the anion and the eight close-contact ring atoms is 3.6 Å with four of the eight atoms being in van der Waals contact ($d \leq 3.5$ Å) (Table 5.3). These are the closest distances observed in this search and, as such, are extremely promising.

1FP8, amylomaltase from *Thermus thermophilus* HB8 (Figure 5.10a) reported by Uitdehaag, *et al*.[143], is not as good of an example as 1GKZ or 2OWR. In this structure Cl 502 was shown to be in close contact with Tyr 59 A with an average distance of 3.7 Å between the chloride anion and the three close contact carbon atoms (Table 5.4). While the distances are comparable to those observed in 1GKZ and 2OWR, the position of the anion (over one of the carbon atoms as opposed to the ring centroid) makes this interaction more similar to a π-type charge-transfer than an anion-π.[40] The remaining anion···arene interactions found by the search were observed at lower angles as shown in Figure 5.6b and Table 5.1, supporting the results of Jackson, *et al*.[136] and Marsili, *et al*.[57] As stated earlier, the number of anion – arene interactions found in this range are insignificant; these examples are included only to illustrate possible anion-π interactions in a protein structure.

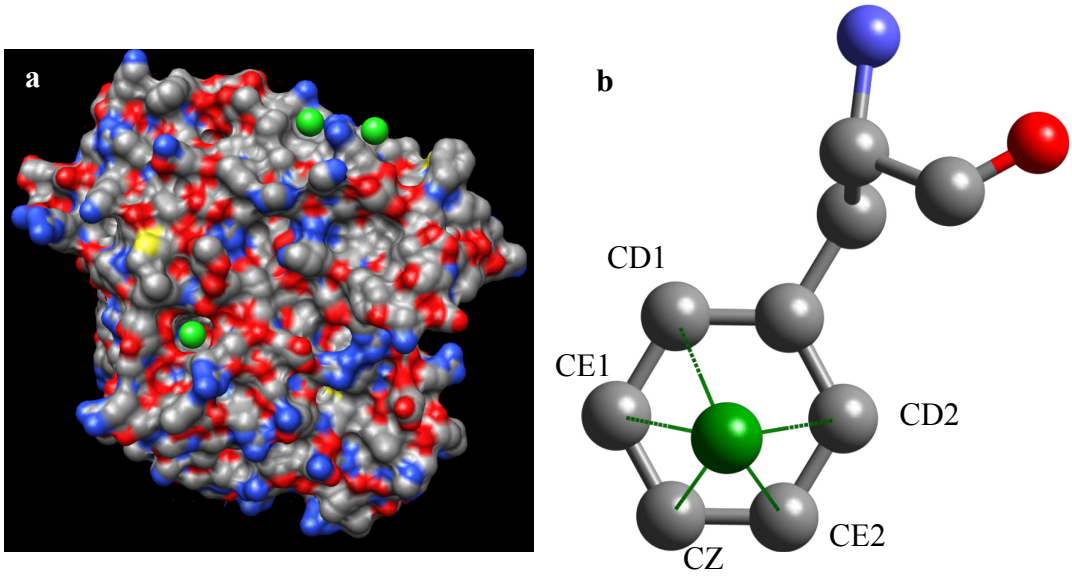

Figure 5.8. Protein 1GKZ (**a**). Interaction between Phe 234 A and Cl 502 A (**b**) with the green lines representing the close contacts (≤ 4.0 Å). Carbon atoms (gray), nitrogen atoms (blue), oxygen atoms (red), sulfur atoms (yellow) and chloride anions (green).

Table 5.2. Distances between Cl 502 A and the carbon atoms from Phe 234 A in close contact.

Ring Atom	C-Cl distance (Å)	Ring Atom	C-Cl distance (Å)
CD1	4.0	CE2	3.8
CE1	3.9	CD2	3.9
CZ	3.8		

Reference Figure 5.8b. Atom labels are standard labels used by the PDB.

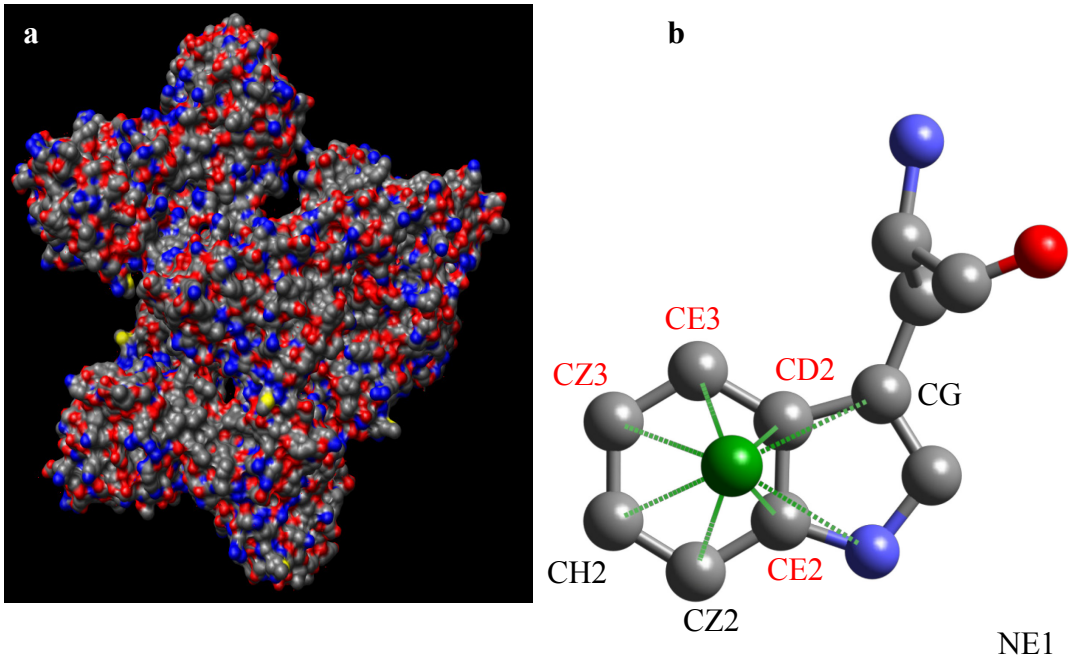

Figure 5.9. Protein 2OWR (**a**). Interaction between Trp 119 C and Cl 600 (**b**) with the green lines representing the close contacts (≤ 4.0 Å). Carbon atoms (gray), nitrogen atoms (blue), oxygen atoms (red), sulfur atoms (yellow) and chloride anions (green).

Table 5.3. Distances between Cl 600 and the carbon atoms from Trp 119 C in close contact.

Ring Atom	C-Cl distance (Å)	Ring Atom	C-Cl distance (Å)
CG	3.9	CH2	3.6
CD2	3.2	CZ2	3.6
CE3	3.4	CE2	3.3
CZ3	3.5	NE1	3.9

Reference Figure 5.9b. Atom labels are standard labels used by the PDB. Values in red represent those contacts with $d \leq 3.5$ Å.

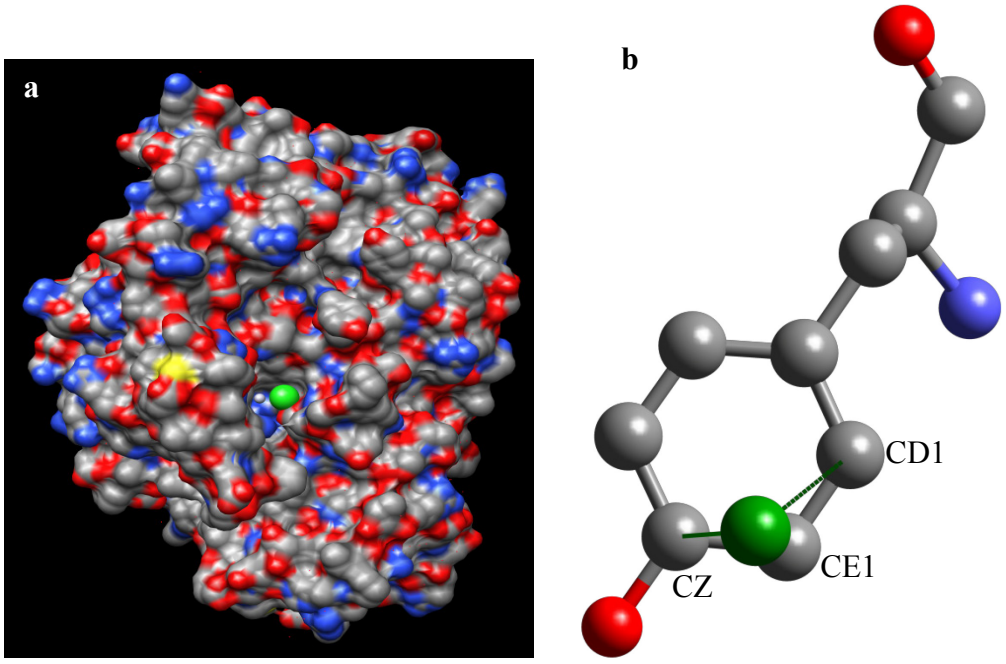

Figure 5.10. Protein 1FP8 (**a**). Interaction between Tyr 59 A and Cl 502 (**b**) with the green lines representing the close contacts (d≤ 4.0 Å). Carbon atoms (gray), nitrogen atoms (blue), oxygen atoms (red), sulfur atoms (yellow) and chloride anions (green).

Table 5.4. Distances between Cl 502 and the carbon atoms from Tyr 59 A in close contact.

Ring Atom	C-Cl distance (Å)
CD1	3.8
CE1	3.5
CZ	3.6

Reference Figure 5.10b. Atom labels are standard labels used by the PDB.

Conclusions

Current literature is sparse on the topic of the biological occurrence of anion-π interactions. The current work includes small molecules composed of biologically relevant species,[121-122] artificial models of biological systems[67,124] and previous searches of the PDB did not provide any evidence of potential anion-π interactions.[57,136] In order to attempt to identify examples of anion-π interactions in protein structures, a new series of searches were performed focusing on the chloride and iodide anions. At this stage, the results of these searches are inconclusive. While anion-π interactions may be present in protein structures, they are not common occurrences for the anions thus far investigated.

CHAPTER VI

SUMMARY AND CONCLUSIONS

Given the large number of claims about anion-π interactions in the literature, many unsupported, there is a compelling need for further research into this topic. Despite a growing body of papers on the subject, fundamental questions as to the nature and definition of anion-π interactions still remain. The controversy surrounding anion-π interactions notwithstanding, research involving application of anion-π interactions is underway.[47,60,67]

As part of ongoing research regarding templation of supramolecular architectures using anion-π interactions, the ligand 3,6-bis(2′-pyrimidyl)-1,2,4,5-tetrazine (bmtz) was synthesized and reacted with $[Cu(NCMe)_4][BF_4]$ to form the octanuclear complex $[Cu_8(bmtz)_6][BF_4]_6 \cdot 6$ MeCN (**1**). Although the complex itself is not templated by an anion, the anions residing along the outside of the cluster participate in crystal packing by means of an anion-π/CH-bonding bridge. There is an *in situ* redox reaction during the formation of **1** resulting in the reduction of bmtz and the formation of a second paramagnetic compound only isolated as an intensely colored blue precipitate (**2**). A direct route to the synthesis of **2** was found and preliminary characterization indicate the presence of the expected copper(II) species, but further work is necessary to fully identify characterize the material. Additionally, the synthesis of **1** requires optimization so that full characterization can be performed. A rich electrochemistry is expected for

the cluster **1**, but sufficiently pure samples have not been isolated to perform cyclic voltammetry experiments.

Computational studies addressing the question of whether or not anion-π interactions can occur between the complex anions tetrafluoroborate ($[BF_4]^-$) and hexafluorophosphate ($[PF_6]^-$) and the olefins tetracyanoethylene (TCNE), 7,7,8,8-tetracyanoquinodimethane (TCNQ), 7,7,8,8-tetracyano-1,2,4,5-tetrafluoroquinodimethane ($TCNQF_4$) and octacyanoquinodimethane ($TCNQ(CN)_4$) have been completed using both Density Functional Theory (DFT) and *ab initio* methods along with critical point analysis (AIM) and Natural Bonding Orbitals (NBO) analysis. While the computational results clearly indicate a favorable interaction between the anions and olefins in all cases, solution (UV/visible spectroscopy) and solid state (single crystal X-ray diffraction) studies have yet to be completed.

Extensive research regarding the simultaneous anion-π and π-type charge-transfer (CT) interactions that occur in the compounds $\{([n\text{-}Bu_4N][X])_3[HAT\text{-}(CN)_6]_2\}3C_6H_6$ (X = Br, I) has been performed in solution and in the solid state in the Dunbar laboratories.[51,73] DFT and NBO computations have been completed and are in full agreement with the experimental work previously reported. While solution and computational evidence point toward the existence of a chloride anion analogue of $\{([n\text{-}Bu_4N][X])_3[HAT\text{-}(CN)_6]_2\}\cdot 3C_6H_6$, no co-crystallized structure involving chloride anions has been achieved. Further work on this topic will focus on this task.

Systematic searches of the Protein Data Bank (PDB) have not revealed conclusive evidence of anion-π interactions involving proteins. To the best of our

knowledge, no such evidence has been reported anywhere in the literature and the question of the biological relevance of anion-π interactions remains to be answered.

REFERENCES

1. Lehn, J.-M. *Supramolecular Chemistry*; VCH: Weinheim, Germany, 1995.

2. Steed, J. W.; Atwood, J. L. *Supramolecular Chemistry*; John Wiley & Sons, Ltd.: Chichester, UK, 2000.

3. *Supramolecular Chemistry of Anions*; Bianchi, A.; Bowman-James, K.; García-España, E., Eds.; Wiley-VCH: New York, 1997.

4. García-España, E.; Díaz, P.; Llinares, J. M.; Bianchi, A. *Coord. Chem. Rev.* **2006**, *250*, 2952-2986.

5. Ballester, P. *Struct. Bond.* **2008**, *129*, 127-174.

6. Gamez, P.; Mooibroek, T. J.; Teat, S. J.; Reedijk, J. *Acc. Chem. Res.* **2007**, *40*, 435-444.

7. Schottel, B. L.; Chifotides, H. T.; Dunbar, K. R. *Chem. Soc. Rev.* **2008**, *37*, 68-83.

8. Biswas, C.; Drew, M. G. B.; Escudero, D.; Frontera, A.; Ghosh, A. *Eur. J. Inorg. Chem.* **2009**, 2238-2246.

9. Convertino, M.; Pellarin, R.; Catto, M.; Carotti, A.; Caflisch, A. *Protein Sci.* **2009**, *18*, 792-800.

10. Egli, M.; Sarkhel, S. *Acc. Chem. Res.* **2007**, *40*, 197-205.

11. Escudero, D.; Estarellas, C.; Frontera, A.; Quiñonero, D.; Deyà, P. M. *Chem. Phys. Lett.* **2010**, *485*, 221-225.

12. Gung, B. W.; Zou, Y.; Xu, Z. G.; Amicangelo, J. C.; Irwin, D. G.; Ma, S. Q.; Zhou, H. C. *J. Org. Chem.* **2008**, *73*, 689-693.

13. Lu, Z. L.; Gamez, P.; Mutikainen, I.; Turpeinen, U.; Reedijk, J. *Cryst. Growth Design* **2007**, *7*, 1669-1671.

14. Matter, H.; Nazaré, M.; Güssregen, S.; Will, D. W.; Schreuder, H.; Bauer, A.; Urmann, M.; Ritter, K.; Wagner, M.; Wehner, V. *Angew. Chem., Int. Ed.* **2009**, *48*, 2911-2916.

15. Mooibroek, T. J.; Gamez, P.; Reedijk, J. *CrystEngComm* **2008**, *10*, 1501-1515.

16. Wan, C.-Q.; Chen, X.-D.; Mak, T. C. W. *CrystEngComm* **2008**, *10*, 475-478.

17. Cabaleiro-Lago, E. A.; Rodríguez-Otero, J.; Peña-Gallego, A. *J. Phys. Chem. A* **2008**, *112*, 6344-6350.

18. Cabaleiro-Lago, E. M.; Peña-Gallego, A.; Rodríguez-Otero, J. *J. Chem. Phys.* **2008**, *128*, 8.

19. Cabellero, A. G.; Croft, A. K.; Nalli, S. M. *Tetrahedron Lett.* **2008**, *49*, 3613-3615.

20. Choudhury, S. R.; Chen, C.-Y.; Seth, S.; Kar, T.; Lee, H. M.; Colacio, E.; Mukhopadhyay, S. *J. Coord. Chem.* **2009**, *62*, 540-551.

21. Escudero, D.; Estarellas, C.; Frontera, A.; Quiñonero, D.; Deyà, P. M. *Chem. Phys. Lett.* **2009**, *468*, 280-285.

22. Escudero, D.; Frontera, A.; Quiñonero, D.; Deyà, P. M. *J. Phys. Chem. A* **2008**, *112*, 6017-6022.

23. Plevin, M. J.; Bryce, D. L.; Boisbouvier, J. *Nature Chem.* **2010**, *2*, 466-471.

24. Quinoñero, D.; Frontera, A.; Escudero, D.; Ballester, P.; Costa, A.; Deyà, P. M. *Theor. Chem. Acc.* **2008**, *120*, 385-393.

25. Tsuzuki, S.; Fujii, A. *Phys. Chem. Chem. Phys.* **2008**, *10*, 2584-2594.

26. Xu, G. H.; Wang, W. *Acta Crystallogr., Sect. E* **2008**, *64*, M1198-U1880.

27. Zang, S. Q.; Mak, T. C. W. *Inorg. Chem.* **2008**, *47*, 7094-7105.

28. Zang, S. Q.; Zhao, L.; Mak, T. C. W. *Organometallics* **2008**, *27*, 2396-2398.

29. Park, C. H.; Simmons, H. E. *J. Am. Chem. Soc.* **1968**, *90*, 2431-2432.

30. Pedersen, C. J. *J. Am. Chem. Soc.* **1967**, *89*, 2495-2496.

31. Schneider, H.-J. *Angew. Chem., Int. Ed. Engl.* **1991**, *30*, 1417-1436.

32. Schneider, H. J.; Werner, F.; Blatter, T. *J. Phys. Org. Chem.* **1993**, *6*, 590-594.

33. Alkorta, I.; Rozas, I.; Elguero, J. *J. Am. Chem. Soc.* **2002**, *124*, 8593-8598.

34. Mascal, M.; Armstrong, A.; Bartberger, M. D. *J. Am. Chem. Soc.* **2002**, *124*, 6274-6276.

35. Quiñonero, D.; Garau, C.; Rotger, C.; Frontera, A.; Ballester, P.; Costa, A.; Deyà, P. M. *Angew. Chem., Int. Ed.* **2002**, *41*, 3389-3392.

36. Park, C. H.; Simmons, H. E. *J. Amer. Chem. Soc.* **1968**, *90*, 2429-2431.

37. Garau, C.; Frontera, A.; Quiñonero, D.; Ballester, P.; Costa, A.; Deyà, P. M. In *Recent Research Developments in Chemical Physics*; Pandalai, S. G., Ed.; Transworld Research Network: Kerala, India, 2004; Vol. 5, p 227-255.

38. Wheeler, S. E.; Houk, K. N. *J. Phys. Chem. A* **2010**, *114*, 8658-8664.

39. Buncel, E.; Norris, A. R.; Russell, K. E. *Q. Rev., Chem. Soc.* **1968**, *22*, 123-146.

40. Berryman, O. B.; Bryantsev, V. S.; Stay, D. P.; Johnson, D. W.; Hay, B. P. *J. Am. Chem. Soc.* **2007**, *129*, 48-58.

41. Bowman-James, K. *Acc. Chem. Res.* **2005**, *38*, 671-678.

42. Hay, B. P.; Bryantsev, V. S. *Chem. Commun.* **2008**, 2417-2428.

43. Quiñonero, D.; Garau, C.; Frontera, A.; Ballester, P.; Costa, A.; Deyà, P. M. *Chem. Phys. Lett.* **2002**, *359*, 486-492.

44. Alberto, M. E.; Mazzone, G.; Russo, N.; Sicilia, E. *Chem. Commun.* **2010**, *46*, 5894-5896.

45. Das, A.; Choudhury, S. R.; Dey, B.; Yalamanchili, S. K.; Helliwell, M.; Gamez, P.; Mukhopadhyay, S.; Estarellas, C.; Frontera, A. *J. Phys. Chem. B* **2010**, *114*, 4998-5009.

46. Garcia-Raso, A.; Albertí, F. M.; Fiol, J. J.; Lagos, Y.; Torres, M.; Molins, E.; Mata, I.; Estarellas, C.; Frontera, A.; Quiñonero, D.; Deyà, P. M. *Eur. J. Org. Chem.* **2010**, 5171-5180.

47. Jones, S. G.; Yau, H. M.; Davies, E.; Hook, J. M.; Youngs, T. G. A.; Harper, J. B.; Croft, A. K. *Phys. Chem. Chem. Phys.* **2010**, *12*, 1873-1878.

48. Lucas, X.; Frontera, A.; Quiñonero, D.; Deyà, P. M. *J. Phys. Chem. A* **2010**, *114*, 1926-1930.

49. Quiñonero, D.; Deyà, P. M.; Carranza, M. P.; Rodríguez, A. M.; Jalon, F. A.; Manzano, B. R. *Dalton Trans.* **2010**, *39*, 794-806.

50. Arunachalam, M.; Ghosh, P. *Org. Lett.* **2010**, *12*, 328-331.

51. Chifotides, H. T.; Schottel, B. L.; Dunbar, K. R. *Angew. Chem., Int. Ed.* **2010**, *49*, 7202-7207.

52. Jian, F.-F.; Wang, J.; Huang, L.-H.; Wang, X.; Xiao, H.-L. *J. Mol. Struct.* **2010**, *973*, 136-143.

53. Smith, G.; Wermuth, U. D. *Acta Crystallogr., Sect. E* **2010**, *E66*, o1173.

54. Smith, G.; Wermuth, U. D.; Young, D. J. *Acta Crystallogr., Sect. E* **2010**, *E66*, o1184-o1185.

55. Wan, C. Q.; Zhao, L.; Mak, T. C. W. *Inorg. Chem.* **2010**, *49*, 97-107.

56. Kim, D.; Tarakeshwar, P.; Kim, K. S. *J. Phys. Chem. A* **2004**, *108*, 1250-1258.

57. Marsili, S.; Chelli, R.; Schettino, V.; Procacci, P. *Phys. Chem. Chem. Phys.* **2008**, *10*, 2673-2685.

58. Hiraoka, K.; Mizuse, S.; Yamabe, S. *J. Phys. Chem.* **1987**, *91*, 5294-5297.

59. Albrecht, M.; Müller, M.; Mergel, O.; Rissanen, K.; Valkonen, A. *Chem.--Eur. J.* **2010**, *16*, 5062-5069.

60. Berryman, O. B.; Hof, F.; Hynes, M. J.; Johnson, D. W. *Chem. Commun.* **2006**, 506-508.

61. Garau, C.; Frontera, A.; Ballester, P.; Quiñonero, D.; Costa, A.; Deyà, P. M. *Eur. J. Org. Chem.* **2005**, 179-183.

62. Mascal, M. *Angew. Chem., Int. Ed.* **2006**, *45*, 2890-2893.

63. Mascal, M.; Yakovlev, I.; Nikitin, E. B.; Fettinger, J. C. *Angew. Chem., Int. Ed.* **2007**, *46*, 8782-8784.

64. Campos-Fernández, C. S.; Schottel, B. L.; Chifotides, H. T.; Bera, J. K.; Bacsa, J.; Koomen, J. M.; Russell, D. H.; Dunbar, K. R. *J. Am. Chem. Soc.* **2005**, *127*, 12909-12923.

65. Schottel, B. L.; Chifotides, H. T.; Shatruk, M.; Chouai, A.; Pérez, L. M.; Bacsa, J.; Dunbar, K. R. *J. Am. Chem. Soc.* **2006**, *128*, 5895-5912.

66. Davis, J. T. *Nature Chem.* **2010**, *2*, 516-517.

67. Gorteau, V.; Bollot, G.; Mareda, J.; Perez-Velasco, A.; Matile, S. *J. Am. Chem. Soc.* **2006**, *128*, 14788-14789.

68. Frontera, A.; Saczewski, F.; Gdaniec, M.; Dziemidowicz-Borys, E.; Kurland, A.; Deyà, P. M.; Quiñonero, D.; Garau, C. *Chem.-- Eur. J.* **2005**, *11*, 6560-6567.

69. Davis, A. P.; Sheppard, D. N.; Smith, B. D. *Chem. Soc. Rev.* **2007**, *36*, 348-357.

70. Gitlin, I.; Carbeck, J. D.; Whitesides, G. M. *Angew. Chem., Int. Ed.* **2006**, *45*, 3022-3060.

71. Yamauchi, O.; Odani, A.; Hirota, S. *Bull. Chem. Soc. Jpn.* **2001**, *74*, 1525-1545.

72. Gallivan, J. P.; Dougherty, D. A. *Proc. Natl. Acad. Sci. USA* **1999**, *96*, 9459-9464.

73. Szalay, P. S.; Galán-Mascarós, J. R.; Schottel, B. L.; Bacsa, J.; Pérez, L. M.; Ichimura, A. S.; Chouai, A.; Dunbar, K. R. *J. Cluster Sci.* **2004**, *15*, 503-530.

74. Campos-Fernández, C. S.; Clérac, R.; Dunbar, K. R. *Angew. Chem., Int. Ed.* **1999**, *38*, 3477-3479.

75. Campos-Fernández, C. S.; Clérac, R.; Koomen, J. M.; Russell, D. H.; Dunbar, K. R. *J. Am. Chem. Soc.* **2001**, *123*, 773-774.

76. Schottel, B. L.; Bacsa, J.; Dunbar, K. R. *Chem. Commun.* **2005**, 46-47.

77. Schottel, B. L. Ph.D. thesis, Texas A&M University, College Station, TX, 2007.

78. Kubas, G. J. *Inorganic Syntheses* **1979**, *19*, 90-92.

79. Geldard, J. F.; Lions, F. *J. Org. Chem.* **1965**, *30*, 318-319.

80. Kaim, W.; Fees, J. *Z. Naturforsch., B Chem. Sci.* **1995**, *50*, 123-127.

81. Glöckle, M.; Hübler, K.; Kümmerer, H.-J.; Denninger, G.; Kaim, W. *Inorg. Chem.* **2001**, *40*, 2263-2269.

82. Hendrich, M.; *SpinCount*, version 3.1.2; Carnegie Mellon University: Pittsburgh, PA.

83. *SMART and SAINT*, Siemens Analytical X-ray Instruments, Inc.: Madison, WI, 1996.

84. Sheldrick, G. M.; *SADABS*, University of Gottingen: Gottingen, Germany, 1996.

85. Sheldrick, G. M. *Acta Crystallogr., Sect. A* **2008**, *A64*, 112-122.

86. Barbour, L. J. *J. Supramol. Chem.* **2003**, *1*, 189-191.

87. Parr, R. G.; Yang, W. *Density-Functional Theory of Atoms and Molecules*; Oxford Press: Oxford, 1989.

88. Frisch, M. J.; Trucks, G. W.; Schlegel, H. B.; Scuseria, G. E.; Robb, M. A.; Cheeseman, J. R.; Montgomery Jr., J. A.; Vreven, T.; Kuden, K. N.; Burant, J. C.; J.M., M.; Iyengar, S. S.; Tomasi, J.; Barone, V.; Mennucci, B.; Cossi, M.; Scalmani, G.; Rega, N.; Petersson, G. A.; Nakatsuji, H.; Hada, M.; Ehara, M.; Toyota, K.; Fukuda, R.; Hasegawa, J.; Ishida, M.; Nakajima, T.; Honda, Y.; Kitao, O.; Nakai, H.; Klene, M.; Li, X.; Knox, J. E.; Hrtatchain, H. P.; Cross, J. B.; Adamao, C.; Jaramillo, J.; Gompersts, R.; Stramann, R. E.; Yazyev, O.; Austin, A. J.; Cammi, R.; Pomelli, C.; Ochterski, J. W.; Ayala, P. Y.; Morokuma, K.; Voth, G. A.; Salvador, P.; Dannenberg, J. J.; Zakrzewski, V. G.; Dapprich, S.; Daniels, A. D.; Strain, M. C.; Farkas, O.; Malick, D. K.; Rabuck, A. D.; Raghavachari, K.; Foresman, J. B.; Ortiz, J. V.; Cui, Q.; Baboul, A. G.; Clifford, S.; Cioslowski, J.; Stefanov, B. B.; Liu, G.; Liashenko, A.; Piskorz, P.; Komaromi, I.; Maritn, R. L.; Fox, D. J.; Keith, T.; Al-Laham, M. A.; Peng, C. Y.; Nanayakkara, A.; Challacombe, M.; Gill, P. M. W.; Johnson, B.; Chen, W.; Wong, M. W.; Gonzalez, C.; Pople, J. A.; *Gaussian03*, Gaussian, Inc.: Pittsburgh, PA, 2003.

89. Becke, A. D. *J. Chem. Phys.* **1993**, *98*, 5648-5652.

90. Lee, C. T.; Yang, W. T.; Parr, R. G. *Phys. Rev. B* **1988**, *37*, 785-789.

91. Krishnan, R.; Binkley, J. S.; Seeger, R.; Pople, J. A. *J. Chem. Phys.* **1980**, *72*, 650-654.

92. McLean, A. D.; Chandler, G. S. *J. Chem. Phys.* **1980**, *72*, 5639-5648.

93. *Cerius*^{2}, versions 4.8 and 4.10; Accelyrs, Inc.: San Diego, CA.

94. Janiak, C. *Dalton* **2000**, 3885-3896.

95. Cotton, F. A.; Wilkinson, G.; Gaus, P. L. *Basic Inorganic Chemistry*; Third ed.; John Wiley & Sons, Inc.: New York, 1995.

96. Collman, J. P.; Christian, P. A.; Current, S.; Denisevich, P.; Halbert, T. R.; Schmittou, E. R.; Hodgson, K. O. *Inorg. Chem.* **1976**, *15*, 223-227.

97. Corey, E. J.; Rohde, J. J.; Fischer, A.; Azimioara, M. D. *Tetrahedron Lett.* **1997**, *38*, 33-36.

98. Liddle, B. J.; Hall, D.; Lindeman, S. V.; Smith, M. D.; Gardinier, J. R. *Inorg Chem* **2009**, *48*, 8404-8414.

99. Reger, D. L.; Gardinier, J. R.; Smith, M. D. *Inorg Chem* **2004**, *43*, 3825-3832.

100 Withers, S. G.; Street, I. P.; Rettig, S. J. *Can. J. Chem.* **1986**, *64*, 232-236.

101. Drago, R. S. *Physical Methods for Chemists*, 2nd ed.; Surfside Scientific Publishers: Gainsville, FL, USA, 1992.

102. Youinou, M. T.; Rahmouni, N.; Fischer, J.; Osborn, J. A. *Angew. Chem., Int. Ed. Engl.* **1992**, *31*, 733-735.

103. Rosokha, Y. S.; Lindeman, S. V.; Rosokha, S. V.; Kochi, J. K. *Angew. Chem., Int. Ed.* **2004**, *43*, 4650-4652.

104. Rosokha, S. V.; Kochi, J. K. In *Halogen Bonding: Fundamentals and Applications*; Springer-Verlag: Berlin, 2008; Vol. 126, p 137-160.

105. Han, B.; Lu, J. J.; Kochi, J. K. *Cryst. Growth Design* **2008**, *8*, 1327-1334.

106. Lu, J. J.; Kochi, J. K. *Cryst. Growth Design* **2009**, *9*, 291-296.

107. Headgordon, M.; Pople, J. A.; Frisch, M. J. *Chem. Phys. Lett.* **1988**, *153*, 503-506.

108. Møller, C.; Plesset, M. S. *Phys. Rev.* **1934**, *46*, 0618-0622.

109. McWeeny, R.; Diercksen, G. *J. Chem. Phys.* **1968**, *49*, 4852-4856.

110. Bader, R. F. W. *Atoms in Molecules: A Quantum Theory*; Clarendon Press: Oxford, 1990; Vol. 22. p 1-438.

111. Bader, R. F. W. *Chem. Rev.* **1991**, *91*, 893-928.

112. Glendening, E. D.; Badenhoop, J. K.; Reed, A. E.; Carpenter, J. E.; Bohmann, J. A.; Morales, C. M.; Weinhold, F.; *GenNBO*, version 5.0W; Theoretical Chemistry Institute, Univerisity of Wisconsin: Madison, WI, 2001.

113. Cramer, C. J. *Essentials of Computational Chemistry*, 2nd ed.; John Wiley & Sons, Ltd.: Chichester, UK, 2004.

114. Dorsey, C. L.; Gabbaï, F. P. *Organometallics* **2008**, *27*, 3065-3069.

115. Furukawa, S.; Okubo, T.; Masaoka, S.; Tanaka, D.; Chang, H. C.; Kitagawa, S. *Angew. Chem., Int. Ed.* **2005**, *44*, 2700-2704.

116. Piglosiewicz, I. M.; Beckhaus, R.; Wittstock, G.; Saak, W.; Haase, D. *Inorg. Chem.* **2007**, *46*, 7610-7620.

117. Hay, P. J.; Wadt, W. R. *J. Chem. Phys.* **1985**, *82*, 299-310.

118. Wadt, W. R.; Hay, P. J. *J. Chem. Phys.* **1985**, *82*, 284-298.

119. Wendt, M.; Weinhold, F.; *NBOView*; University of Wisconsin: Madison, Wisconsin, 2001.

120. Turner, D. R.; Paterson, M. J.; Steed, J. W. *J. Org. Chem.* **2006**, *71*, 1598-1608.

121. Garcia-Raso, A.; Alberti, F. M.; Fiol, J. J.; Tasada, A.; Barceló-Oliver, M.; Molins, E.; Escudero, D.; Frontera, A.; Quiñonero, D.; Deyà, P. M. *Inorg. Chem.* **2007**, *46*, 10724-10735.

122. García, B.; Garcia-Tojal, J.; Ruiz, R.; Gil-García, R.; Ibeas, S.; Donnadieu, B.; Leal, J. M. *J. Inorg. Biochem.* **2008**, *102*, 1892-1900.

123. Burger, K.; Hennig, L.; Tsouker, P.; Spengler, J.; Albericio, F.; Koksch, B. *Amino Acids* **2006**, *31*, 55-62.

124. Banerji, N.; Bhosale, R.; Bollot, G.; Butterfield, S. M.; Furstenberg, A.; Gorteau, V.; Hagihara, S.; Hennig, A.; Maity, S.; Mareda, J.; Matile, S.; Mora, F.; Perez-Velasco, A.; Ravikumar, V.; Kishore, R. S. K.; Sakai, N.; Tran, D. H.; Vauthey, E.; Int Union Pure Applied Chemistry: Turin, Italy, 2008, p 1873-1882.

125. Gorteau, V.; Bollot, G.; Mareda, J.; Matile, S. *Org. Biomol. Chem.* **2007**, *5*, 3000-3012.

126. Perez-Velasco, A.; Gorteau, V.; Matile, S. *Angew. Chem., Int. Ed.* **2008**, *47*, 921-923.

127. Dawson, R. E.; Hennig, A.; Weimann, D. P.; Emery, D.; Ravikumar, V.; Montenegro, J.; Takeuchi, T.; Gabutti, S.; Mayor, M.; Mareda, J.; Schalley, C. A.; Matile, S. *Nature* **2010**, *2*, 533-538.

128. Ahuja, R.; Samuelson, A. G. *CrystEngComm* **2003**, *5*, 395-399.

129. Capó, M.; Benet-Buchholz, J.; Ballester, P. *Inorg. Chem.* **2008**, *47*, 10190-10192.

130. Garau, C.; Frontera, A.; Quiñonero, D.; Ballester, P.; Costa, A.; Deyà, P. M. *Chem. Phys. Lett.* **2003**, *382*, 534-540.

131. Garau, C.; Quiñonero, D.; Frontera, A.; Ballester, P.; Costa, A.; Deyà, P. M. *New J. Chem.* **2003**, *27*, 211-214.

132. Garau, C.; Quiñonero, D.; Frontera, A.; Escudero, D.; Ballester, P.; Costa, A.; Deyà, P. M. *Chem. Phys. Lett.* **2007**, *438*, 104-108.

133. Hay, B. P.; Custelcean, R. *Cryst. Growth Design* **2009**, *9*, 2539-2545.

134. Mooibroek, T. J.; Black, C. A.; Gamez, P.; Reedijk, J. *Cryst. Growth Design* **2008**, *8*, 1082-1093.

135. Quiñonero, D.; Frontera, A.; Escudero, D.; Ballester, P.; Costa, A.; Deyà, P. M. *ChemPhysChem* **2007**, *8*, 1182-1187.

136. Jackson, M. R.; Beahm, R.; Duvvuru, S.; Narasimhan, C.; Wu, J.; Wang, H.-N.; Philip, V. M.; Hinde, R. J.; Howell, E. E. *J. Phys. Chem. B* **2007**, *111*, 8242-8249.

137. Willis, M. A.; Song, F.; Zhuang, Z.; Krajewski, W.; Chalamasetty, V. R.; Reddy, P.; Howard, A.; Dunaway-Mariano, D.; Herzberg, O. *Proteins: Struct., Funct., Bioinf.* **2005**, *59*, 648-652.

138. Drenth, J.; Mesters, J. *Principles of Protein X-ray Crystallography*; 3rd ed.; Springer: New York, 2007.

139. McRee, D. R.; David, P. R. *Practical Protein Crystallography*; 2nd ed.; Academic Press: San Diego, CA, 1999.

140. Sacchettini, J. C. Texas A&M University, College Station, TX. Personal Communication, 2010.

141. Machius, M.; Chuang, J. L.; Wynn, R. M.; Tomchick, D. R.; Chuang, D. T. *Proc. Natl. Acad. Sci. USA* **2001**, *98*, 11218-11223.

142. Schormann, N.; Grigorian, A.; Samal, A.; Krishnan, R.; DeLucas, L.; Chattopadhyay, D. *BMC Struct. Biol.* **2007**, *7*, No pp given.

143. Uitdehaag, J. C. M.; Euverink, G. J.; van der Veen, B. A.; van der Maarel, M.; Dijkstra, B. W. Structure and Mechanism of the Amylomaltase from Thermus thermophilus HB8. [Online], Sept. 2, 2003. Protein Data Bank http://www.pdb.org/pdb/explore/explore.do?structureId=1FP8 (accessed Aug. 31, 2010).

144. Luka, Z.; Pakhomova, S.; Luka, Y.; Newcomer, M. E.; Wagner, C. *Protein Sci.* **2007**, *16*, 1957-1964.

VITA

Edward Sterling Funck
c/o Dr. Kim R. Dunbar
Department of Chemistry, Texas A&M University
College Station, TX 77840-3255
esfunck2@gmail.com

EDUCATION

Texas A&M University, College Station, TX, USA

M.S. Chemistry (2011)

Thesis: Investigation of Anion-π Interactions in Inorganic, Organic and Biological Systems.

Advisor: Prof. Kim R. Dunbar

Grove City College, Grove City, PA, USA

B.S. Chemistry (2005)

PROFESSIONAL EXPERIENCE

Texas A&M University, College Station, TX, USA

Research Assistant, Department of Chemistry (July 2005-May 2010)

Teaching Assistant, Department of Chemistry (Sept. 2005-Dec. 2009)

Instructor's Assistant, Department of Chemistry (Sept. 2006-May 2010)

Research Assistant (Research Experience for Undergraduates), Department of Chemistry (June 2004-Aug. 2004)

The Pennsylvania State University, State College, PA, USA

Research Assistant (Research Experience for Undergraduates), Department of Chemistry (June 2003-Aug. 2003)